EVALUATING SUBUNIT INTERFACIAL INTERACTIONS AND CHLORIDE ADDUCTION INDUCED GAS-PHASE STABILIZATION OF DIUBIQUITIN USING ESI-IM-MS AND COLLISIONAL ACTIVATION METHODS

A Dissertation

by

NICOLE DEANNE WAGNER

Submitted to the Office of Graduate and Professional Studies of
Texas A&M University
in partial fulfillment of the requirements for the degree of

DOCTOR OF PHILOSOPHY

Chair of Committee,	David H. Russell
Committee Members,	Simon W. North
	Emile A. Schweikert
	Paul D. Straight
Head of Department,	Simon W. North

August 2017

Major Subject: Chemistry

ABSTRACT

Native electrospray ionization ion mobility mass spectrometry (ESI-IM-MS) allows for the investigation of complex heterogeneous mixtures of intact biomolecules according to their mass, charge, and size, which can provide unique insight into higher order protein structure (*i.e.* tertiary, quaternary, *etc.*), solution-phase perturbations, and dynamics. However, this method is more of a "coarse-grained" approach providing relative size information rather than more detailed characterization of local structures. Here we demonstrate the use of the complementary technique collision induced unfolding (CIU) for the characterization of noncovalent intra/intermolecular interactions of the model protein ubiquitin (Ubq), its bioactive oligomers, and the effect of chloride adduction on conformational preference.

Ubq is a relatively small protein that participates in a wide-array of bioactivities as defined by the ability to form a variety of oligomeric states. A key facet to the quaternary structure and thus function of Ubq oligomers is the site of covalent-linkage between the subunits. Here we present the investigation of the recently reported non-covalent homodimer of Ubq (ncUbq) and four diubiquitin (diUbq) molecules covalently-linked through different lysine side-chains. Despite that each covalent-linkage site induces distinct conformational preferences owing to steric hindrance induced by the covalent tether, ESI-IM-MS lacks sufficient resolution to differentiate these conformers; however, the CIU fingerprints of each are distinctly different. Furthermore, the CIU

fingerprint of ncUbq suggests a high degree of conformational similarity to diUbq covalently linked through K48.

ESI-IM-MS is an inherently gas-phase technique, raising the question: How much does the solvent-free ion resemble the solution-phase structure of the analyte, and under what conditions might this structure be preserved? Here, using ESI-IM-MS and CIU, we provide evidence that chloride adduction to Ubq results in gas-phase stabilization of a more compact conformer; furthermore, the more compact conformers of chloride adducted K48-linked diUbq ions demonstrate gas-phase unfolding patterns characteristic of the "native-like" structure reported in the previous sections. Thus we present evidence that chloride adduction to Ubq and K48-linked diUbq ions results in the gas-phase stabilization of the "native-like" conformation of the analyte ion and inducing additional resistance to gas-phase unfolding.

DEDICATION

For my family

ACKNOWLEDGEMENTS

I would like to thank my graduate research advisor Dr. David H. Russell for sharing a small portion of his vast expertise with me and for guiding me through the research and publication process. Perhaps the greatest lesson I learned is that a project ending is not a failure unless you do nothing with what you had learned in the process.

I would like to thank the various members of the Russell group, both past and present, for help both intellectual and psychological with a special thank you to Greg Matthijetz, Dr. Doyong Kim, Dr. Kerry Wooding, Dr. Shuhua Chen, Chunying Xiao, Shiyu Dong, Michael Hebert, and Chris Mallis. You've made me feel at home and like I've always had someone to turn to.

Thank you to my parents (Daniel and Deborah), grandparents (David, Teresa, Dean, and Patricia), brother (Matthew), sister (Jenifer), and aunt and uncle (Denise and Eddie) for your love, support, and encouragement. I'd like to thank Dr. Jessica Spear for being the best friend I could have asked for. You made Texas A&M and College Station infinitely more entertaining; I've really missed you these last couple of years. Lastly, thank you to my fiancé Jordan Embree for your love and support while weathering life in College Station and for keeping a smile on my face, even if I didn't want to smile just then.

CONTRIBUTORS AND FUNDING SOURCES

Contributors

This work was supported by a dissertation committee consisting of Professor David H. Russell (advisor), Professor Emile A. Schweikert of the Department of Chemistry, Professor Simon H. North of the Department of Chemistry, and Professor Paul A. Straight of the Department of Biochemistry and Biophysics.

Theoretical CCS values were calculated via the MOBCAL trajectory method by Dr. Doyong Kim. All other work conducted for the dissertation was completed by the student independently.

Funding Sources

This work was made possible in part by the Department of Energy, Division of Chemical Sciences, Basic Energy Science under Grant Number DE-FG02-04ER15520.

NOMENCLATURE

CCS	Collision Cross-Section
CID	Collision Induced Dissociation
CIU	Collision Induced Unfolding
diUbq	Covalently-linked Diubiquitin
ESI	Electrospray Ionization
HDX	Hydrogen-Deuterium Exchange
IMS	Ion Mobility Spectrometry
IM-MS	Ion Mobility-Mass Spectrometry
m/z	Mass-to-charge Ratio
MS	Mass Spectrometry
nESI	nano-Electrospray Ionization
MDS	Molecular Dynamics Simulations
ncUbq	Noncovalent Ubiquitin Homodimer
NMR	Nuclear Magnetic Resonance
polyUbq	Covalently-linked Polyubiquitin Chains
SASA	Solvent Accessible Surface Area
TWIG	Travelling Wave Ion Guide
TWIMS	Travelling Wave Ion Mobility Spectrometry
Ubq	Ubiquitin

TABLE OF CONTENTS

Page

LIST OF FIGURES

Page

LIST OF TABLES

Page

1. INTRODUCTION

Understanding protein higher order structure and interfacial interactions is crucial to understanding protein binding motifs, *i.e.* an interactome, in order to better understand their diverse cellular function. Rough estimates for protein binding in the yeast cell suggest that the average protein participates in as few as three to as many as ten interactions with different binding partners.[1] Due to the complex, dynamic and often transient nature of quaternary and quinary structures, characterization of an interactome is particularly challenging. X-ray crystallography is an excellent structural analysis technique capable of atomistic detail; however, the ability to crystallize dynamic proteins/protein complexes with a high degree of conformational entropy in a well-ordered crystal is no simple feat. Nuclear magnetic resonance (NMR) spectroscopy is similarly capable of high resolution structural analysis and relaxation measurements; however, the deconvolution of complex conformational mixtures and relaxation results is an ongoing investigation often requiring the use of computational deconvolution methods.[2-4]

With the advent of soft ionization techniques, *i.e.* matrix assisted laser desorption ionization (MALDI) and electrospray ionization (ESI), mass spectrometry (MS) has evolved to become an excellent complementary technique for evaluation of structural biology. In particular, ESI-MS allows for the characterization of complex mixtures of intact proteins/protein complexes retaining "native" or "native-like" noncovalent interactions with high sensitivity.[5-9] Ion mobility spectrometry (IMS) is a gas-phase

electrophoretic separation technique that separates ions on the basis of their ion-neutral collision cross sections (CCS) which correlates to the ion's three-dimensional structure. The integration of IMS with ESI-MS has yielded a symbiotic relationship capable of complex conformational analyses of heterogeneous mixtures of ions; consequently, ESI-IM-MS is exceptionally useful for evaluation of heterogeneous populations of tertiary and quaternary structures. However, IM-MS CCS values are essentially a "coarse-grained" approach providing only a rough measurement of overall size.[10] In an effort to circumvent this issue, molecular dynamics simulations (MDS) have proven an effective complementary technique to IM-MS experiments yielding more atomistic detail.[11-13] In addition, techniques such as chemical footprinting, hydrogen-deuterium exchange (HDX), tandem MS, and collisional activation techniques can be used to extract more detail. More recently, new applications of gas-phase activation methods have been applied to the characterization of complex quaternary structure, such as surface induced dissociation and collision induced unfolding (CIU).[6, 9, 14-15] In particular, CIU has been applied to examine differences in protein complex interfaces, intramolecular interactions, and lipid and anion binding induced stabilization.[7, 15-21] CIU is the stepwise increase in the internal energy of the ion through collisional activation with a buffer gas and subsequent structural analysis using IM-MS. As such, CIU results in a gas-phase unfolding fingerprint that is often unique and representative of the ion's noncovalent interactions (See for **Figure 1.1** an example compilation of a CIU heat map from individual IMS CCS profiles.)

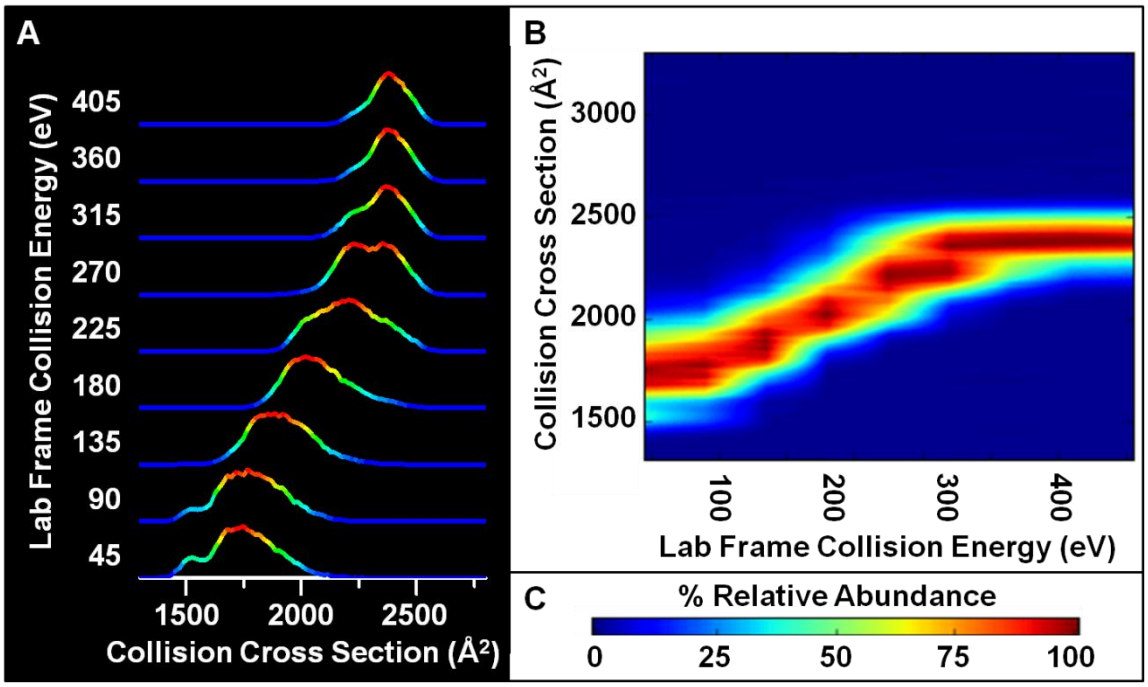

Figure 1.1. Example compilation of a CIU heat map from raw CCS profiles acquired using different collision energies (K48-[diUbq + 9H]$^{9+}$ from water/0.1% formic acid).

Overall, each analytical technique has strengths and limitations; therefore, a more complete analysis of protein structure and characterization of protein-protein dynamic interactions can be achieved when analytical information is drawn from a variety of sources. For example, recently a hybrid x-ray crystallography and NMR relaxation analysis was demonstrated to provide a more complete analysis of protein dynamics.[22] An additional study utilized x-ray crystallography, NMR, IM-MS, and CIU analyses to study the conformational dynamics of a labile protein upon ligand binding.[23] Here we demonstrate the complementarity of ESI-IM-MS in conjunction with CIU experiments for the analysis of a model protein and its conformationally dynamic oligomeric states previously studied using NMR and x-ray crystallography.

Ubiquitin (Ubq) is a highly conserved, 76 amino acid protein that is expressed in all eukaryotic cells with little structural deviation. The structure of Ubq has been well characterized using X-ray crystallography and nuclear magnetic resonance spectroscopy; the monomeric form of Ubq occupies a stable β-grasp fold structure in aqueous solutions over a pH range of 1.2 to 8.4 (See **Figure 1.2** for the x-ray crystal structure of Ubq).[24-25] The surface of Ubq is peppered with acidic and basic residues (thirteen of each) and two

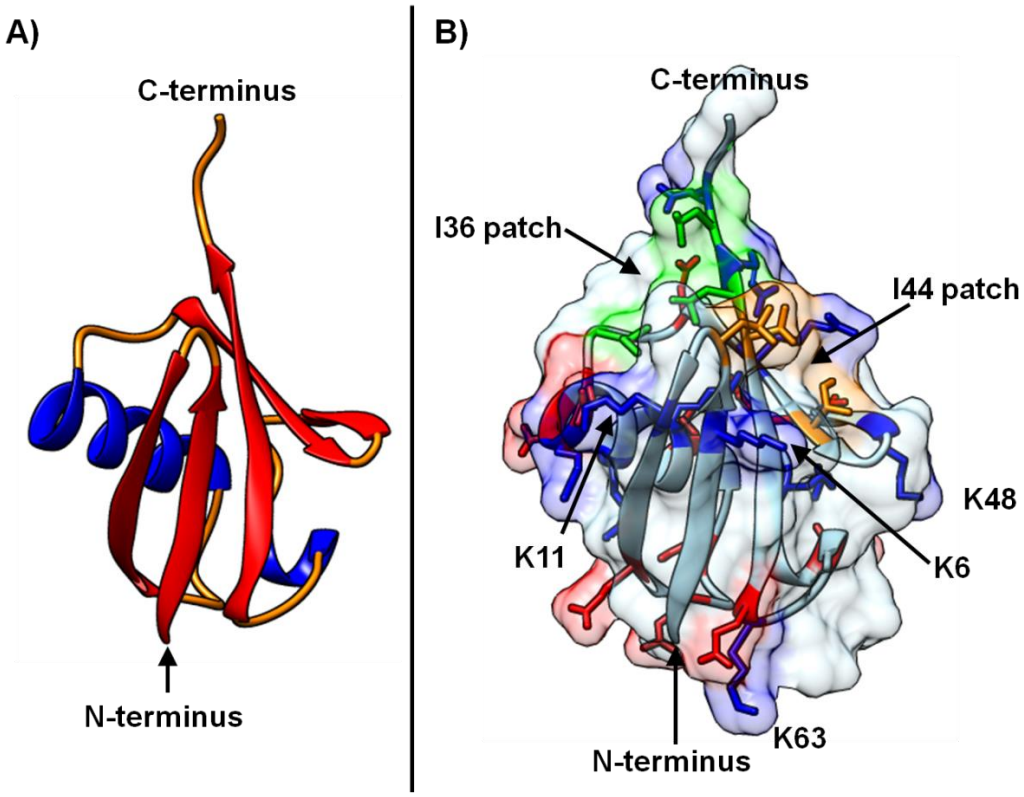

Figure 1.2. Two representations of the PDB structure of Ubq (1UBQ) as determined by x-ray crystallography. (A) illustrates β-grasp fold structure observed of Ubq where helices and the β-sheet are shown in blue and red, respectively. (B) shows the locations of the hydrophobic patches (I44 and I36 are shown as orange and green, respectively) and all acidic (red) and basic (basic) residues. Note that the most common sites of covalent linkage are denoted.

hydrophobic surfaces. The I44 hydrophobic patch consists of L8, I44, and V70, and the I36 hydrophobic patch consists of I36, L71, and L73.[26-27] Low charge states of Ubq ions analyzed by ESI-IM-MS are well reported to have CCS values similar to that calculated for the native-fold in solution.[28-30] However, the more biologically relevant forms of Ubq are its oligomeric forms.

Polyubiquitylation is a post-translational modification wherein a chain of Ubq subunits is covalently linked to a substrate protein through an isopeptide bond between the C-terminus and a substrate amino group. These chains range in length from two moieties to more than ten via sequential C-terminus - amine isopeptide bonds.[27] Due to the presence of eight amino groups in Ubq (the N-terminus and seven lysine side-chains), polyubiquitin chains (polyUbq) populate a diverse array of homogeneous, mixed, and branched oligomers, each resulting in a unique tag encrypting diverse biological function. Interestingly, the structure of each subunit in a polyUbq chain differs little from that of monoUbq; in particular, both hydrophobic patches are preserved and often participate in interfacial interactions between the covalently linked subunits or as part of a binding motif.[26, 31-35] However, the location of the covalent linkage results in unique conformational preferences, associated binding motifs, and function.[27, 36-40]

For example, K48-linked tetraUbq performs the most well-known Ubq function as the tag for proteosomal degradation of a misfolded protein or an antigen in the 26S proteosome complex.[36, 41-42] Other chains propagating through alternative linkage types may protect the tagged substrates from proteosomal degradation, but also produces

alternative functions.[27, 43-44] For example, K63-linked polyUbq is implicated in several biological functionalities including DNA repair,[45-46] inflammation,[47] immune response,[41] cellular trafficking,[45] and antiviral response.[48] K11-linked polyUbq is involved in the regulation of cell division and mitosis.[32] K6-linked polyUbq chains linked to the parkin protein are associated with the regulation of mitophagy.[49] Due to the diverse biological functionality encoded by polyubiquitination, this single post-translational modification has been implicated in a variety of medical conditions: dysfunction of the ubiquitin-proteasome pathway is reportedly involved in the pathogenesis of Parkinson's, Huntington's, and Alzheimer's diseases,[50-51] and K48- and K63-linked polyUbq molecules are involved in the oncogenesis of several cancers making them targets for cancer therapy research.[52] Consequently, a better understanding of the unique conformational preferences and induced binding domains defined by the covalent-linkage could improve understanding of a variety of biological processes and aid in targeted potential applications.

Diubiquitin (diUbq) molecules provide a means to directly probe the structural propensities and interfacial interactions characteristic of each covalent linkage site. Many structures of various diUbq molecules have been previously reported using NMR and x-ray crystallography. K48-linked diUbq reportedly occupies a "closed" structure stabilized through I44/I44 hydrophobic interfacial interactions (See **Figure 1.3A)**.[37]

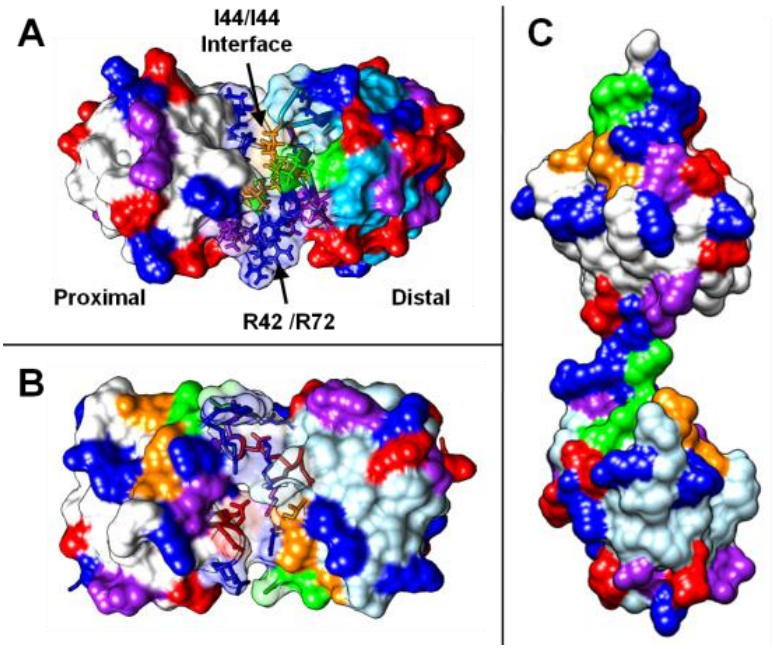

Figure 1.3. PDB reported structures for (A and B) K48- and (C) K63-linked diUbq, illustrating the different noncovalent interactions responsible for dimer conformational preference. K48-linked diUbq is shown as a "closed" conformation with I44/I44 hydrophobic patch interaction (A, PDB 2PEA) and an "open" conformation with electrostatic interactions (B, PDB 3NS8). K63-linked diUbq is shown with an "open" conformation (C, PDB 2JF5). Note residues are color coded as (blue) basic, (red) acidic, (purple) glutamine and asparagine, (orange) I44 hydrophobic patch, and (green) I36 hydrophobic patch. The calculated CCS values for each are 1780 $Å^2$, 1816 $Å^2$, and 2086 $Å^2$ (A-C, respectively). Reprinted with permission from [97].

Under more acidic conditions, R42 and R72 located in close proximity to the I44 patch are more likely to be protonated which results in coulombic repulsion. This added destabilization induces the preference for electrostatic interfacial interactions, exposing the I44 patches to the solvent for potential binding in an "open" conformation (**Figure 1.3B**).[34, 53] K63-linked diUbq will not form hydrophobic patch interactions due to the steric hindrance induced by the covalent tether; note that K63 is near the N-terminus whereas the hydrophobic patches are near the C-terminus. Consequently, K63-linked

diUbq reportedly adopts an extended "open" conformation (**Figure 1.3C**) or "closed" conformations stabilized by electrostatic interfacial interactions.[38, 40, 54-55] The structural preferences of K6- and K11-linked diUbq molecules are less well understood. Two distinct structures for K11-linked diUbq are reported under physiological conditions – one of which adopts I36/I36 hydrophobic interactions and the other is stabilized via electrostatic interactions.[32, 56-57] A single crystal structure for K6-linked diUbq adopting I36/I44 interfacial interactions has been reported.[58] More recent NMR and small angle neutron scattering (SANS) results have reported that a single structure is a woefully incomplete representation of the conformational space occupied by the different diUbq molecules.[59] Recent reports suggest that because the C-terminus of Ubq is inherently flexible, diubiquitin (diUbq) molecules adopt a dynamic ensemble of solution-phase conformations, and thus these single structures are likely an oversimplification of diUbq conformational preference and interfacial binding, further complicating potential analyses.[59-60]

Recent investigations have shown that Ubq may form purely noncovalent oligomers in solution.[61-62] The occurrence of the noncovalent dimer (ncUbq) is especially useful for evaluating the relative stability of Ubq subunit interfacial interactions in that preference for a particular interface would suggest relative interfacial affinities without covalent linkage induced steric hindrance. Tang *et al.* reported NMR data suggesting that ncUbq is stabilized via I44/I44 interfacial interactions, reminiscent of that observed of K48-linked diUbq. [61] Prag *et al.* used x-ray crystallography to investigate a noncovalent Ubq tetramer that overlaps perfectly with the structure of K11-

linked tetraUbq exhibiting primarily electrostatic interactions. [62] Using cryogenic ESI-IM-MS, Servage *et al.* expanded upon these initial findings to suggest that water is integral to maintaining the stability of ncUbq.[63] The proximity of several basic residues (K6, K11, R42, R72, and H68) to the I44 hydrophobic patch may serve to promote occlusion of the water from the hydrophobic interface; furthermore, water-bridging may serve to reduce coulombic repulsion of said basic residues that may destabilize the noncovalent interface as observed of K48-linked diUbq.[34, 53, 63]

In Section 2, we introduce the application of CIU for the differentiation of polyUbq conformational architectures when ESI-IM-MS could not; furthermore, we utilize the CIU fingerprint information found for K48- and K63-linked diUbq to evaluate the structural propensity of ncUbq ions. In Section 3, we expand upon the interpretation of diUbq CIU fingerprints using two additional diUbq linkage types and solvent induced denaturation. The most common Ubq covalent linkage sites found in yeast cells are observed through the residues K48 (29.1%), K11 (28%), K63 (16.3%) and K6 (10.9%),[64] as such diUbq molecules covalently linked through these four linkage sites are used in Section 3.

Because ESI-IM-MS is an inherently gas-phase technique, the relevance of structural information derived from ESI-IM-MS to analysis of native solution-phase biomolecular structure remains an unresolved issue. Stated more specifically, "…for how long, under what conditions, and to what extent, can solution structure be retained without solvent?"[65] Current opinion in the field suggests that in the final stages of desolvation, the biomolecule experiences a mechanism akin to "freeze-drying",[66] *i.e.*, the

evaporative cooling inherent to the desolvation of an ESI nanodroplet provides a route for capturing ions that retain solution-phase conformer distributions.[63, 67-68] Furthermore, the intramolecular interactions induced by droplet shrinkage and charge solvation may stabilize the biomolecule and inhibit unfolding.[69-70] However, care must be taken in choosing instrumental parameters, for these solvent-free "solution-phase" conformations may revert to a gas-phase equilibrium structure if the ions experience collisional activation as they traverse the instrument.[71-72]

Recent investigations have reported that anion adduction to ESI-IM-MS analytes results in the preferential detection of more compact protein conformers[73] and the stabilization of quaternary structures.[74-75] In Section 4 we report the gas-phase stabilization of compact Ubq ions using chloride adduction. We theorize that the complex network of noncovalent interactions via the chloride adducts result in substantial stabilization capable of preserving the more "native-like" conformation of the protein despite collisional activation. However, due to the "coarse-grained" nature of CCS measurements, the observed compact conformers may be the product of anion adduction induced conformational collapse to an alternative compact conformer rather than a "native-like" conformation. Finally, in Section 6, using the comparison of CIU profiles acquired of K48-linked diUbq ions and chloride adducted K48-linked diUbq ions, we report the retention of "native-like" conformers upon chloride adduction to K48-linked diUbq.

2. DEFINING NON-COVALENT UBIQUITIN HOMODIMER INTERFACIAL INTERACTIONS THROUGH COMPARISONS WITH COVALENTLY-LINKED DIUBIQUITIN[*]

2.1. Introduction

Ubiquitin (Ubq), a small regulatory protein that is conserved in all eukaryotic cells, functions as a tag for many bioactivities as regulated by its oligomeric state. These bioactive oligomers are formed via an isopeptide bond between the C-terminal carboxyl group of an Ubq subunit and the amino group at either the N-terminus or one of the seven lysine side-chains of another Ubq subunit. Ubq bioactivities are encoded by distinct quaternary structures dependent upon the linkage site(s), chain length, branching, and specific non-covalent interactions.[27, 36-40] Recent investigations have shown that Ubq also forms a non-covalent homodimer (ncUbq) in solution.[61, 63] Tang *et al.* reported nuclear magnetic resonance (NMR) data that they interpreted as evidence that ncUbq populates an ensemble of conformers where residues surrounding the I44 hydrophobic patch (L8, I44, V70) of each subunit form the dimer interface.[61] Prag *et al.* reported a crystal structure of the noncovalent tetramer (teUbq) exhibiting purely electrostatic interfaces.[62] Such differences may arise owing to preferences for "specific interfaces" to remain "dry", whereas "crystal packing interfaces" tend to be "wet".[76] On the basis of cryo-ion mobility-mass spectrometry (cryo-IM-MS) experiments, Servage *et*

[*] Reprinted with permission from Wagner, N. D.; Russell, D. H., Defining Noncovalent Ubiquitin Homodimer Interfacial Interactions through Comparisons with Covalently Linked Diubiquitin. *J. Am. Chem. Soc.* **2016,** *138* (51), 16588-16591. Copyright 2016 American Chemical Society.

al. suggested that water mediates formation and retention of ncUbq ions through formation of intermolecular water-bridges, and that the dimer disassociates to form monomers upon complete evaporation of the water.[63] Here, we report collision-induced unfolding (CIU) fingerprints that provide additional evidence that ncUbq exhibits similar interfacial interactions and structural stability to diubiquitin (diUbq) covalently-linked through K48.

Two covalently-linked diUbq were chosen for this study because they each exhibit distinctly different conformations owing to very different interfacial interactions: K48-linked diUbq and K63-linked diUbq. **Figure 1.3** shows representative structures of K48-linked diUbq "closed" and "open" conformers and an "open" conformer of K63-linked diUbq. The two subunits of both diUbq retain much of the native monomeric structure despite the isopeptide linkage, including the preservation of the I44 (L8, I44, V70) and I36 (I36, L71, L73) hydrophobic patches.[27] Under physiological conditions, K48-linked diUbq preferentially adopts "closed" conformations stabilized by hydrophobic interactions between the two I44 patches (**Figure 1.3A**).[37] Increased protonation of the five basic residues in close proximity to the I44 patch (K6, K11, R42, R72, and H68) induces the preference for electrostatic interfacial interactions, *i.e.* an "open" conformation (**Figure 1.3B**).[34, 37, 53] Reports suggest that K48-linked diUbq exists in equilibrium between the two conformer types.[34, 77] K63-linked diUbq is incapable of forming I44/I44, I44/I36, and I36/I36 interactions and adopts an ensemble of conformer types in solution, *viz.* an "open" conformation as shown in **Figure 1.3C** and two conformers forming electrostatic subunit interfaces. [38, 40, 54-55] Other linkage

types (K6-, K11-, etc.) are reported to exhibit a variety of dynamic interfacial interactions involving either electrostatic interactions or the I36 patch. [32, 56-58] As such, the hydrophobic I44/I44 interface reported for K48-linked diUbq and the electrostatic interface reported for K63-linked diUbq make each an appropriate model for comparison to ncUbq.

2.2. Experimental Methods

2.2.1. Sample Preparation

K6-, K11-, K48- and K63-linked diUbq were purchased from R&D Systems Inc. (Minneapolis, MN, USA), and bovine ubiquitin was purchased from Sigma Aldrich, Inc. (St. Louis, MO, USA). All were used without further purification. Each was dissolved in 18 MΩ water (Barnstead Easy Pure II, Thermo Scientific) and stored at -20 ˚C for later use. All solutions were prepared with 0.1% formic acid or 25 mM ammonium acetate (pH adjusted to ~7.4). The final concentrations of the covalently-linked diUbq were 10 µM. To drive formation of the noncovalent dimer, the final concentration of ubiquitin for noncovalent dimer studies was 75 µM.

2.2.2. ESI-IM-MS and CIU

IM-MS spectra and CIU curves were acquired via a Waters Synapt G2 HDMS mass spectrometer (Manchester, UK). Instrument conditions were chosen to minimize collisional heating as the ions traverse the various regions of the instrument: sample cone, 10V; extraction cone, 1V; trap bias, 25 V; API gas flows, off; helium cell flow rate, 200 mL/min; IMS nitrogen flow rate, 60 mL/min; TWIMS wave height, 20V;

TWIMS wave velocity, 300 m/s.[72] "Helium equivalent" CCS values were calibrated as previously described using reported CCS_{He} values for acid denatured ubiquitin, cytochrome c, and myoglobin.[78] Noncovalent dimer ions were mass selected in the quadrupole; mass selection was not necessary for covalently linked dimers. Collisional activation was applied via increasing the voltage drop between the exit of the quadrupole and the entrance to the TWIG-trap region filled with the collision gas argon. Note that a 5 V drop was necessary to maintain transmission through the trap and transfer regions and will be referred to as low collision energy. Reported lab-frame collision energies were calculated as the product of ion charge and acceleration voltage. CIUSuite was used to assemble all heat maps and difference plots.[20] All CCS profiles at each collision energy were normalized to the CCS of maximum abundance.

2.2.3. Theoretical Structures

Chimera UCSF was used for visualization of PDB files.[79] The MOBCAL trajectory method was used to calculate theoretical CCS values from PDB files.[80,81]

2.3. Results and Discussion

The ESI mass spectrum of Ubq obtained by cryo-IM-MS is dominated by ions corresponding to $[Ubq + 7H]^{7+}$ and $[ncUbq + 14H]^{14+}$ ions;[63] however, the ESI mass spectrum obtained using ambient conditions contains ions corresponding to $[Ubq + 7H]^{7+}$ and $[Ubq + 8H]^{8+}$ in high abundance, and low abundances of $[ncUbq + 9H]^{9+}$, $[ncUbq + 10H]^{10+}$, and $[ncUbq + 11H]^{11+}$ (see **Figure 2.1** for full mass spectra). The differences in the mass spectra are attributed to the presence of hydrating water

molecules in the cryo-IM-MS experiment; note that a large fraction of fully desolvated $[ncUbq + 14H]^{14+}$ ions disassociate to form $[Ubq + 7H]^{7+}$ ions.[63]

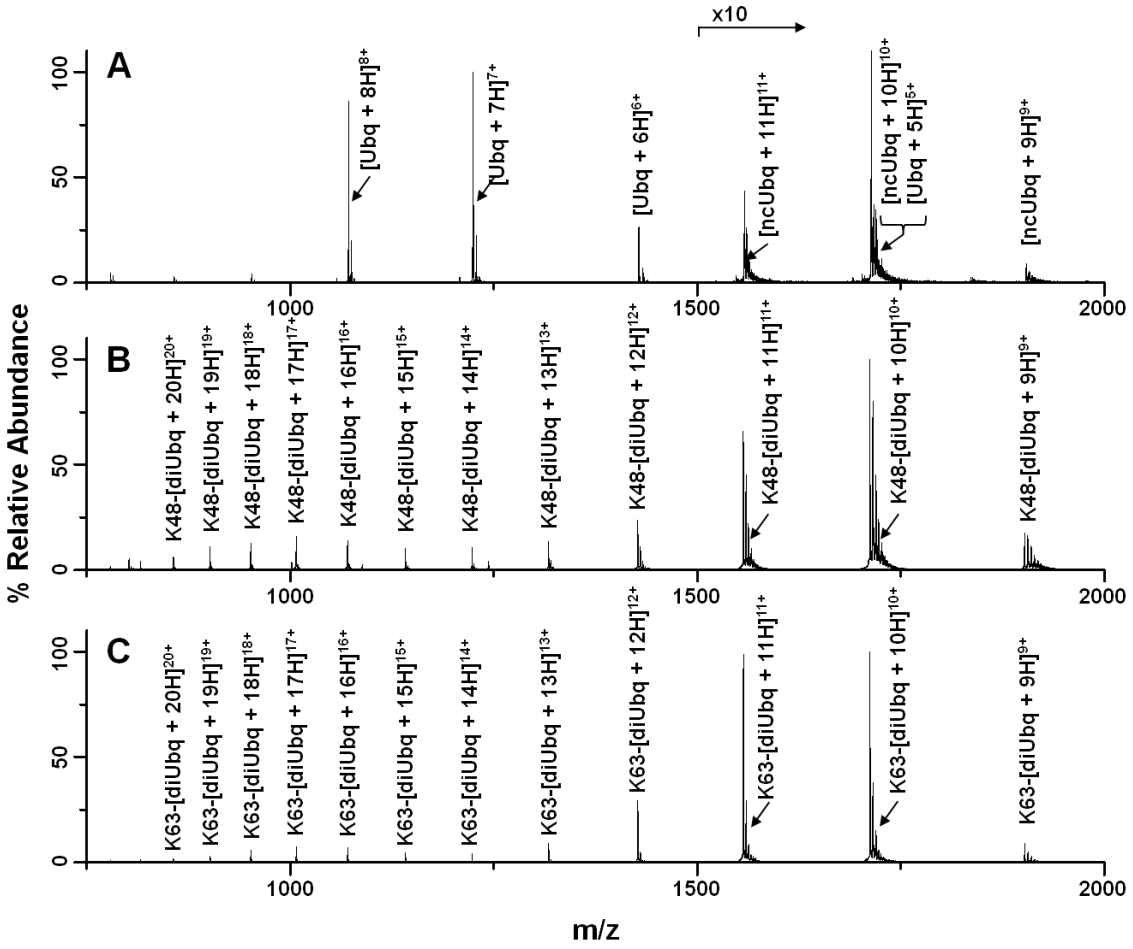

Figure 2.1. (A) Full mass spectrum of 75µM ubiquitin acquired from water and 0.1% formic acid. The ion signals with m/z greater than 1500 were amplified by 10 in order to better depict the dimer signals. (B) and (C) Full mass spectra for K48-linked and K63-linked diubiquitin, respectively, acquired from water and 0.1% formic acid (Note: no signal amplification). Reprinted with permission from [97].

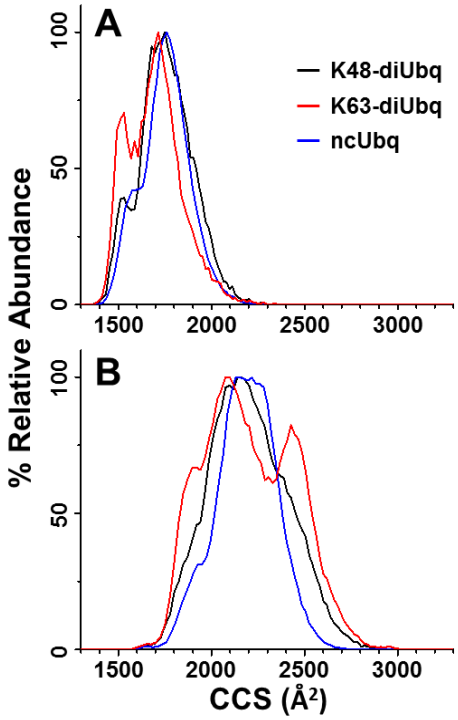

Figure 2.2. CCS profiles acquired from water and 0.1% formic acid of (A) the 9+ and (B) the 11+ charge states of (black) K48-linked diUbq, (red) K63-linked diUbq, and (blue) ncUbq. All CCS profiles were acquired under ambient conditions and using collision energies of 45 eV and 55 eV for 9+ and 11+ ions, respectively (the minimum required to maintain ion transmission). Reprinted with permission from [97].

The following discussion will be limited to $[ncUbq + 9H]^{9+}$ and $[ncUbq + 11H]^{11+}$ ions owing to overlap of $[ncUbq + 10H]^{10+}$ and monomeric $[Ubq + 5H]^{5+}$ ions. **Figure 2.2** shows ambient, low internal energy CCS profiles for the 9+ and 11+ charge states of K48- and K63-linked diUbq and ncUbq. Interestingly, under experimental conditions that sample low internal energy ions,[72] each of the ions exhibit similar, conformationally broadened CCS profiles that are practically indistinguishable (see **Figure 2.1** for calculated theoretical CCS values). The 9+ charge state ions of each type suggest at least two conformational populations: a more compact conformer family

smaller than all calculated values, *i.e*. compact (~1500 $Å^2$), and a more extended conformer family at ~1780 $Å^2$. These observed CCS values provide strong evidence that the 9+ charge states of each ion exhibit a distribution of conformations similar in size to the reported PDB structures of K48-linked diUbq; note that the calculated CCS values for both conformations of K48-linked diUbq are within the experimental error (±2%) and thus not differentiable using IMS. The 11+ charge state ions of each diUbq demonstrate more conformational heterogeneity and are distinctly larger than the calculated CCS for the K48-linked conformers. The centroid for the CCS profiles are closer to the value calculated for the fully "open" conformation of K63-linked diUbq; however, the detection of the ncUbq 11+ ion suggests that some form of interfacial interactions are preserved. The larger CCS values are attributed to intermediate conformations along the gas-phase unfolding pathway still retaining some form of interfacial interactions. Note that the CCS profiles of K48-and K63-$[diUbq + 14H]^{14+}$ - ions suggest that these ions are in an open conformation and that the subunits have significantly unfolded (see **Figure 2.3**). These results suggest that the $[ncUbq + 14H]^{14+}$ ion population has disassociated upon complete desolvation similarly to that reported previously.[63]

Collision-induced unfolding (CIU) and collision-induced dissociation (CID) are increasingly used to investigate conformational changes induced by increasing ion internal energies.[7, 16, 18-20] CIU combined with IM-MS provides a unique unfolding

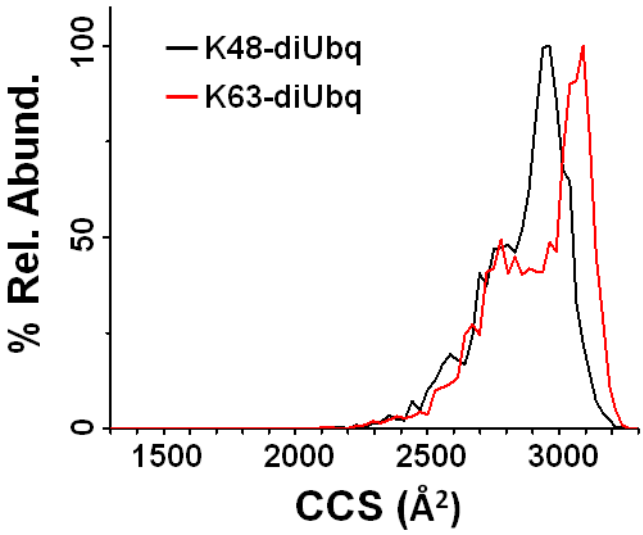

Figure 2.3. CCS profiles of the 14+ charge state of (black) K48- and (red) K63-linked diUbq acquired from 0.1% formic acid/99.9% water. Note that the calculated theoretical CCS values for closed K48-linked diUbq (PDB: 2PEA) and open K63-linked diUbq (PDB: 2JF5) are 1780 Å2 and 2086 Å2, respectively. Reprinted with permission from [97].

fingerprint for ions adopting a variety of noncovalent interactions. Here, CIU was used to probe the unfolding fingerprints of the K48- and K63-linked diUbq and ncUbq ions in an effort to elucidate conformational differences/similarities defined by their subunit interfacial interactions. At the collision energies used, covalently-linked diUbq does not undergo CID; however, upon destabilization of the ncUbq interface, disassociation to form two intact subunits is observed providing further insight into the relative stability of the ncUbq interface.

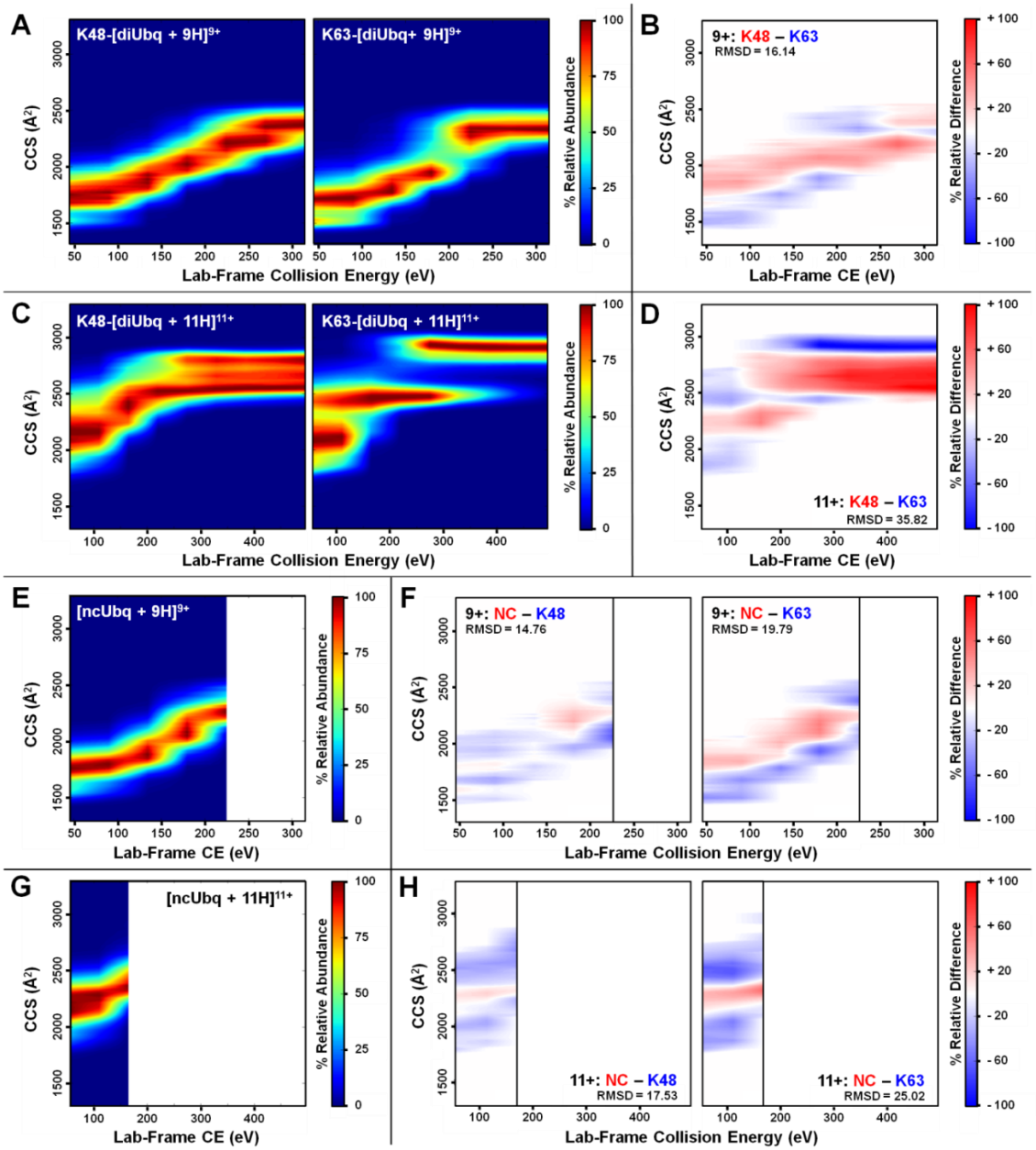

Figure 2.4. (A) and (C) CIU heat maps for 9+ and 11+ charge states, respectively, of K48- and K63-linked diUbq ions. (B) and (D) the difference plots resulting from subtraction of (red) K48- and (blue) K63-linked diUbq CIU profiles for the (B) 9+ and (D) 11+ charge states, respectively. (E) and (G) CIU heat maps for $[ncUbq + 9H]^{9+}$ and $[ncUbq + 11H]^{11+}$ ions, respectively. (F) Difference plots comparing the CIU unfolding pattern of $[ncUbq + 9H]^{9+}$ to those of (right) K48- and (left) K63-$[diUbq + 9H]^{9+}$ ions. (H) Difference plots comparing the CIU unfolding pattern of $[ncUbq + 11H]^{11+}$ to those of (right) K48- and (left) K63-$[diUbq + 11H]^{11+}$ ions. Note that all collision energies are reported as lab-frame kinetic energy and that each CCS profile is normalized to the most abundant feature. Reprinted with permission from [97].

Figure 2.4A and **Figure 2.4B** show CIU heat maps and the resulting difference plot,[20] respectively, for the 9+ charge state of K48- and K63-linked diUbq ions. A difference plot is generated by subtraction of two CIU heat maps where features observed of each fingerprint are differentiated as red or blue.[20] For example in **Figure 2.4B**, CCS values observed of K48-linked diUbq are shown in red, whereas those for K63-linked diUbq are shown in blue. The difference plot reveals that K63-[diUbq + 9H]$^{9+}$ ions exhibit a higher abundance of the more compact conformer population than do K48-[diUbq + 9H]$^{9+}$ ions, followed by gradual unfolding up to ~175 eV of collision energy. Upon additional collisional heating, K63-[diUbq + 9H]$^{9+}$ ions undergo a sharp transition from intermediate to extended conformers. Conversely, primarily gradual unfolding is observed for K48-[diUbq + 9H]$^{9+}$ ions, and the collision energy required to populate the most extended conformers of K48-[diUbq + 9H]$^{9+}$ ions is greater than that required to form extended conformers of K63-[diUbq + 9H]$^{9+}$ ions.

Figure 2.4C and **Figure 2.4D** show CIU heat maps and difference plot, respectively, for the 11+ charge state of K48- and K63-linked diUbq ions. The CIU heat map for K63-[diUbq + 11H]$^{11+}$ ions reveal that a portion of the ions undergo significant unfolding (to ~2500 Å^2) even at the lowest collision energy; whereas, ~200 eV of collisional energy is required for K48-[diUbq + 11H]$^{11+}$ ions to populate an intermediate conformer with a similar CCS. Furthermore, the collisional activation of K48-[diUbq + 11H]$^{11+}$ ions does not result in distinct unfolding intermediates and produces more compact extended conformers than those observed of K63-[diUbq + 11H]$^{11+}$ ions.

Overall, we find that K48- and K63-linked diUbq each exhibit unique unfolding fingerprints, attributable to different tertiary structures and intramolecular stabilization.

Figure 2.4E and **Figure 2.4G** show the CIU heat maps for the 9+ and 11+ charge states of ncUbq. The unfolding patterns of the ncUbq ions are visually most similar to those of K48-linked diUbq ions with the same charge state. This observation is further supported by the difference plots shown in **Figure 2.4F** and **Figure 2.4H.** The $[ncUbq + 9H]^{9+}$ ion unfolding pattern tracks closely with that of K48-$[diUbq + 9H]^{9+}$ ions up to ~200 eV of collision energy, where some fraction of the total population of K48-$[diUbq + 9H]^{9+}$ ions remains more compact. The 11+ charge states of ncUbq and K48-linked diUbq are less similar to one another than those of the 9+ ions; specifically, the K48-$[diUbq + 11H]^{11+}$ ion conformational population is more broad, i.e. more heterogeneous, than the $[ncUbq + 11H]^{11+}$ conformer population. Overall, we attribute the similarity between the ncUbq and K48-linked diUbq ion CIU fingerprints to similarities in conformation and noncovalent interactions. The CIU fingerprints for both charge states of K63-linked diUbq differ dramatically from those of the ncUbq ions, further strengthening this assessment. Note that CIU heat maps for K6- and K11-linked diUbq ions,[27] are more similar to K63-linked diUbq than to K48-linked diUbq and ncUbq ions. These comparisons provide further support for our assignment (see **Figure 2.5**; note the large change in CCS rather than gradual unfolding). The CIU heat maps for ncUbq ions are truncated due to collision-induced disassociation (See **Figure 2.6** for a detailed description of the CID of ncUbq ions). Interestingly, both the $[ncUbq + 9H]^{9+}$

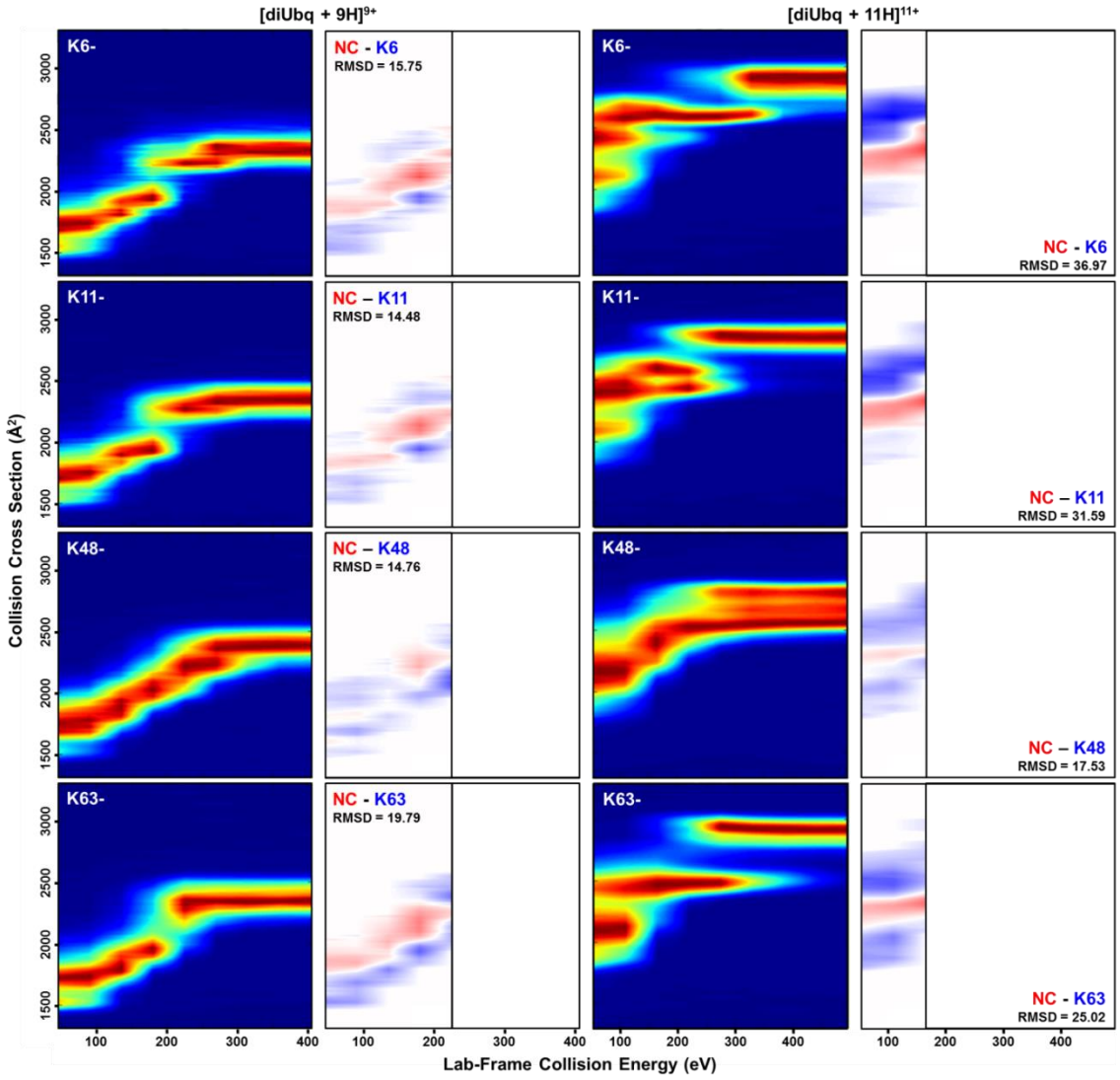

Figure 2.5. CIU heat maps and difference maps for the 9+ and 11+ charge states (left to right) of K6-, K11-, K48-, and K63-linked diUbq ions (top to bottom). Solution conditions were 99.9% water and 0.1% formic acid. K6-, K11-, and K63-linked diUbq ions undergo a dramatic change in CCS not observed of K48-linked diUbq or ncUbq, seen as a red spot in the 9+ difference plots. Note that K11-linked diUbq reportedly adopts electrostatic interfacial interactions and I36/I36 interfacial interactions; K6-linked diUbq reportedly adopts I36/I44 interfacial interactions. [32, 56-58] Reprinted with permission from [97].

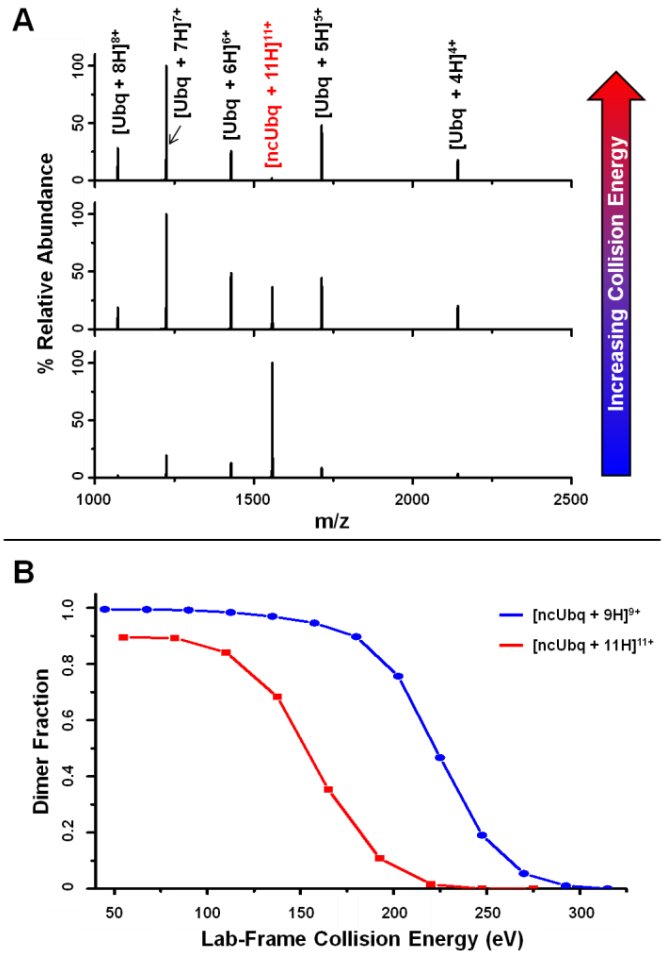

Figure 2.6. (A) MS-CID-MS product ion mass spectra resulting from mass selection of $[ncUbq + 11H]^{11+}$ ions and application of differing collision energies (55 eV, 165 eV, and 275 eV from bottom to top). (B) Plot depicting the surviving fraction of mass selected (red) $[ncUbq + 11H]^{11+}$ and (blue) $[ncUbq + 9H]^{9+}$ ions as a function of collision energy. Reprinted with permission from [97].

and $[ncUbq + 11H]^{11+}$ ions are stable through collision energies that produce intermediate conformers of K48-linked diUbq but disassociate prior to formation of the most extended conformations of K48-linked diUbq. The disassociation of ncUbq ions occurs at collision energies larger than those resulting in extended K63-linked diUbq conformers. This further supports our hypothesis that the noncovalent interactions

stabilizing ncUbq are more similar to those of the K48-linked diUbq ions. Furthermore, the disassociation of ncUbq at a collision energy below that required for formation of the most extended conformers of K48-linked diUbq suggests that this final transition corresponds to complete disruption of the K48-linked diUbq noncovalent interface.

Overall, we have shown that the tertiary structures of the closed conformations of K48- and K63-linked diUbq are differentiable using CIU, suggesting that the method is sensitive to differences in protein-protein interfacial interactions. Furthermore, the results of CIU support previously published results suggesting that ncUbq adopts an I44/I44 hydrophobic interface in solution as opposed to primarily electrostatic interactions.[61, 63] Fushman suggested that the prevalence of the K48-linked diUbq hydrophobic interface in solution is pH dependent; *i.e.* the preference for the I44/I44 interface is dependent upon the protonation state of basic residues in close proximity to the interface.[34] Due to this pH dependence, control studies were performed for ncUbq and K48- and K63-linked diUbq using buffered solution. The buffered solutions produced 7-9+ charge states of each (see **Figure 2.7** for the full MS). When the CIU fingerprints produced from buffered solution were compared to the 9+ ions produced from acidic solution, the difference plots show little deviation (see **Figure 2.8**). The most notable difference between the CIU patterns from buffered and acidic solutions correspond to collapsed conformers that are observed at low collision energies from acidic solution (~1500 $Å^2$). We attribute these more collapsed conformers to an acid-induced, molten globule conformation.[82] Note that 11+ ncUbq and diUbq ions were not

observed from buffered solution and as such may be more representative of acid destabilized conformations.

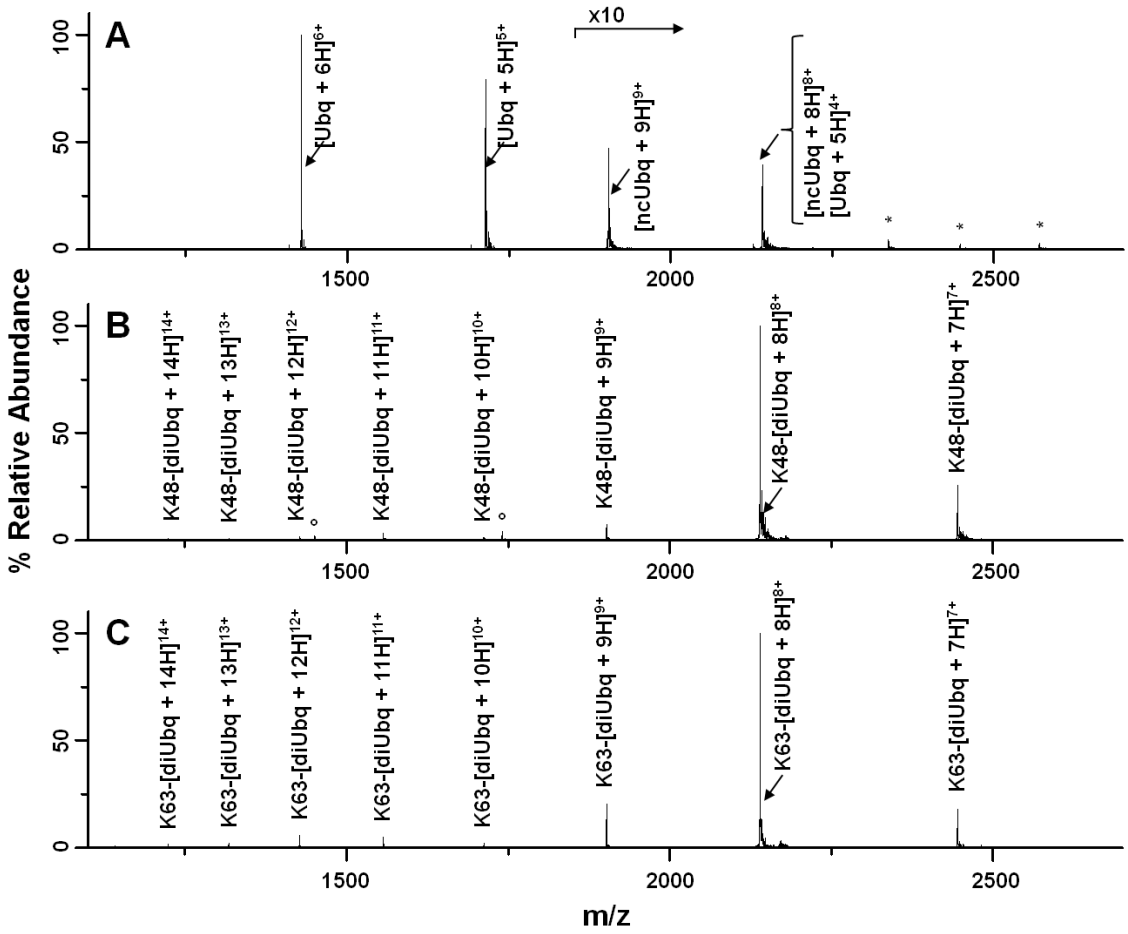

Figure 2.7. (A) Full mass spectrum of 75µM ubiquitin acquired from 25 mM NH4OAc, pH 7.4. The ion signals with m/z greater than 1500 were amplified by 10 in order to better depict the dimer signals. An asterisk indicates a multimer larger than a dimer. (B) and (C) Full mass spectra of K48-linked and K63-linked diubiquitin, respectively, acquired from 25 mM NH4OAc, pH 7.4 (Note: no signal amplification). Open circles indicate low abundance [M + 132] ions, which likely correspond to fragmentation at the C-terminal end of the distal ubiquitin (y2 fragment of the distal ubiquitin covalently linked to the K48 of the proximal ubiquitin). Reprinted with permission from [97].

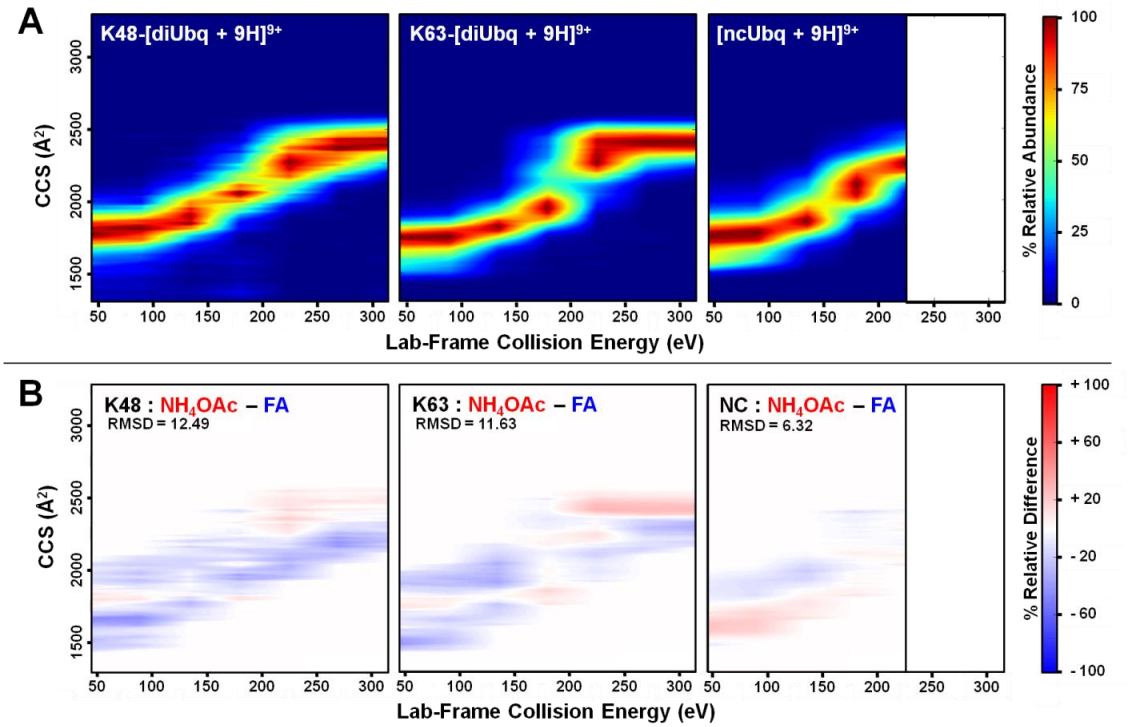

Figure 2.8. (A) CIU heat maps for the 9+ charge state of K48- and K63-linked diUbq and ncUbq. Solution conditions were water/25 mM ammonium acetate, pH 7.4. Note that the noncovalent dimer population has been significantly depopulated at collision energy 225 eV. (B) Difference plots are shown for comparison of the CIU heat maps acquired from (red) ammonium acetate solution vs. (blue) 0.1% formic acid solution (CIU heat maps acquired from 0.1% formic acid solution are shown in Figure 3). Reprinted with permission from [97].

Liu *et al.* predicted a dissociation constant for ncUbq of 4.4 mM, higher than the concentrations used in this study.[61] Electrospray ionization (ESI) produces charged nanodroplets that contain the analyte of interest. The effective concentration of the analyte may increase as the droplet size decreases; therefore, in the late stages of droplet evolution, the concentration of Ubq may approach the K_D of ncUbq. Consequently, it is possible that the ncUbq ions presented in this study may not be representative of initial solution-phase conformations, but rather "ESI-induced" dimerization.[83] The cryo-IM-

MS experiment has the advantage of monitoring hydrated proteins en route to complete desolvation. Servage *et al.* report that $[ncUbq + 14H]^{14+}$ ions exhibit a hydration trendline, whereas, $[Ubq + 7H]^{7+}$ does not.[63] The absence of Ubq hydration suggests that nonspecific dimerization of Ubq is preferred either during the ESI process or in solution.

2.4. Conclusions

Covalently-linked diubiquitin (diUbq) is known to adopt specific interfacial interactions owing to steric hindrance induced by the covalent tether. K48-linked diUbq preferentially forms hydrophobic interfacial interactions between the two I44 faces under physiological conditions, whereas K63-linked diUbq preferentially forms electrostatic interfacial interactions. Here, we have shown using collision-induced unfolding (CIU) ion mobility-mass spectrometry (IM-MS) that the recently reported non-covalent dimer of ubiquitin (ncUbq) exhibits structural preferences and interfacial interactions that are most similar to that of K48-linked diUbq.

Servage *et al.* speculated that the basic residues surrounding the hydrophobic patch serve as hydration sites, resulting in two modes of interfacial stabilization: to promote occlusion of water from the hydrophobic interface and to reduce coulombic repulsion via water bridging.[63] A recent report suggests that charged residues serve as recognition sites for both mono- and pUbq by the proteosome prior to forming final hydrophobic interactions.[84] Arginine is one of three residues found with greater than 10% incidence in protein hot spots.[85] The proximity of the R42 and R72 residues from both ubiquitin subunits to the interface of "closed" K48-linked diUbq[34, 37, 53] and the

precedence for arginine participation in hot spots suggests that these residues would have a strong impact on the binding strength of the ncUbq subunit interface. An ionic hydrogen bond between a guanidinium ion and a proximal guanidine group would impart significant stabilization to the subunit interface, especially upon desolvation; whereas, if multiple guanidine groups are protonated, then coulombic repulsion may induce disassociation of the hydrophobic interface. The similarities between the ncUbq and K48-linked diUbq CIU patterns and the effects of pH portend the inclusion of the arginine residues as part of the ncUbq hot spot. In conclusion, CIU provides further evidence for the ncUbq hot spot to include the I44 hydrophobic patch and proximal R42/R72 arginine residues.

3. ESI-IM-MS AND COLLISION INDUCED UNFOLDING PROVIDES INSIGHT INTO THE LINKAGE DEPENDENT NON-COVALENT INTERACTIONS OF DIUBIQUITIN IONS

3.1. Introduction

Many biological processes are attributable to specific protein-protein interactions, in fact the majority of proteins function primarily as a subunit in a larger protein complex rather than as a single entity; for example, in the yeast cell, rough estimates suggest that the average protein may participate in 3-10 interactions with other binding partners.[1] Characterizing an interactome is challenging, particularly due to the dynamic and often transient nature of higher order structures. Electrospray ionization ion mobility mass spectrometry (ESI-IM-MS) has established widespread applicability for evaluating the conformational preference of biological molecules.[11, 86-88] IM-MS is capable of rapid characterization of heterogeneous conformational mixtures via separation of ions based on their three-dimensional shape and charge, *i.e.* their ion-neutral collision cross section (CCS). MS, tandem MS, and IM-MS have been used with moderate success for the characterization of protein complex identities and quaternary structure.[6, 8, 89-92] More recently, new applications of gas-phase activation methods have been applied to the characterization of complex quaternary structure, such as surface induced dissociation and collision induced unfolding (CIU).[6, 9, 14-15] In particular, CIU is the stepwise increase in the internal energy of the ion through collisional activation with a buffer gas and subsequent structural analysis using IM-MS. As such, CIU results in a

gas-phase unfolding fingerprint that is often unique and representative of the ion's noncovalent interactions. For example, CIU has been applied to examine differences in protein complex interfaces, intramolecular interactions, and lipid and anion binding induced stabilization.[7, 15-21]

Ubiquitin (Ubq) is a 76 amino acid protein with a highly conserved primary structure that has been studied extensively both in solution and as a solvent-free, gas-phase ion.[25, 30, 93-95] Despite transfer into the gas-phase, low charge states of Ubq ions are known to exhibit CCS values similar to that reported for the native-fold in solution.[28-30, 72, 96] Ubq displays diverse biological functionality as a tag, *i.e.* ubiquitylation, for cellular processes as defined by its oligomeric state; polyubiquitylation is a post-translational modification wherein a chain of Ubq subunits is covalently linked to a target molecule. Each Ubq subunit of a polyubiquitin (polyUbq) tag is linked through a specific isopeptide bond between the C-terminus of one subunit and an amino group of another subunit. The functionality of a specific polyUbq tag is encoded by its distinct quaternary structure and the resulting binding motif induced by differences in linkage site, chain length, and branching.[27, 36-40] Ubq contains eight amino groups (seven lysine side-chains and the N-terminus) that may form the covalent linkage, each encoding unique cellular functions. For example, K48-linked tetraUbq functions primarily as a tag for the proteosomal degradation of the target protein within the 26S proteasome complex.[36, 42] The ubiquitin-proteasome pathway is used to degrade misfolded proteins and antigens;[41] furthermore, the dysfunction of this pathway is implicated in the pathogenesis of several neurodegenerative diseases.[50-51] K11-linked polyUbq is linked to regulation of cell

division and mitosis,[32] whereas K63-linked tetraUbq is implicated in DNA repair,[45-46] inflammation,[47] immune response,[41] trafficking,[45] and antiviral response.[48] And both K48- and K63-linked polyUbq types have been implicated in the oncogenesis of several cancers and as such are a target for cancer therapy.[52] Overall, a more detailed understanding of the conformational preferences and noncovalent interactions defined by the covalent-linkage could aid in understanding its diverse functionality and potential applications.

Ubiquitin monomers (monoUbq) adopt highly stable, compact β-grasp fold structures, as characterized by NMR and X-ray crystallography,[24-25] and a high degree of this tertiary structure is maintained for each subunit of polyUbq, including the I44 (L8, I44, V70) and I36 (I36, L71, L73) hydrophobic patches.[27] Here, we examine four diUbq molecules linked through K6, K11, K48, and K63 to better understand the interfacial interactions induced by the different covalent linkage types; the most common linkage types in yeast cells are observed linked through the residues K48 (29.1%), K11 (28%), K63 (16.3%) and K6 (10.9%).[64] Under physiological conditions, K48-linked diUbq exists in equilibrium wherein conformers are stabilized by interactions of the I44/I44 hydrophobic patches or purely electrostatic interactions that expose the I44 patches for binding.[34, 37, 77] In more acidic environments, the electrostatic interface is reportedly preferred due to protonation of basic residues (K6, K11, R42, R72, and H68) in close proximity to the I44 patches and the resulting coulombic repulsion.[34, 53] Due to steric hindrance, K63-linked diUbq molecules cannot form interfacial interactions between the hydrophobic patches and instead occupy an ensemble of conformations including closed

conformations stabilized by electrostatic interactions.[40, 55] The conformational preferences of K6- and K11-linked diUbq are less well defined. Two solution phase conformers of K11-linked diUbq have been reported: one stabilized through I36/I36 interfacial interactions and the other through electrostatic interactions.[32, 56-57] A single crystal structure for K6-linked diUbq exhibiting I36/I44 interfacial interactions has been reported.[58]

We have recently reported that IMS alone is insufficient to differentiate the conformational preferences of K48- and K63-linked diUbq ions; however, collision-induced unfolding (CIU) supplies an added dimension capable of differentiating dissimilar noncovalent interactions.[97] We used CIU to evaluate the conformational differences not apparent in low-energy CCS profiles between the low charge states of the noncovalent Ubq homodimer, K48- and K63-linked diUbq ions. The results suggest that the conformational preference of K48- and K63-linked diUbq are differentiable using CIU; furthermore, noncovalent Ubq dimer ions exhibit similar noncovalent interfacial interactions and likely similar conformational preferences to that of K48-linked diUbq ions. Here we report an expanded investigation into the conformational preferences of K6-, K11-, K48-, and K63-linked diUbq using ESI-IM-MS, CIU, and solvent induced denaturation.

3.2. Experimental Methods

3.2.1. Sample Preparation

K6-, K11-, K48- and K63-linked diubiquitin were purchased from R&D Systems Inc. (Minneapolis, MN, USA). All were used without further purification. Each was dissolved in 18 MΩ water (Barnstead Easy Pure II, Thermo Scientific) and stored at -20°C for later use. All solutions were prepared with a final concentration of 10 μM in either 99.9/0.1% (v/v %) water/formic acid or 49.9/50/0.1% (v/v %) water/methanol/formic acid.

3.2.2. ESI-IM-MS and CIU Analysis

ESI-IM-MS spectra were acquired using a Waters Synapt G2 HDMS mass spectrometer (Manchester, UK). Instrument conditions were chosen to minimize instrumental heating: sample cone, 10V; extraction cone, 1V; trap bias, 25 V; API gas flows, off; helium cell flow rate, 200 mL/min; IMS nitrogen flow rate, 60 mL/min; TWIMS wave height, 20V; TWIMS wave velocity, 300 m/s.[72] CCS values were calibrated as previously described using reported values for acid and acetonitrile denatured ubiquitin, cytochrome c, and myoglobin.[78] All CCS profiles were normalized to the most abundant feature.

Different collision energies for CIU were imparted by changing the voltage drop between the exit of the quadrupole and the entrance to the TWIG-trap region filled with the collision gas argon. Note that a 5 V drop was necessary to maintain transmission through the trap and transfer regions and will be referred to as low collision energy. Reported lab-frame collision energies were calculated as the product of ion charge and

acceleration voltage. CIUSuite was used to assemble all CIU heat maps from IM-MS spectra; the "compare" function of CIUSuite was used to produce difference plots, used to draw attention to differences in CIU heat maps, and to produce RMSD values, used to summarize those differences.[20] The MOBCAL trajectory method was used to calculate theoretical CCS values from PDB files.[80,81]

3.3. Results and Discussion

3.3.1. Charge-Induced Unfolding of DiUbq Ions

Figure 3.1 shows the full ESI-IM-MS mass spectra and CCS profiles acquired using instrument conditions that minimize collisional activation to preserve more native-like conformations[72] for K6-, K11-, K48-, and K63-linked diUbq acquired from 99.9% water and 0.1% formic acid. All ions discussed throughout the paper are charged only through differences in protonation; therefore, ions of the form $[diUbq + nH]^{n+}$ will be abbreviated as $diUbq^{n+}$ for the remainder of the text. The charge state distributions observed of all four diUbq types from water/formic acid exhibit a narrow distribution of high abundance, low charge states (10 – 11+) and a broad distribution of low abundance, high charge states (13 – 25+). Note, however, that the abundances of each charge state differ for the different linkage sites of diUbq.

It has been shown that ESI-MS charge state distributions can be correlated to protein conformational preference.[98-99] That is, the charge state of a protein in the ESI mass spectrum is related to the solvent accessible surface area (SASA), as related to

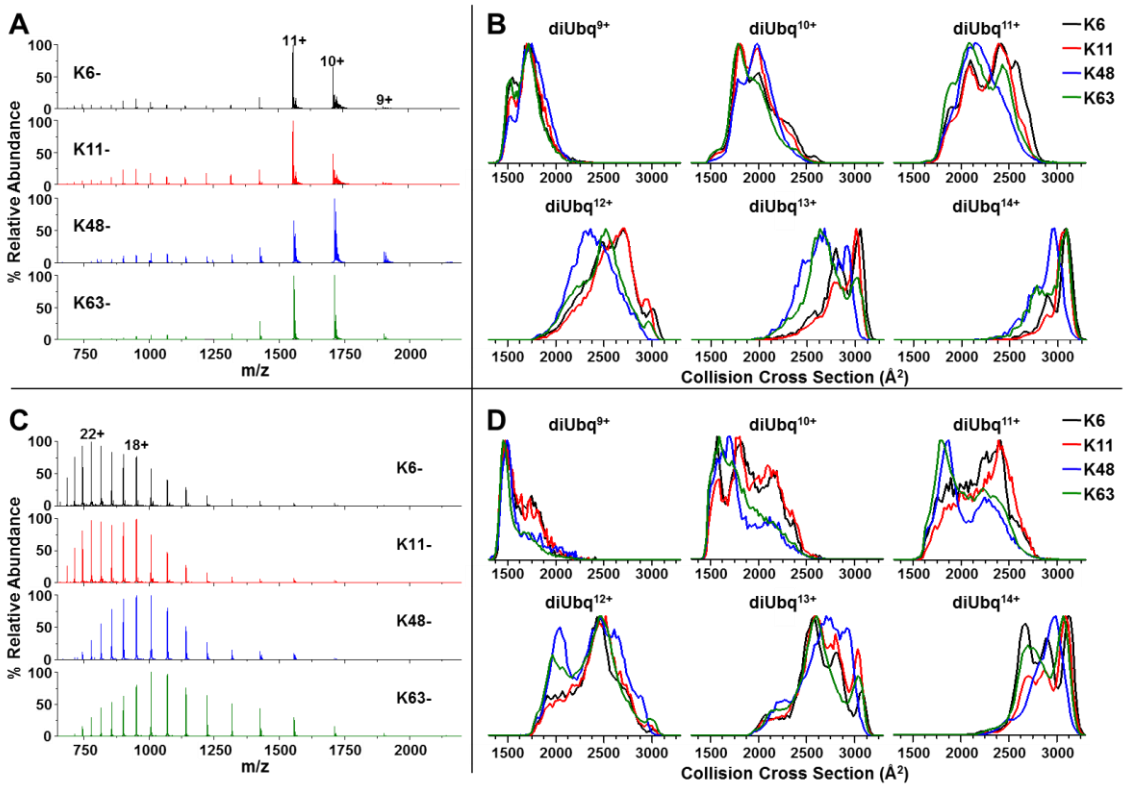

Figure 3.1. (A,C) Full mass spectra and (B,D) CCS profiles acquired with minimal collsional activation for K6- (black), K11- (red), K48- (blue), and K63- (green) linked diUbq acquired from (A,B) 99.9% water and 0.1% formic acid and (C,D) 50% methanol, 49.9% water and 0.1% formic acid. Select charge states are labelled.

solvent exposure of basic/acidic residues and the presence of intramolecular interactions.[100-102] Under acidic conditions, monoUbq produces a narrow distribution of low charge states centered around the Ubq^{7+} ion and a low abundance of higher charge states, which suggests retention of native-like states, but the observed higher charge states, IMS CCS profiles, and radical-directed fragmentation experiments provide evidence for a small population of unfolded conformers.[30, 103] The mass spectra acquired for all four diUbq linkage types from water/formic acid illustrate similar behavior,

suggesting retention of native-like conformations (**Figure 3.1A**). Note, however, that the abundances of the charge states differ for the different linkage sites of diUbq, suggesting differing exposure of basic residues owing to differences in conformation or intramolecular bonding. K63- and K48-linked diUbq in particular populate on average lower charge states than do K6- and K11-linked diUbq. This finding is consistent with results reported by Lee *et al.*; *viz.* complexation of the K6 or K11 side-chains of monoUbq by host-guest chemistry destabilizes the native conformation and induces preference for higher charge states.[104]

The CCS profiles of diUbq ions (**Figure 3.1B**) indicate sensitivity to the charge state of the ion and to the linkage site when higher charge state ions are sampled; however, the CCS profiles of $diUbq^{9+}$ ions are relatively narrow for all linkage types and suggest two conformational families: ~1500 $Å^2$ and 1750 $Å^2$. The larger of the two CCS values is similar to the theoretical CCS values of K48-linked diUbq reported previously (1780 $Å^2$ for the "closed" conformation PDB 2PEA, 1816 $Å^2$ for the "open" conformation PDB 3NS8),[97] suggesting that these ion populations retain much of the solution phase structure. Furthermore, K63-$diUbq^{9+}$ is not observed populating an open conformation (calculated CCS of 2086 $Å^2$, PDB 2JF5). The smaller of the two CCS values was previously defined as that of acid-induced molten globule conformations through comparison with CCS profiles acquired from buffered solution.[97] The MOBCAL calculated theoretical CCS values for diUbq structures reported in the PDB are 1829 $Å^2$ and 1845 $Å^2$ for K6- and K11 -linked diUbq, respectively (PDB structures 2XK5, 2XEW, respectively). The percent difference between these structures and those

reported for K48-linked diUbq is approximately 3%; consequently, the inability to differentiate K6-, K11-, and K48-linked conformations using IM-MS is unsurprising.

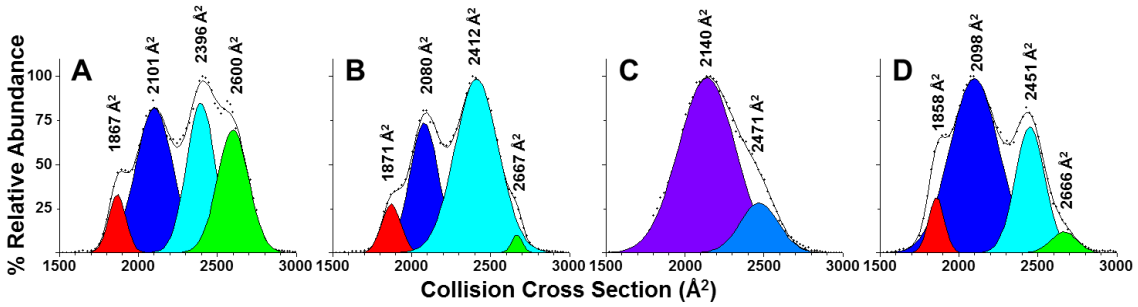

Figure 3.2. Deconvolution of (A) K6-, (B) K11-, (C) K48-, and (D) K63-diUbq^{11+} CCS profiles. The raw data is represented as data points, the cumulative fit is represented as a black line, and the fitted peaks are filled such that like colors depict fit peaks.

The CCS profiles of the higher charge states shift to larger CCS values suggesting increasing degrees of gas-phase unfolding due to their increasing coulombic repulsion and lab-frame collision energies. The diUbq^{10+} and diUbq^{11+} ions of all four linkage types exhibit broad distributions with distinct conformational populations. Peak deconvolution of diUbq^{11+} ion CCS profiles is shown in **Figure 3.2**. The CCS profiles of K6-, K11-, and K63-diUbq^{11+} ions each demonstrate four broad conformational families where CCS centroid values vary less than 3% for each linkage type; the primary difference between the 3 linkage types is the relative abundance of the different conformational families. The K48-diUbq^{11+} distributions are better represented with a fit that involves two more broadened peaks with CCS centroid values shifted relative to the other linkage types. The CCS profiles of diUbq^{12+} ions are still broad, but relatively

featureless; however, the degree of unfolding varies relative to linkage site. The majority of K6- and K11-diUbq^{13+} ions populate a narrow distribution of extended conformers; whereas, the K48- and K63-diUbq^{13+} ions retain a broad distribution of ions with largely intermediate CCS values. diUbq^{14+} ions of all linkage types populate primarily narrow CCS distributions of extended conformers that likely represent gas-phase equilibrium conformations.

3.3.2. Solvent Induced Denaturation of DiUbq

Addition of >40% methanol to acidic solution (pH ~ 2), monoUbq is known to populate the "denatured" A-state conformation, wherein part of the N-terminal portion of the β-sheet is retained, but the rest of the structure is in a flexible conformation with a high degree of α-helical character.[24, 105-107] The mass spectra acquired of monoUbq exhibit a broad distribution of high charge state ions consistent with the increased SASA.[30, 94] The calculated CCS for the A-state of monoUbq is larger than that of the N-state, and experimental CCS profiles of monoUbq are consistently shifted to larger CCS when acquired from methanolic solutions with low pH.[30, 96, 108] **Figure 3.1C** and **Figure 3.1D** show the full ESI-MS mass spectra and CCS profiles, respectively, for K6-, K11-, K48-, and K63-linked diUbq acquired from 49.9% water, 50% methanol, and 0.1% formic acid. The ESI mass spectra of diUbq acquired from these denaturing conditions indicate a broad distribution of high charge states, similarly suggesting increased SASA, but the spectra differ for each linkage type. K48-linked diUbq exhibits a more narrow charge state distribution centered at the 18+ charge state. K6- and K11-linked diUbq exhibit bimodal charge state distributions centered on the 18+ and 22+ charge states.

K63-linked diUbq exhibits an even broader charge state distribution, possibly trimodal, centered at the 17+ charge state. The presence of multiple broad distributions of high charge states for K6-, K11-, and K63-linked diUbq from the denaturing solution conditions suggests a high degree of conformational heterogeneity in solution. The distribution of charge states for K6- and K11-linked diUbq are significantly higher than those observed for K48- and K63-linked diUbq indicative of further increased SASA.

The CCS profiles of low charge state diUbq ions of all four linkage types acquired from acidic 50% methanol solution (**Figure 3.1D**) suggest that the ions adopt more compact conformers than those observed from acidic aqueous solution. This observed preference for compact conformers is contrary to the larger CCS observed for monoUbq under similar conditions suggesting the collapse of the ion's tertiary structure. Interestingly, the CCS of the more compact $diUbq^{9+}$ conformer observed from denaturing conditions is similar to that of the ~1500Å^2 $diUbq^{9+}$ conformer previously attributed to an acid-induced molten globule conformation. Thus, we attribute the more compact conformer observed from denaturing conditions to a collapsed, partially folded conformation likely possessing a high degree of α-helical character or a molten globule type conformation .

3.3.3. Gas-Phase Unfolding of DiUbq Ions

CIU is similar to gas-phase annealing, *viz.* collisional activation (unfolding) is followed by collisional cooling (thermalization) prior to IM separation; consequently, CIU provides information concerning the gas-phase potential energy surface *en route* to

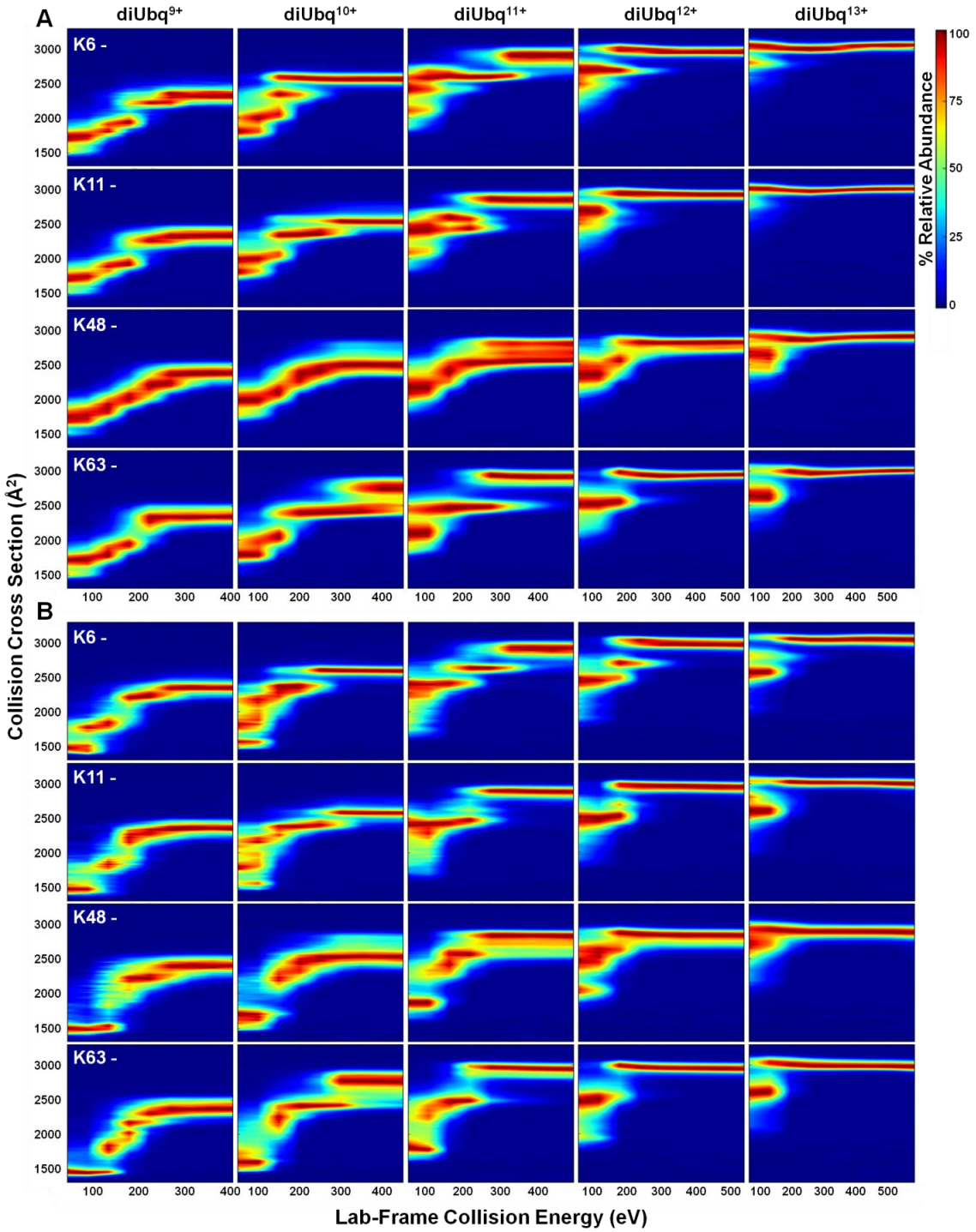

Figure 3.3. CIU heat maps for K6-, K11-, K48-, and K63-linked diUbq (top to bottom) with 9-13+ charge states (left to right) acquired from (A) 99.9% water and 0.1% formic acid and (B) 49.9% water, 50% methanol, and 0.1% formic acid.

the gas-phase equilibrium conformation as defined by their noncovalent interactions. CCS profiles for the four linkage types of diUbq were acquired with increasing collisional activation and assembled into heat maps, or CIU fingerprints, to illustrate the changing conformational preference of the protein en route to the gas-phase equilibrium conformation (**Figure 3.3**, see **Figure A.1-A.4** for raw CCS profiles used to assemble CIU plots). Overall, the CIU fingerprints of each linkage type acquired under N-state conditions differ noticeably from one another (**Figure 3.3A**). These differences are highlighted by the use of difference plots (**Figure A.5-A.8**) and calculated RMSD values (summarized in **Figure 3.4**).

The RMSD values and difference plots indicate that the CIU of K48-linked diUbq differs most significantly from the other linkage types due to the absence of distinct unfolding intermediates and generally more compact extended conformers than those observed of the other linkage types. Specifically, the CIU fingerprints of lower charge states of K48-linked diUbq indicate that the ions undergo gradual unfolding until the late stages of the unfolding process, whereas the CIU profiles of K6-, K11-, and K63-linked diUbq indicate interconversion between distinct intermediate conformers. Furthermore, K48-diUbq^{10+}, diUbq^{11+}, and diUbq^{12+} populate three distinct extended conformers, most apparent of the 11+ ion, that remain stable until fragmentation. An exception to the exclusively large RMSD values observed for K48-linked diUbq ions are the large RMSD values observed for K63-diUbq^{10+} ions due to large differences in the late stages of unfolding. The most extended conformer of K63-[diUbq + 10H]$^{10+}$ is

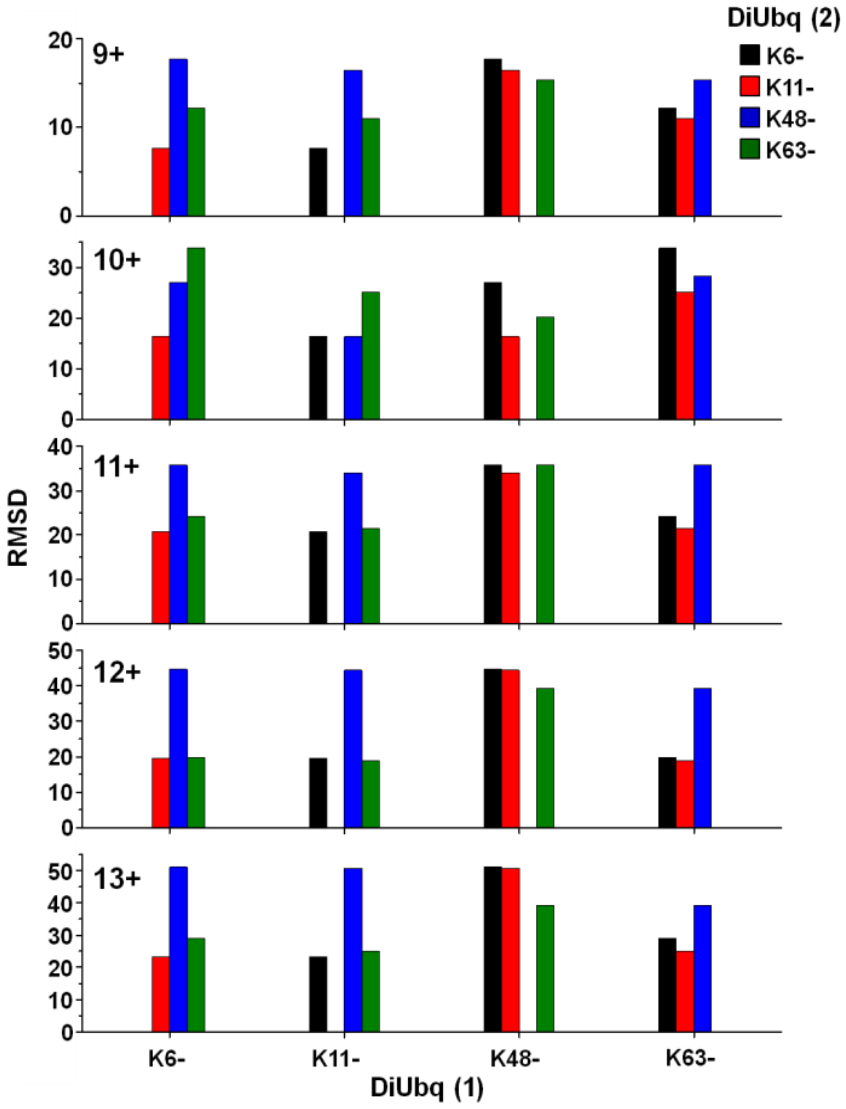

Figure 3.4. Root-mean-square deviation values calculated for two CIU heats maps, DiUbq (1) minus DiUbq (2). For example the blue bar in the 9+, K11 cluster represents the RMSD value for K11- and K48-diUbq^{9+} ion CIU profiles.

observed only after a high degree of collisional activation and in much higher abundance than a similar conformer observed of K11- and K48-diUbq^{10+} (see **Figure A.1** for details). The distinct unfolding intermediates of K6-, K11-, and K63-linked diUbq ions exhibit similar CCS values to one another but differing stabilities. This suggests that

these ions populate similar conformational populations en route to the gas-phase equilibrium structure. This observation is consistent with that reported by Eschweiler *et al.* wherein collisional activation of albumin homologues populate very similar conformational unfolding intermediates, but the stability of each varied with differing 1^{o} structure.[109]

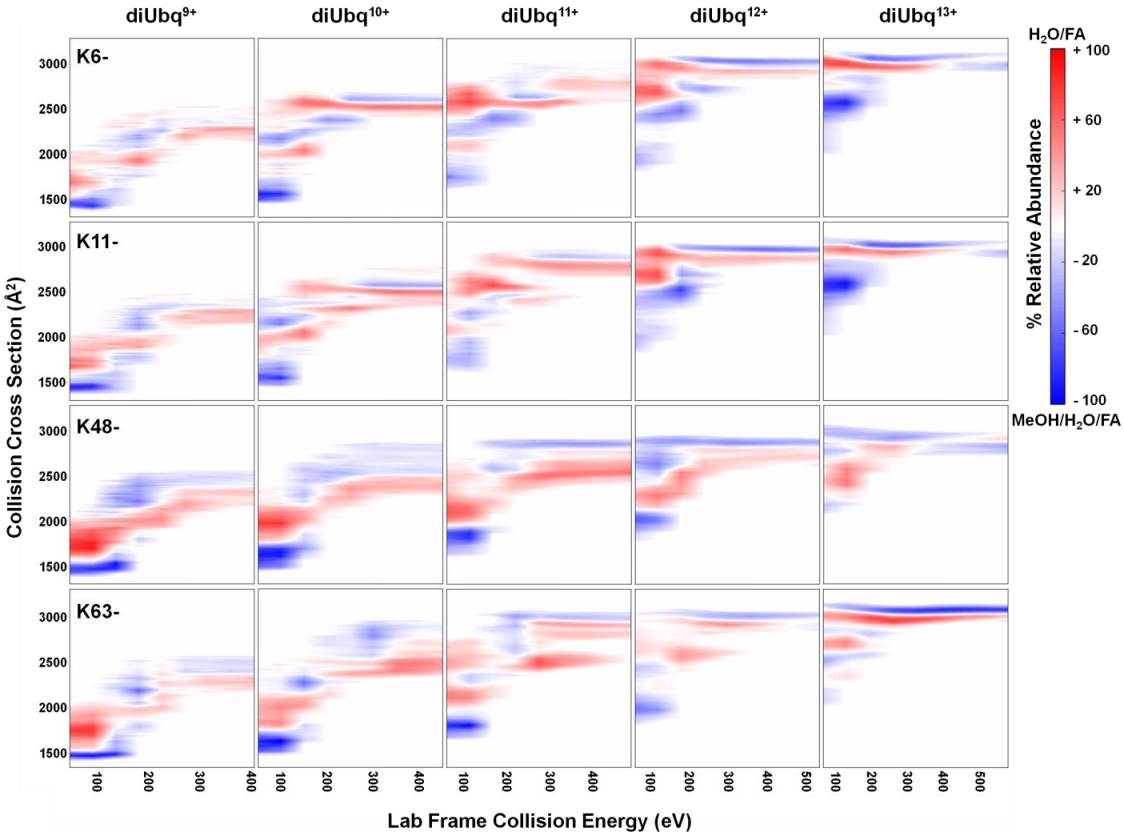

Figure 3.5. Difference plots calculated using CIUSuite, where the CIU heat maps of diUbq ions acquired from 50% methanol/49.9% water/0.1% formic acid (blue) are subtracted from the CIU profiles acquired from 99.9% water/0.1% formic acid (red). Note that the difference plots for all other charge states can be found in the Supporting Information.

The CIU fingerprints of the diUbq ions acquired from denaturing conditions bear striking differences from those acquired from "native" conditions, but also interesting similarities in the late stages of unfolding (**Figure 3.3B**). These observations are demonstrated most vividly by difference plots (see **Figure 3.5**). As discussed previously, the CCS profiles of the "denatured" diUbq ions are shifted to lower CCS than those acquired from "native" conditions. Interestingly, the CIU profiles of K48-linked diUbq ions acquired from the denaturing conditions exhibit the distinct unfolding intermediates observed of the other linkage types in "native" conditions. This suggests that the gradual unfolding observed previously is characteristic of the native K48-linked diUbq solution-phase structure. The CCS profiles of all diUbq linkage types acquired from "native" and "denatured" conditions converge to similar conformational families upon application of high collision energies. This provides an indication as to when all aspects of the solution-phase "conformational memory" is lost in favor of gas-phase equilibrium conformations. The CIU profiles of K48-linked diUbq acquired from both solution conditions are increasing similar with increasing charge state. Oddly, the gas-phase equilibrium conformers of the higher charge states of K6-, K11-, and K63-linked diUbq ions acquired from the denaturing solution conditions adopt a smaller CCS than those acquired from more native conditions.

Shi *et al.* have previously reported that the relative abundances of different extended conformers of monoUbq are influenced by the addition of methanol.[108, 110] The addition of methanol appears to have a similar influence on the conformational preference of extended K48-diUbq^{11+} conformers; specifically, the more compact of the

extended conformers is less preferred. The most likely explanation for these differences in gas-phase equilibrium conformation would be differences in charge location as defined during the ESI process. The residues K6, K11, and K63 are located near the N- and C-termini, meaning fully extended conformations of diUbq covalently linked through those residues are nearly linear. Contrarily, K48 is located near the center of the sequence, meaning a fully extended conformation of K48-linked diUbq would resemble a "T" shape. Consequently, differences in charge location would more likely result in multiple extended conformations upon collisional activation.

3.3.4. Unraveling Differences in Noncovalent Intramolecular DiUbq Interactions

The effect of collisional activation on the conformation of multidomain proteins is oft-debated, mainly due to observed asymmetric charge partitioning between dissociated subunits. Wysocki *et al.* suggest that asymmetric charge partitioning is evidence that collisional activation results in subunit unfolding,[14] whereas Loo and Loo posit that charge state differences may be a function of salt bridge rearrangement such that collisional activation may still result in disassociation of the subunit interface.[111] Eschweiler *et al.* have recently used chemical probes to monitor the sequential unfolding of albumin domains; distinct unfolding intermediate transitions were correlated with the loss of subunit bound ligands suggesting sequential subunit unfolding upon collisional activation.[109] We have previously suggested that the subunit interface of K48-linked diUbq ions persists until the late stages of unfolding via comparisons with noncovalent Ubq dimer unfolding and disassociation energies.[97]

The specific gas-phase unfolding pathway of monoUbq has been previously discussed by Skinner *et al.* using electron capture dissociation experimental results[69] and Chen *et al.* using molecular dynamics simulations.[72] The N- and C-terminal β-strands located in the center of the β sheet structure are in particular only weakly stabilized in the gas-phase, meaning collisional activation likely results first in the loss of the five stranded β-sheet structure. This "weakness" provides much insight into the unfolding patterns observed of the diUbq ions. The residues of the I44 patch are located on three individual β-strands, including both the N- and C-terminal; consequently, any subunit interfacing with the other via the I44 patch would benefit from significant stabilization of the β-sheet. The residues from the I36 patch are located on the C-terminal β-strand, but not on the N-terminal β-strand, such that participation of the I36 patch in the subunit interface will have no effect on the stability of the β-sheet. K48-linked diUbq preferentially forms I44/I44 interfacial interactions unless coulombic repulsion of R42 and R72 in close proximity to the I44 hydrophobic faces induces the preference for electrostatic interfacial interactions.[34, 37] Based upon the aforementioned possible influence of I44 patch interactions on the stability of each subunit, it would be expected that an I44/I44 interface would impart dramatic stabilization of both Ubq subunits. We have previously reported that the unique gradual unfolding observed in the CIU fingerprints of K48-diUbq^{9+} and diUbq^{11+} are indicative of I44/I44 hydrophobic interfacial interactions; furthermore, the R42 and R72 residues play an important role in stabilization of the subunit interface.[63, 97] The observed gradual unfolding of the

additional charge states further supports the differentiation of the K48-linked diUbq subunit interface as unique from that observed of other linkage sites.

As noted repeatedly, K6-, K11-, and K63-linked diUbq ions demonstrate substantial CIU similarity. With increasing collision energy, each undergoes conversion between distinct intermediates en route to the most extended conformations. As discussed previously, K63-linked diUbq is stabilized exclusively by electrostatic interactions; consequently, the most obvious conclusion that can be drawn from the similarity between the CIU fingerprints of K6-, K11-, and K63 linked diUbq is that the lower charge states of all three linkage types exhibit electrostatic interfacial interactions. The gas-phase stability of an electrostatic interface would depend greatly on the number of salt bridges and ionic hydrogen bonds formed between the subunits resulting in differing stabilities, dependent on linkage site and charge state. Thus, differences in the unfolding pathway could be the product of different available electrostatic interactions induced by the changing proximities of charge groups induced by the covalent linkage site. A solution phase structure of K11-linked diUbq is reported that demonstrates electrostatic interfacial stabilization; however, another reports an I36/I36 interface.

Both K6- and K11-linked diUbq have reported conformations utilizing the I36 hydrophobic patch for interfacial interaction. The crystal structure of K6-linked diUbq, specifically, was reported to exhibit an I36/I44 interface, where the I36 patch of the proximal Ubq subunit interacts with the I44 patch of the distal Ubq subunit. Thus it would be expected that the proximal subunit would unfold upon collisional activation due to the instability of its β-sheet, followed by the unfolding of the distal subunit. Both

subunits of K11-linked diUbq would be expected to unfold upon collisional activation due to the preference for an I36/I36 interface. As such, K6- and K11-linked diUbq would be expected to demonstrate significantly different unfolding pathways. Consequently, the resemblance between the K6-, K11-, and K63-linked diUbq CIU fingerprints could be attributed to two scenarios: all three adopt electrostatic interfacial interactions, or the unfolding pathway of interfacial interactions involving I36 is comparable to that demonstrated by K63-linked diUbq ions.

3.4. Conclusions

Here we demonstrate the use of ESI-IM-MS and CIU to probe the differences in noncovalent intramolecular interactions responsible for the conformational heterogeneity of the most abundant covalent linkage types of diUbq. The ESI mass spectra of each linkage type suggest that the ions sampled are "native-like" in conformation. Furthermore, the CCS profiles of $diUbq^{9+}$ ions are centered on a CCS similar to theoretical CCS values calculated from PDB structures; however, because the CCS of the "native-like" conformers are within the error of the IMS experiment, solution-phase and gas-phase denaturation provides the additional information necessary to differentiate the conformational differences induced by the covalent linkage site.

Unfolding upon removal of solvent, driven by Coulomb repulsion as well as collisional activation, shows that K48-linked diUbq is unique in its conformational preference and gas-phase stability. We posit that this difference is the result of added stabilization of the β-sheet structure induced by I44/I44 interfacial interactions. Solvent

induced denaturation disrupts the hydrophobic patches apparent in the native fold of the subunits and reduces the burial of hydrophobic side-chains within the interior of the structure; therefore, any remaining noncovalent interactions are unlikely to involve hydrophobic interactions. Upon solvent induced denaturation, the gradual unfolding observed of K48-linked diUbq ions is no longer observed in favor of distinct unfolding intermediates. Reported K6- and K11-linked diUbq structures suggest interfacial interactions either involving the I36 patch or electrostatic interactions. Due to the inaccessibility of hydrophobic patch interactions induced by covalent linkage through K63, electrostatic interactions are preferred for K63-linked diUbq interfacial interactions. K6-, K11-, and K63-linked diUbq ions demonstrate very similar unfolding pathways including distinct unfolding intermediate conformers very similar in CCSs but differing in relative stabilities. Therefore, the similarities between the K6-, K11-, and K63-linked diUbq CIU profiles could be indicative that K6- and K11-linked diUbq ions also adopt primarily electrostatic interfacial interactions. However, interfacial interactions involving the I36 patch would not lead to substantial stabilization of the weakly bound β-sheet structure and thus such structures may unfold in a similar manner to those of K63-linked diUbq ions. Overall we have shown that ESI-IM-MS and CIU can provide a wealth of information concerning the noncovalent interactions stabilizing the conformational preference of diUbq ions; however, as with many IMS experiments, molecular dynamics simulations or solution-phase NMR would be excellent complementary techniques to provide more detailed atomistic information.

4. PRESERVING MORE "NATIVE-LIKE" CONFORMATIONS OF UBIQUITIN IONS IN THE GAS-PHASE VIA CHLORIDE ADDUCTION*

4.1. Introduction

Native electrospray ionization mass spectrometry (nESI-MS) has evolved as an important technique for structural biology; in particular, the integration of ion mobility (IM) with nESI-MS, *i.e.*, nESI-IM-MS, has provided an approach complementary to other structural MS techniques such as hydrogen/deuterium exchange (HDX) and chemical foot-printing. The contribution of IM to structural characterization lies in the ability to separate ions on the basis of size-to-charge in the form of ion-neutral collision cross section (CCS) measurements, *i.e.*, the 3-dimensional shape of the ion, which can then be related to the protein tertiary structure. An unresolved issue related to the IM CCS measurement is whether the 3-D shape of the gas-phase ion can be related to the solution-phase conformation; stated differently, "…for how long, under what conditions, and to what extent, can solution structure be retained without solvent?"[65] Current opinion in the field suggests that in the final stages of desolvation, the biomolecule experiences steps that are similar to "freeze-drying",[66] *i.e.*, the evaporative cooling inherent to desolvation of the ESI nanodroplet provides a route for capturing ions that retain solution-phase conformer distributions,[63, 67-68] preserving intramolecular

* Reprinted with permission from Wagner, N. D.; Kim, D.; Russell, D. H., Increasing Ubiquitin Ion Resistance to Unfolding in the Gas Phase Using Chloride Adduction: Preserving More "Native-Like" Conformations Despite Collisional Activation. *Anal. Chem.* **2016,** *88* (11), 5934-5940.Copyright 2016 American Chemical Society.

interactions that stabilize the protein and inhibit unfolding.[69] Recent studies also illustrate that solvent-free "solution-phase" conformations may revert to a gas-phase equilibrium structure if the ions experience collisional activation as they traverse the instrument.[71-72]

Protein dynamics, activity, and function are closely correlated to the protein's three-dimensional structure which varies with the local environment, specifically solvent polarity, pH, and the presence of salts. The latter has spawned an entire field of research focused on probing the intricacies of salt effects on protein conformation, *i.e*. the Hofmeister series.[112-117] Anions generally exhibit the strongest influence on the structure of a protein owing to their high affinity for the protein backbone.[112, 116-118] An exhaustive survey of the protein database yielded over 6000 proteins and protein complexes that exhibit a "halide motif", *i.e*. "the interaction motif of a non-bonded halogen ion with two or more electrophiles simultaneously." [119] Many of these examples of "halide motifs" result in the stabilization of the protein or protein complex. Furthermore, anions have been shown to induce refolding of misfolded proteins and protein complexes,[120-121] and addition of a salt to an acid-unfolded protein induces refolding to a compact molten globule conformation.[120]

In the field of mass spectrometry, the adduction of anions to positively charged peptide and protein ions was first noted by Chait *et al.*, who suggested that anions adducted to the protein dissociate via loss of the neutral conjugate acid; this manifests in the mass spectrum as a lower average charge.[122] It has recently been reported using IM-MS that anion adducted protein ions can result in the preference for more compact

conformations.[73] More recently, anion adduction to protein complexes has been shown to result in the stabilization of quaternary structure, whereby loss of the adducted anions and the concurrent partitioning of internal energy results in formation of complex ions having lower E_{int}.[74-75]

Here, we use collisional activation to expound on the retention of more native-like protein conformations in the gas-phase upon chloride adduction. Ubiquitin (Ubq) has been extensively studied in both the solution as well as the solvent-free, gas-phase ion.[25, 95] Furthermore, it has been previously reported that the addition of different salts to Ubq at neutral pH results in significant stabilization via anion binding.[123] Using mild ESI conditions Ubq forms a large number of chloride adduct ions, thus it is an excellent model system for studies of the effects of chloride adduct ions on the protein conformer preference. Low charge states of Ubq ions formed by ESI from both neutral and acidic solutions are known to have CCS values similar to that of the native fold in solution,[28-30] and the effects of E_{int} on the conformer preference has been investigated using both ESI IM-MS and molecular dynamics simulations.[29, 72, 96] The addition of methanol to acidified solutions of Ubq is known to induce formation of the denatured A-state.[94, 96, 105, 124-125] Here, methanol was used to investigate the effect(s) of differing solution-phase protein structure(s) on the retention of chloride adducts. The results clearly show that chloride adducts greatly increase the preference for more compact conformers. Specifically, the direct interaction of chloride with the protein results in significant stabilization of a more native-like protein conformation.

4.2. Experimental Methods

4.2.1. Sample Preparation

Bovine ubiquitin (Sigma-Aldrich, St. Louis, MO, USA) was dissolved in 18 MΩ water (Barnstead Easy Pure II, Thermo Scientific) and desalted using a Millipore centrifugal filter; after dilution, the final protein concentration was 10 μM. Each solution contained 0.1% Certified ACS Plus Grade hydrochloric acid (~12.6mM, Fisher Scientific, Pittsburg, PA, USA) in order to supply chloride anions in excess. HPLC grade methanol was purchased from EMD Millipore (Billerica, MA, USA).

4.2.2. ESI-IM-MS

A Waters Synapt G2 HDMS instrument (Manchester, UK) was used for all ESI IM-MS experiments, and all results reported were acquired in the positive ion mode. As previously described, instrument conditions can be tuned to preserve ions having low internal energy (E_{int});[72] cooler instrument conditions are essential for retaining Ubq-chloride adducts. The instrument conditions used were as follows: sample cone 10 V, extraction cone 1 V, trap bias 25 V, helium cell flow rate 200 mL/min, IMS nitrogen flow rate 50 mL/min. The wave height and wave velocity in the TWIMS drift cell were 20 V and 600 m/s, respectively.

CCS values were calibrated as previously described.[78] Theoretical isotope distributions were calculated using Data Explorer Version 4.3. The molecular formula of each protein-adduct ion was determined and used to calculate theoretical isotope distributions with which to verify the identity of each ion.

4.2.3. CID and CIU-IM-MS

Collisional activation experiments were performed via collisions with background gas (argon) in the TWIG trap by changing the voltage drop between the end of the quadrupole and the beginning of the trap, as was described previously; note that a 5 V difference was necessary for ion transmission and, as such, was the smallest voltage drop used. Collision voltages are reported rather than collision energies because the number of collisions involved in the activation step is unknown. Two distinct collisional activation experiments were used. The first was performed following quadrupole mass selection of a chloride adducted Ubq ion population; the mass selected ions were collisionally activated, and the resulting mass spectrum and mobility profiles were acquired and analyzed for collision-induced dissociation (CID product ions) and collision-induced unfolding (CIU). The second collisional activation experiment involved no mass selection in the quadrupole, whereby all ions produced via ESI were transmitted, activated by collisions, and the post-activation ions were analyzed via TWIMS and MS with particular interest paid to CIU.

4.3. Results and Discussion

Recent molecular dynamics simulations have shed much light on how the presence of counter anions impacts a biomolecule's conformational preference during and after the desolvation process. Consta *et al.* report the effect of Na^+ and Cl^- on the final charge state of a polyethylene glycol polymer; Cl^-/Na^+ clusters form, but only Na^+ remains adducted to the polymer.[126] In terms of biomolecules, Konermann and

coworkers have reported the effect of Na^+ and Cl^- on protein structure throughout desolvation.[127] Collectively, these studies show how 1) ions remain adducted to a biomolecule despite desolvation, 2) a protein's structure changes very little throughout desolvation despite the presence of ionic adducts, 3) anionic adducts are clustered around basic residues or cationic adducts, 4) Cl^- facilitates intramolecular non-covalent interactions, and 5) cationic adducts associate with acidic residues or Cl^- adducts. Here, the model protein Ubq will be used to discuss each of these findings using H_3O^+ and Cl^-, as well as elaborate on the effects of ion adduction after desolvation.

4.3.1. Ubq-chloride Adducts $[M + nH + xCl]^{(n-x)+}$ Are Observed Using nESI-MS

The ESI mass spectrum of acidified aqueous solutions of Ubq contains abundant ions of the type $[M + nH + xCl]^{(n-x)+}$. **Figure 4.1** contains selected regions of the mass spectrum showing Ubq ions produced from HCl acidified water (0.1%, pH < 2) and 60/40 (*% v/v*) methanol/water (0.1%, pH < 2). The formal charge states range from 5^+ to 13^+ (see **Figure 4.2** for full mass spectra). Abundant ions of the type $[M + nH + xCl]^{(n-x)+}$ are observed. For example, the signal at *m/z* 1714 corresponds to the $[M + 5H]^{5+}$ ion, and the signal at *m/z* 1721 corresponds to $[M + 6H + Cl]^{5+}$ ions, i.e. $[M + 6H]^{6+}$ ions plus a single Cl^- adduct resulting in an overall charge state of 5+. Ubq electrosprayed from HCl acidified methanol/water (60/40) solutions takes on more Cl^- adducts than when electrosprayed from HCl acidified water. For example, the most abundant adduct ions in the distribution of 5+ charge state ions from water are the $[M + 9H + 4Cl]^{5+}$, whereas the most abundant ions from the methanol/water solution are $[M + 10H + 5Cl]^{5+}$.

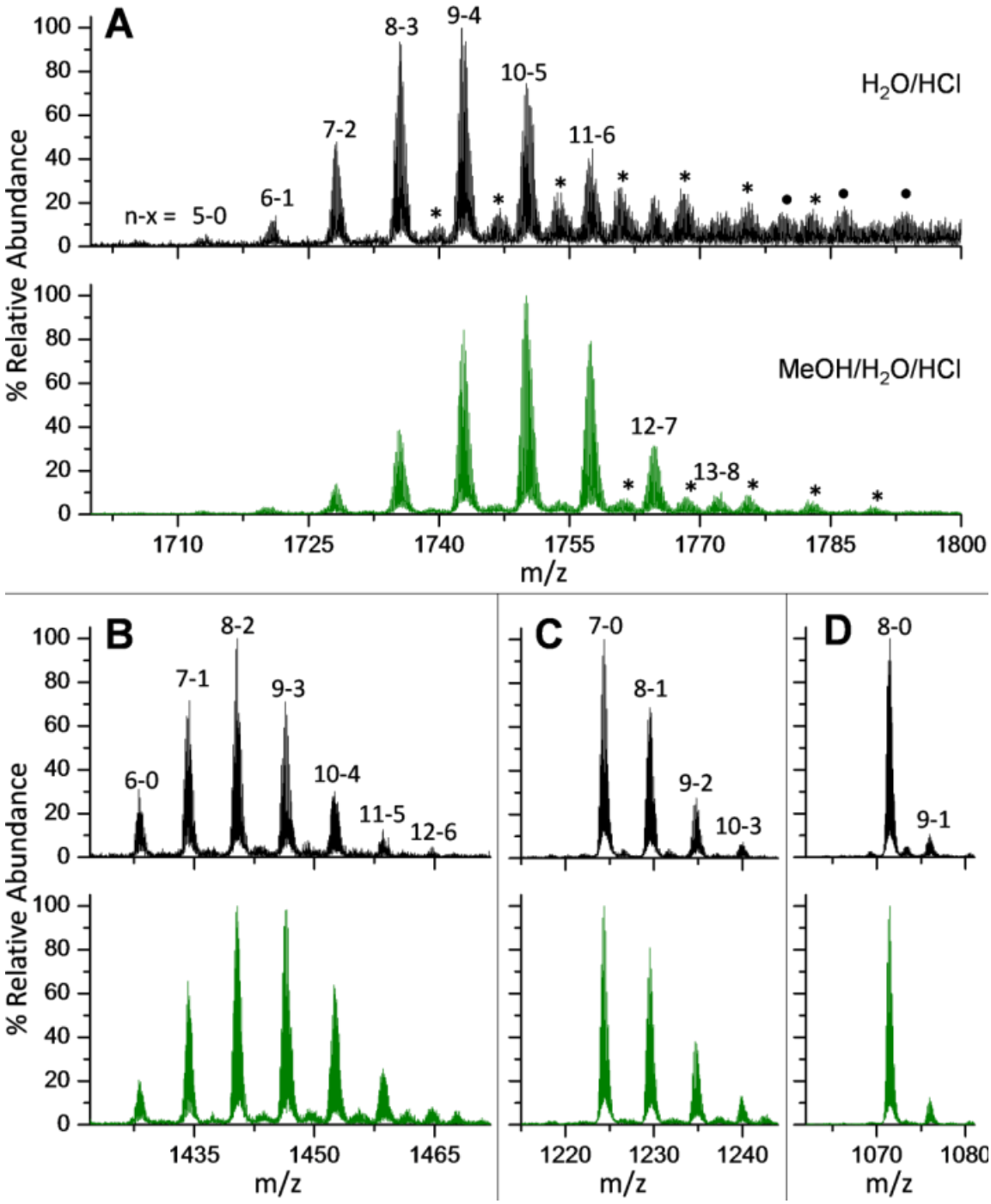

Figure 4.1. Selected regions of the ESI mass spectra of HCl acidified Ubq (0.1% HCl in 99.9% water (top black) and 60/40 methanol (bottom green)). The notation above the peaks denotes n and x; $[M + nH + xCl]^{(n-x)+,}$ n – x = 5, 6, 7, and 8, (A - D). The ions labeled with an asterisk denote ions containing both Cl- and water adducts. Reprinted with permission from [21.]

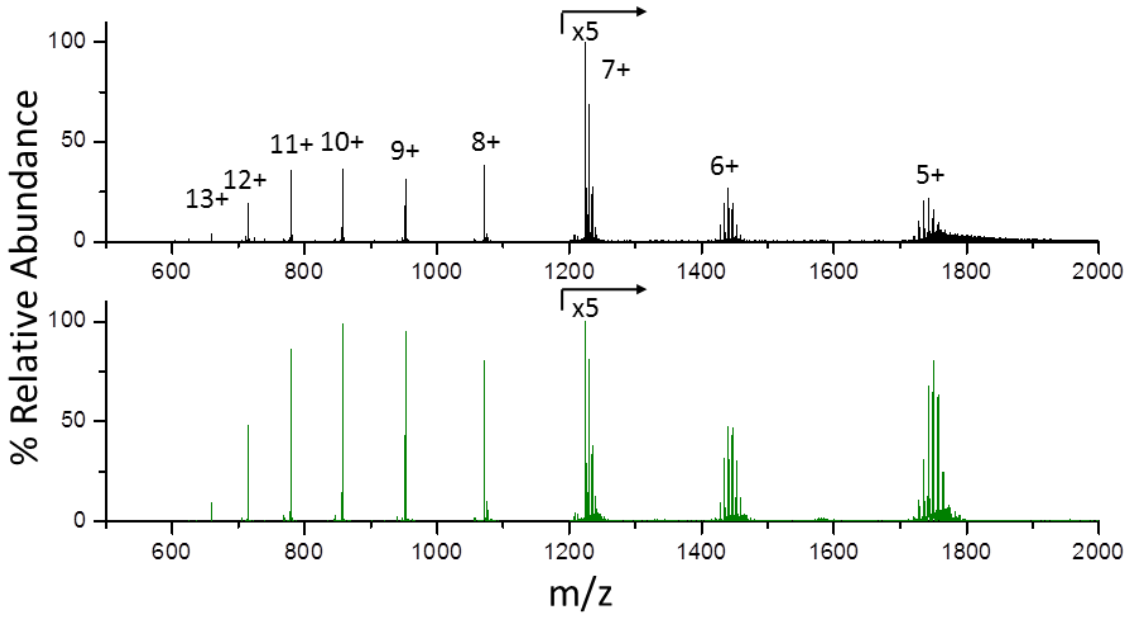

Figure 4.2 Full mass spectra of Ubq acquired from 99.9% water / 0.1% formic acid (top) and 60% methanol / 39.9% water / 0.1% formic acid (bottom). Note that the lower charge state ion abundances are attenuated due to the partitioning of the signals across multiple ion populations, *viz.* $[M + nH + xCl]^{(n-x)+}$ and $[M + nH + xCl + yH_2O]^{(n-x)+}$ ions. The ion signals with *m/z* greater than 1200 Da are amplified by five to illustrate the distribution of ion signals. Reprinted with permission from [21].

The effect of methanol on the solution phase structure of Ubq is well reported. Ubq is reported to occupy the A-state when in solution with greater than 40% methanol and a pH less than 2.[94, 105, 128] The A-state of Ubq exhibits significantly more solvent accessible surface area due to the overall lack of a defined tertiary structure, the result of which are more basic and polar sites exposed to the solvent, *i.e.*, more sites exposed that are amenable to Cl^- adduction. Therefore, it is not unexpected that Ubq ions retain more Cl^- adducts when electrosprayed from 60% methanol and a pH of 2.

4.3.2. $[M + nH + xCl]^{(n-x)+}$ Ions Exhibit More Compact Conformations Than $[M + nH]^{n+}$ Ions

Williams *et al.* have previously reported that intermediate charge states of protein ions that exhibit more extended conformations adopt more compact conformations upon anion adduction; however, no effects were reported for Cl^- adduction.[20] **Figure 4.3** contains the CCS profiles of all $[M + nH + xCl]^{(n-x)+}$ ions electrosprayed from water/0.1% HCl (black) and 60/39.9/0.1 (*% v/v/v*) methanol/water/HCl (green). As noted previously, Ubq ions populate three types of conformers – compact, intermediate, and extended – that fall in the range of CCS values of ~900 – 1000 $Å^2$, ~1050 – 1350 $Å^2$, and >1400 $Å^2$, respectively.[72] This same terminology will be used in the following discussion.

The CCS profiles of all $[M + nH + xCl]^{(n-x)+}$ ions electrosprayed from 60/40/0.1% methanol/water/HCl (**Figure 4.3,** green) are similar to those for water (black); however, there is a distinct shift in the centroid of compact conformers. Clemmer *et al.* have previously suggested that this shift is evidence for the so-called A-state of Ubq, which has been detected in solutions of acidified methanol/water with a pH>2.[96] Note that similar shifts for the compact conformer are observed for both 5+ and 6+ ion populations.

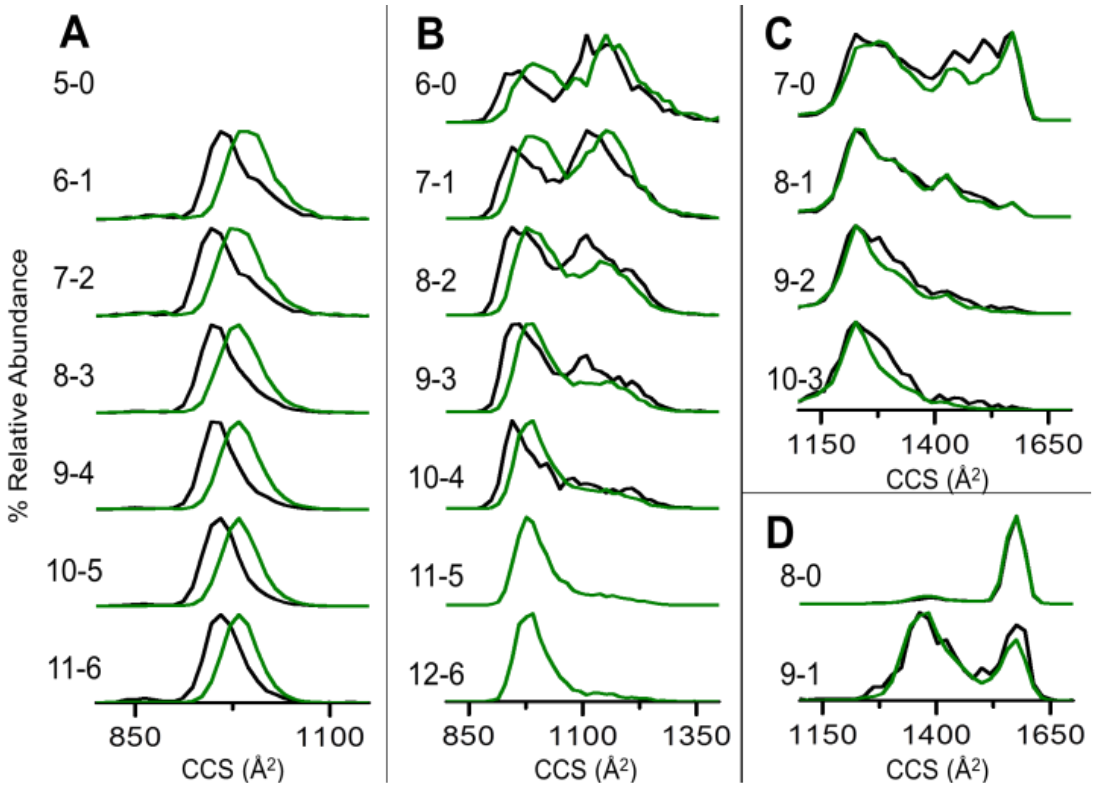

Figure 4.3. CCS profiles of [M + nH + xCl](n-x)+ ions from 0.1% HCl/99.9% water (black) and 60/40% methanol/water (green). The CCS profiles of A through D correspond to Ubq ions where n – x = 5, 6, 7, and 8, respectively. Reprinted with permission from [21.]

Chen *et al.* report instrument conditions at which the internal energy (E_{int}) of an ion can be minimized, thereby preserving more native-like conformers, using Ubq as an example.[72] Using instrument tuning parameters that minimize collisional heating, $[M + 6H]^{6+}$ Ubq ions exhibit CCS profiles that indicate solely compact conformers. Varying the instrument conditions results in depopulation of the compact conformer populations in favor of intermediate and extended conformers; the instrument conditions used in this experiment result in an identical CCS profile for $[M + 6H]^{6+}$ under the same conditions.[72] The $[M + 6H]^{6+}$ CCS profiles observed in this study are indicative of

relatively high E_{int}, whereas under the same instrumental conditions, the CCS profiles for $[M + nH + xCl]^{(n-x)+}$ ions clearly demonstrate an increased preference for more native-like conformer populations with the retention of increasing numbers of Cl^- adducts. Although compact conformers are not observed for $[M + nH + xCl]^{(n-x)+}$ ions where (n-x) = 7 or 8 regardless of Cl^- adduction, $[M + nH + xCl]^{(n-x)+}$ ions do exhibit significantly depopulated extended conformers. The CCS profile of the $[M + 7H]^{7+}$ ion population indicates that the ions adopt both intermediate and extended conformations, and retention of Cl^- adducts in the 7+ ion series results in an increased preference for intermediate conformers; the CCS profile of the $[M + 9H + 2Cl]^{7+}$ ion in particular indicates almost exclusively intermediate conformers.

The adduction of Cl^- to a positively-charged Ubq ion results in the reduction of the total positive charge on the protein. For example, $[M + 10H]^{10+}$ ions exhibit solely an extended conformation (see **Figure 4.4**), but the adduction of 5 Cl^- to produce 5+ ions results in a CCS profile with almost exclusively compact conformers. This extreme transition indicates a significant decrease in coulombic repulsion that would otherwise result in significant unfolding. Due to the charge reduction induced by the adduction of an anion, the most abundant $[M + nH + xCl]^{(n-x)+}$ ions are observed with low overall charge states.

It should be noted that $[M + nH + xCl]^{(n-x)+}$ ions could differ structurally from those produced from a solution with a different salt or without a salt; ion mobility may not have sufficient resolution to distinguish such similarly-sized proteins. In solution, the

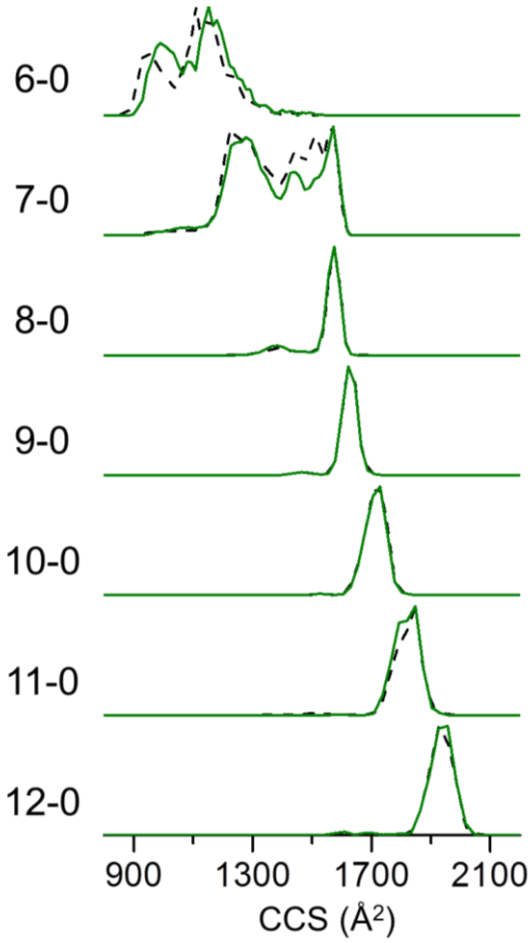

Figure 4.4. CCS profiles of $[M + nH]^{n+}$ ions using solution conditions of 0.1% HCl with 99.9% water (black dash) and 60% methanol (solid green). Reprinted with permission from [21].

effect of various salts on the structure of a protein has been well-studied and is broadly referred to as the Hofmeister effect. The concentration of HCl used for these experiments (~12.6 mM) was much lower than the lower limit at which the Hofmeister series becomes relevant (hundreds of mM). However, the actual concentration of the salt in the final stages of the ESI process increases significantly. MDS simulations concerning the evolution of an ESI droplet containing both a protein and a salt shed

some light onto the dynamics of such a system.[127, 129] Initially, fission events carry away both Na^+ and Cl^-, further reducing the concentration of the Cl^-. After droplet fission, Cl^- does not leave the droplet; consequently, subsequent water evaporation dramatically increased the concentration of the anion in the droplet. Furthermore, MDS simulations have found that the pH of the droplet varies significantly throughout the desolvation process.[130] Therefore, the protein could refold in the late stages of desolvation due to Hofmeister or pH effects.

Hamada *et al.* have previously reported that after acid-induced unfolding, high salt concentration induces the formation of the compact molten globule state of apo-myoglobin and cytochrome c.[120] It has been previously determined that Ubq does not exhibit acid-induced unfolding in aqueous solution; as such it would not be expected that Ubq would undergo the same folding pathway as the cited proteins. However, the addition of acid to Ubq in a methanolic solution clearly results in acid-induced unfolding to the A-state; therefore, it is possible that the high concentration of anions in the final stages of electrospray ionization could induce the formation of a molten globule conformation. A molten globule state by definition exhibits significant exposure of side-chains and as such would be similarly amenable to Cl^- adduction. Note that no changes in the CCS centroids but rather changes to the relative abundance of each conformer population are observed. Interestingly, $[M + nH + xCl]^{(n-x)+}$ ions produced from water/acid and methanol/acid show similar trends in conformer preference.

4.3.3. Cl^- Ions are Associated with Amine/Amide Moieties – the CID of HCl

Chait *et al.* have previously reported charge reduction in the presence of anions; the authors claim that the anions adduct to the peptide or protein and dissociate as the neutral conjugate acid.[122] **Figure 4.5** contains the mass spectra of Ubq ions after mass selection of $[M + 9H + 3Cl]^{6+}$ ions are subjected to low energy collisional activation (see *Section 3.2* for details) thereby inducing successive loss of HCl. Note that the black traces **(Figure 4.5A**, upper spectrum) were acquired using the lowest possible collision voltages (5V). Increasing the collision voltage, (**Figure 4.5A**, lower spectrum) increases the abundance of product ions from HCl loss. Collision voltages greater than 20 V are sufficient to completely dissociate all Cl^- adducts to the $[M + 6H]^{6+}$ ion (data not shown). Collisional activation of the mass-selected $[M + 9H + 3Cl]^{6+}$ Ubq ion population clearly demonstrates the facile dissociation of HCl under transmission conditions. A change in charge state was not observed upon collisional activation of $[M + nH + xCl]^{(n-x)+}$ ions indicating that the dissociation product was the neutral acid. Halides have been shown to associate with/cluster around basic residues; moreover, Cl^- can form stable backbone interactions with amide moieties of the protein backbone.[131] Both instances would result in the dissociation of HCl upon collisional activation. Furthermore, Zhou *et al.* report that when Cl^- hydrogen bonds to an ammonium ion, the bond length between the Cl^- and an ammonium proton is significantly shorter than the N-H ammonium bond.[132] Thus it comes as no surprise that collisional activation of an ammonium-Cl^- interaction should result in loss of HCl.

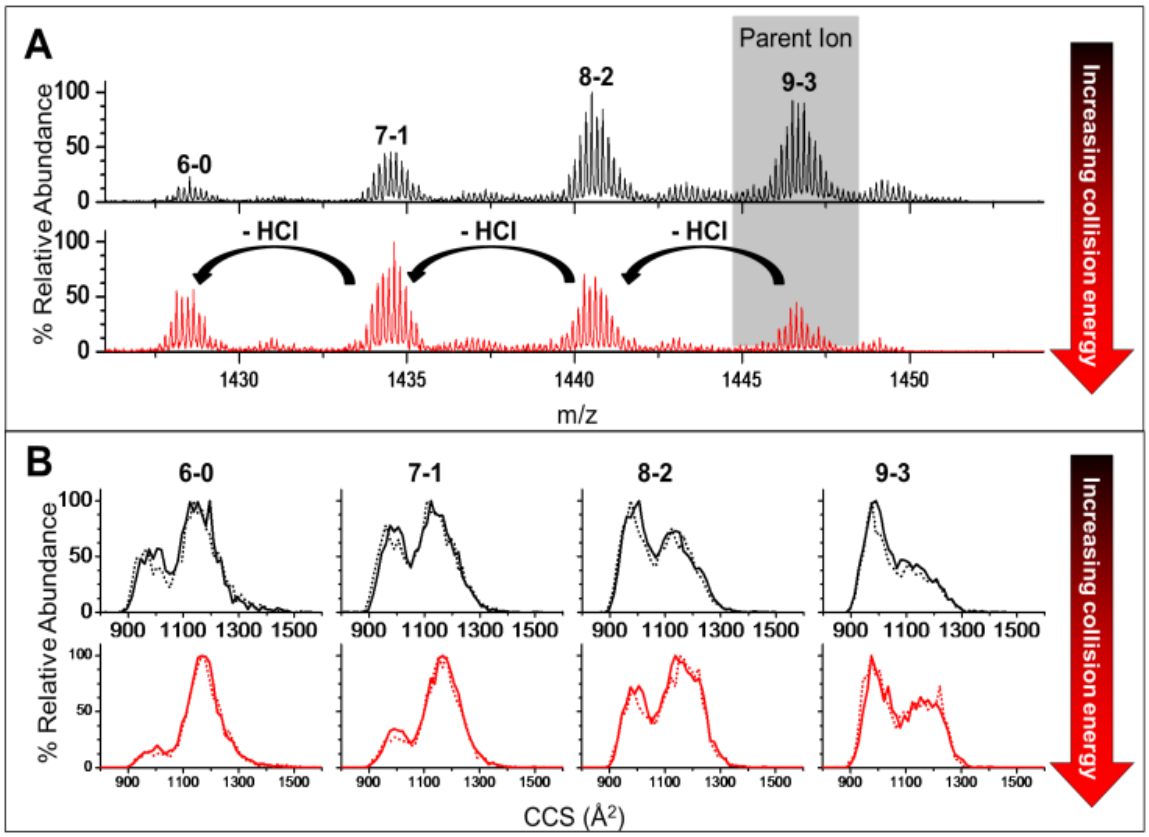

Figure 4.5. (A) The MS-MS mass spectra for $[M + 9H + 3Cl]^{6+}$ ions taken using two different collision energies which leads to collision-induced dissociation by loss of HCl. The upper spectra were acquired using the lowest possible collisional heating conditions while maintaining good ion transmission (5V, see *Experimental Section* for details). (B) A comparison of CCS profiles for ions produced by loss of HCl from mass selected $[M + 9H + 3Cl]^{6+}$ (solid) and without mass selection ion (dashed). Reprinted with permission from [21].

Ruotolo *et al.* suggested that anion dissociation upon collisional activation, particularly Cl^-, will stabilize a protein complex; *i.e.* the dissociation of the anion carrying away excess energy is responsible for maintaining a low E_{int}.[74] The CCS profiles for $[M + nH\ xCl]^{(n-x)+}$ ions produced via dissociation of HCl from the $[M + 9H + 3Cl]^{6+}$ ion are shown; the CCS profiles of $[M + nH\ xCl]^{(n-x)+}$ ions acquired without

quadrupole mass selection are shown overlaid for comparison (see **Figure 4.5B)**. The similarity between these CCS profiles indicates that conformer preference is independent of parent ion identity. If the dissociation of HCl carries away excess energy, then subsequent collisions obfuscate that effect. The number of Cl^- adducts retained by the protein and the degree of collisional activation are the determining factors for the CCS profiles of $[M + nH + xCl]^{(n-x)+}$ ions, *i.e.*, the identity of the parent ion is irrelevant to the final conformer preference of the protein. Upon loss of HCl, the protein ions are more prone to collision induced unfolding resulting in an increase in heat induced conformational diversity.

4.3.4. Strong Noncovalent Interactions Induce Resistance to Unfolding – Preserving More Compact Conformers

Williams and coworkers proposed that the Cl^- is likely participating in salt bridging which is responsible for more compact $[M + nH + xCl]^{(n-x)+}$ conformer ions;[73] we assert that this is an oversimplification of the potential interactions between the protein and Cl^-. Williams *et al.* later reported that halides participate in ionic hydrogen bonds with a peptide, the strength of which was directly proportional to anion gas-phase basicity and indirectly proportional to the gas-phase basicity of the ammonium groups; furthermore, Cl^- participated in an ammonium–Cl^-–ammonium complex, where the ammonium held the proton more closely than the anion.[133] In addition, the possibility of Cl^-–backbone interactions, as mentioned previously,[131] could result in basic-side-chain–Cl^-–backbone amide ionic hydrogen bonds. Due to differences in proton affinity, a single ionic hydrogen bond between an amine group and Cl^- would simply result in dissociation

of HCl; however, multiple ionic hydrogen bonds would be much more stabilizing and more difficult to dissociate. Warnke *et al.* claim that side-chain – backbone interactions destabilize the protein in the gas-phase by disrupting the hydrogen bond network of the protein.[134] Conversely, Zhou *et al.* report that these "halide motifs" can stabilize the native-fold of a protein;[119] specifically, the concerted stabilization energy of a "halide motif" in the gas phase can exceed 100 kcal/mol.[41] A broad range of stabilization energies for ionic hydrogen bonds are reported, *i.e.*, ~5-35 kcal/mol;[135] the increased stabilization attributed to a "halide motif" is the product of the concerted stabilization via multiple noncovalent interactions. In effect, Cl^- adduction "stitches" together regions of the protein, which increases the energy necessary for the protein to unfold.

Collisional activation of $[M + nH + xCl]^{(n-x)+}$ ions results in not only loss of HCl, but also collision induced unfolding (CIU) (see heat maps in **Figure 4.6**). The formation of strong non-covalent interactions is further supported by the resistance of $[M + nH + xCl]^{(n-x)+}$ ions to CIU; $[M + nH + xCl]^{(n-x)+}$ ions retain relatively more compact conformers than $[M + nH]^{n+}$ ions after CIU. Mild CIU of the $[M + nH]^{6+}$ ion population is sufficient to completely depopulate the compact conformer, indicating loss of the native-like conformer. Where x = 1 or 2, the relative percentage of the 5+ and 6+ Ubq populations that undergoes collisional unfolding is similar for the $[M + nH]^{n+}$ and $[M + nH + xCl]^{(n-x)+}$ ions. Most interestingly, $[M + 10H + 4Cl]^{6+}$, $[M + 8H + 1Cl]^{7+}$, and $[M + 9H + 2Cl]^{7+}$ ions do not exhibit CIU; specifically, $[M + 10H + 4Cl]^{6+}$ ions appear to hinder formation of intermediate conformers, and the $[M + 8H + 1Cl]^{7+}$ and

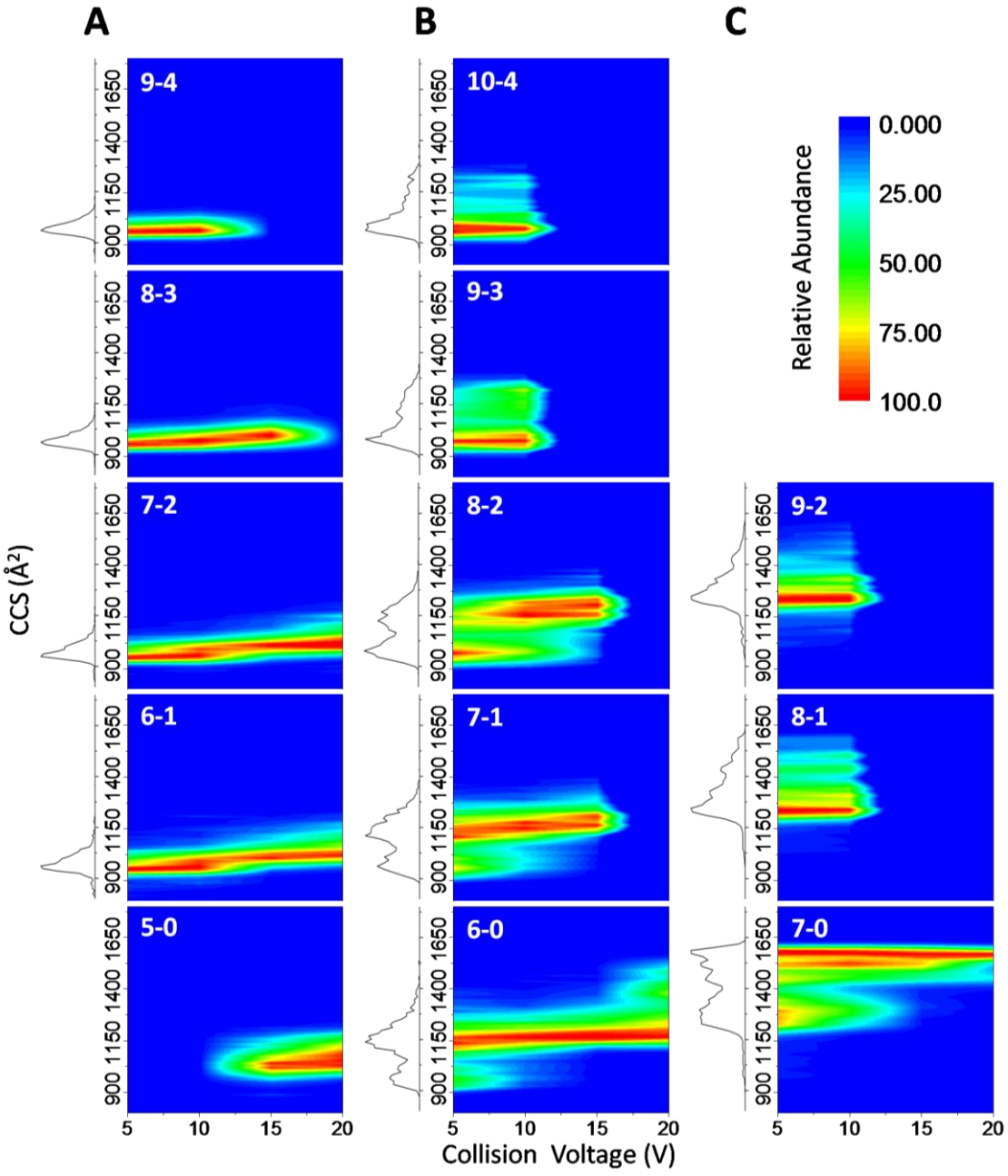

Figure 4.6. Heat maps showing the effect of collisional activation on the CCS profiles of $[M + nH + xCl]^{(n-x)+}$ Ubq ions with a total charge of 5+, 6+, and 7+ (A-C, respectively). Quadrupole mass selection was not used in this experiment, see *Experimental* for details. The CCS profiles observed using a collision voltage of 5V is shown to the left of each heat map for detail. Note that the $[M + 5H]^{5+}$ is not observed in appreciable abundance without collisional induced dissociation of HCl from $[M + nH + xCl]^{5+}$ ions. Reprinted with permission from [21].

$[M + 9H + 2Cl]^{7+}$ ions appear to hinder formation of extended conformers. For these ions, the Cl^- appears to be stabilizing the compact 5+/6+ ions and intermediate 7+ Ubq ions. This stabilization of the more compact conformers is indicative of coordinated interaction between Cl^- and multiple sites on the protein, *i.e.*, "halide motif". Overall, the results indicate that these interactions "stitch" together the backbone of the protein into a compact conformation that resists unfolding to a more extended conformation.

4.3.5. Cl^- Facilitates the Retention of Water Adducts

In all previous studies, both experimental and computational, concerning the impact of counter anions on the ESI process and subsequent conformational preference of a protein, either Na^+ or NH_4^+ was used in conjunction with the anion. In terms of the Hofmeister series, it has been claimed that anions have a more direct interaction with the protein and, consequently, a more dramatic effect on conformational preference; however, any potential influence of the cation cannot be ruled out. In fact, Na^+ was shown to directly bind to the macromolecule.[127, 129] In order to examine the effect of the anion alone on conformational preference, HCl was chosen to supply Cl^-; as stated previously, acidification has little to no effect on the conformational preference of Ubq unless the solution is >40% methanol.

A second series of ions (denoted by *) is observed from aqueous Ubq solutions and have thus far not been discussed; the most abundant ions of this series is observed of 5+ Ubq ions (**Figure 4.1A**). The ions of this series are shifted by 18 Daltons relative to the Cl^- adduct ions. These ions are assigned as H_2O/H_3O^+ adducts, $[M + nH + xCl]^{5+}$ •

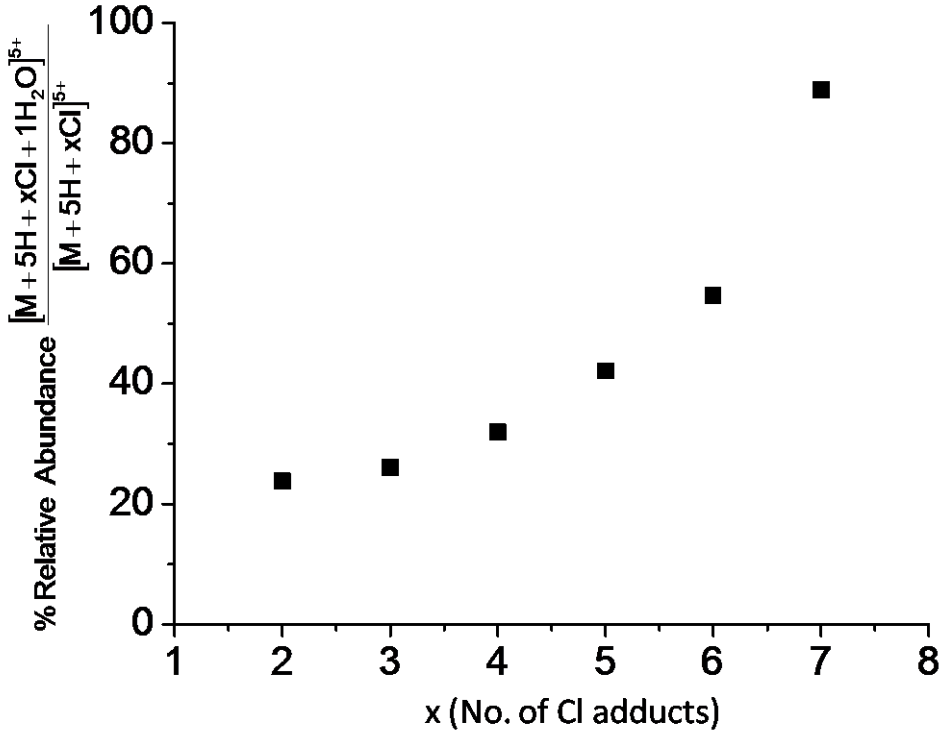

Figure 4.7. Plot showing the relative abundance of $[M + nH + xCl]^{5+}$ ions vs. the abundance of $[M + nH + xCl + yH_2O]^{5+}$ for different numbers of Cl^- adducts (x). Reprinted with permission from [21.]

$(H_2O)_i$. Note that the water adduct ions are observed in lower abundance in the methanol/water solutions, as would be expected since the water content is reduced. The identity of all $[M + nH + xCl + yH_2O]^{5+}$ ions was verified using calculated theoretical isotope distributions. As shown in **Figure 4.7**, there is a direct correlation between the number of Cl^- adducts and the relative abundance of Ubq ions with both Cl^- and water adducts. This implies that Cl^- adduction facilitates the retention of the water adduct. These results suggest that either the water/hydronium v ion is directly bound to a Cl^-

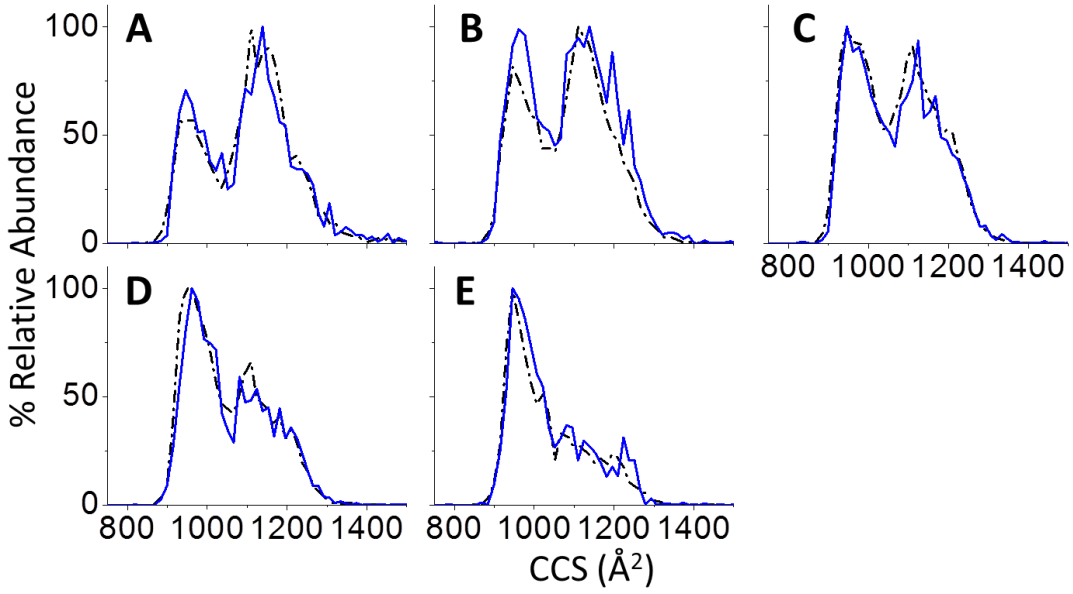

Figure 4.8. CCS profiles of $[M + nH + xCl + yH_2O]^{6+}$ ions where x = 0-4 (A-E respectively) and where y = 0 (black) and y = 1 (blue). Reprinted with permission from [21].

adduct (as in the aforementioned simulations[127]), the interaction between a water molecule and the protein is strengthened by the presence of Cl^-, or the Cl^- adduct facilitates the formation of a cavity from which the water cannot escape. The adduction of water had no effect on the ion CCS distribution; CCS profiles of water/ Cl^-adducted ions are identical to the ion population directly preceding it (see **Figure 4.8** for $[M + nH + xCl + yH_2O]^{6+}$ ion CCS profiles; note that $[M + 5H]^{5+}$ ions are already compact and as such would not be expected to change conformation upon adduction). The fact that the presence of water adducts appears to have no impact on conformational preference supports the possibility that the water adducts are associating with the Cl^- adducts as

reported by the simulations. Further-more, this finding supports the assumption that H_3O^+ has minimal effect on the conformational preference of Ubq; Cl^- is responsible for all previously discussed observations.

4.4. Conclusions

In this study, we have sought to understand how the presence of counter anions impacts the conformational preference of the model protein Ubq after desolvation. From the results of the aforementioned Na^+/Cl^-/Ubq theoretical desolvation study,[127] it would be expected that Ubq should adduct many more Cl^- and H_3O^+ ions than that observed in this study. The deficiency in ion adduction is easily explained by the facile dissociation of Cl^- observed using MS-MS; adducts not participating in direct interactions with the protein may be more easily dissociated still than those that are directly forming ionic hydrogen bonds. Because only dissociation of HCl is observed, it can be assumed that those ions retained are directly bound to the protein. This study has shown that if the protein retains those Cl^- adducts, then the protein exhibits a more native-like conformation and resists collisional unfolding. In effect, the adduction of Cl^- decreases the effect of coulombic repulsion and the "web-like" coordinated interactions between the anion and the protein stabilizes the "native-like" structure of the protein. Analogous to the use of Cl^- for crystallizing a protein to facilitate x-ray crystallographic analysis, Cl^- participates in a lattice network of coordinated interactions that "freezes" the protein in its native-like state, despite transfer from solution into the gas-phase and collisional activation.

5. CHLORIDE ADDUCTION TO K48-LINKED DIUBIQUITIN INDUCES PRESERVATION OF MORE "NATIVE-LIKE" CONFORMATIONS AND INCREASED GAS-PHASE STABILITY

5.1. Introduction

Electrospray ionization mass spectrometry (ESI-MS) has established a foothold in the field of structural biology, especially with the use of other MS techniques such as tandem MS, hydrogen/deuterium exchange (HDX), chemical foot-printing, and the integration of ion mobility (*i.e.* ESI-IM-MS). ESI-IM-MS in particular provides the ability to separate ions on the basis of size-to-charge in the form of ion-neutral collision cross sections (CCS), a measure of the rotationally averaged 3-dimensional shape of the ion. Due to the fact that ESI-IM-MS is an inherently gas-phase technique, the relationship between the IM CCS measurement and the solution-phase conformational preference remains a large concern in the field; stated differently, "…for how long, under what conditions, and to what extent, can solution structure be retained without solvent?"[65] Current opinion suggests that evaporative cooling[63, 66-68] and the formation of intramolecular interactions in the late stages of desolvation[46] provide a route for capturing solvent-free "native-like" conformations despite transfer into the gas phase.[69] However, the retention of said "native-like" conformation is highly dependent upon the degree of collisional activation experienced by the ion in transmission through the instrument and the resulting increasing in ion internal energy (E_{int}).[71-72]

Anion adduction has been shown to result in the preference for more compact conformations of protein ions[21, 73] and the stabilization of protein complexes.[74-75] Han *et al.* suggest that dissociation of anion adducts from protein complexes results in lower average E_{int} inducing not conformational stabilization, but instead minimizing the effect of collisional activation.[74-75] We have previously shown that Cl^- adduct ions impart a significant degree of gas-phase stabilization to compact conformers of the model protein ubiquitin (Ubq).[21] Halides have been shown to associate with/cluster around basic residues, and Cl^- can form stable backbone interactions with amide moieties of the protein backbone;[131] therefore, in the case of Ubq, we claim instead that the complex network of intermolecular interactions between the protein and Cl^- adducts stabilizes the "native-like" structure and prevents unfolding in the gas phase.[21] However, ESI-IM-MS provides only a single parameter with which to deduce differences structure,[10] and the possibility remains that the observed anion adduction induced preference for more compact conformers is not the result of retention of "native-like" structure, but instead anion adduction induced conformational collapse to an alternative compact conformer.

Ubq participates in a diverse array of bioactivities as defined by its oligomeric state, connected through an isopeptide bond between the C-terminal carboxyl group of an Ubq subunit and the amino group of either the N-terminus or a lysine side-chain of another Ubq subunit. These Ubq oligomers vary in terms of covalent linkage site, branching, and homo/heterogeneity resulting in unique quaternary structures, available binding motifs, and bioactivities; however, the tertiary structure of each Ubq subunit remains largely unchanged.[5] The most common linkage site, through K48,[64] is integral to

cellular function and immune response in that K48-linked tetraUbq tags misfolded proteins and antigens for proteosomal degradation in the 26S proteosome.[36, 41-42] K48-linked diUbq has been previously reported to adopt two distinct conformer types, "closed" conformers forming hydrophobic interfacial interactions between the I44 hydrophobic patch (L8, I44, and V70) of each subunit, and "open" conformers wherein the I44 patches are exposed and primarily electrostatic interactions between the subunits are observed.[34, 37, 53] These two conformational families exist in a dynamic equilibrium that will shift to preference for the "open" conformations at low pH. [12, 31]

We have previously reported that ESI-IM-MS alone is insufficient with current resolution limits to differentiate the quaternary structures of diUbq ions covalently-linked through different lysine side chains despite that their reported structures are very different; however, the collisional activation technique termed collision induced unfolding (CIU) was found to be capable of this differentiation.[86] CIU is the sequential gas-phase collisional activation of solvent-free ions resulting in an increase in E_{int} and subsequent denaturation. Consequently, a CIU fingerprint can be acquired relating to the ion's noncovalent inter/intramolecular interactions. For example, CIU has been applied to examine differences in protein complex interfaces, intramolecular interactions, and lipid and anion binding induced stabilization.[7, 15-21] K48-linked diUbq in particular exhibits a unique CIU fingerprint characteristic of its I44/I44 interfacial interactions.[86] Upon collisional activation, K48-linked diUbq ions exhibit gradual unfolding rather than the distinct conformational transitions observed of other linkage type diUbq ions.[86] When the possibility for I44/I44 interfacial interactions is perturbed using solvent

induced unfolding, K48-linked diUbq ions no longer undergo gradual unfolding, but instead transition through distinct intermediates observed of other linkage type diUbq ions (See Section 3 for details). Here we investigate the ability of chloride adduct ions to increase the gas-phase stability of more "native-like" conformations of K48-linked diUbq using ESI-IM-MS and CIU. Furthermore, the previously discussed unique CIU fingerprint of protonated diUbq ions can be used to differentiate retention of more "native-like" conformers vs. an alternative conformation upon Cl^- adduction.

5.2. Experimental Methods

5.2.1. Sample Preparation

K48-linked diubiquitin was purchased from R&D Systems Inc. (Minneapolis, MN, USA) and was used without further purification. The protein was dissolved in 18 MΩ water (Barnstead Easy Pure II, Thermo Scientific) and stored at -20°C for later use. All solutions containing HCl were prepared with a final concentration of 10 μM protein, 10 mM of hydrochloric acid (Fisher Scientific, Pittsburg, PA, USA), and either water or 50% water/50% methanol. Formic acid containing solutions were prepared with a final concentration of 10μM protein, 0.1% formic acid, and either 99.9% water or 49.9% water/50% methanol. Ammonium acetate buffered solutions were prepared with a final concentration of 10μM protein and 25mM ammonium acetate in water (pH adjusted to ~7.4).

5.2.2. ESI-IM-MS

A Waters Synapt G2 HDMS instrument (Manchester, UK) was used for all ESI IM-MS experiments, and all results reported were acquired in the positive ion mode. As previously described, instrument conditions can be tuned to preserve ions having low internal energy (E_{int});[72] cooler instrument conditions are essential for retaining ubiquitin-halide adducts. The instrument conditions used were as follows: sample cone, 10V; extraction cone, 1V; trap bias, 25 V; API gas flows, off; helium cell flow rate, 200 mL/min; IMS nitrogen flow rate, 60 mL/min; TWIMS wave height, 20V; TWIMS wave velocity, 300 m/s. CCS values were calibrated as previously described.[78] Theoretical isotope distributions were calculated using Data Explorer Version 4.3. The molecular formula of each protein-adduct ion was determined and used to calculate theoretical isotope distributions with which to verify the identity of each ion.

5.2.3. ESI-CA-IM-MS

Collisional activation was induced by changing the voltage drop between the exit of the quadrupole and the entrance to the TWIG-trap region filled with the collision gas argon. Note that a 4 V drop was necessary to maintain transmission through the trap and transfer regions and will be referred to as low collision energy. In order to adjust the relative collisional activation of the different adduct ions for differences in analyte ion mass, collision energies are reported as center-of-mass frame collision energy (CE_{com}) calculated as:

$$CE_{com} = qV \frac{m_{Ar}}{m_{Ar}+m_{ion}} \quad (1)$$

where q is the ion's charge, V the accelerating voltage, m_{Ar} the mass of the collision gas, and m_{ion} the mass of the analyte ion.

CIU is commonly depicted in the form of heat maps showing changes in CCS as a function of collision energy; however, collisional activation also induces the dissociation of the adduct ions as the neutral conjugate acid.[21, 122] Consequently, CIU heat maps of the $[Ubq + nH + xX]^{(n-x)+}$ ions are difficult to interpret. To better facilitate interpretation, the "weighted centroid" of the CCS profile of each adduct ion at each collision energy was calculated using Equation 2:

$$CCS\ Centroid_{weighted} = \frac{\sum(CCS_i * RA_i)}{\sum RA_i} \quad (2)$$

where CCS_i and RA_i are the CCS value and relative abundance of each data point in the CCS profile.

5.3. Results and Discussion

5.3.1. K48-linked diUbq-Chloride Adducts Ions Are Observed Using nESI-MS

In Section 4, we have shown that monoUbq electrosprayed from HCl acidified solution produces abundant Cl^- adducted protein ions; furthermore, the number of Cl^- adducts increases upon solvent induced denaturation.[21] Chloride adducted ions are similarly observed of K48-linked diUbq ions. **Figure 5.1** shows the full ESI mass spectra of K48-linked diUbq ions acquired from various solution conditions, and **Figure 5.2** shows selected regions of the mass spectra showing K48-linked diUbq ions produced from HCl acidified solutions for various charge states. Mass spectra of K48-linked

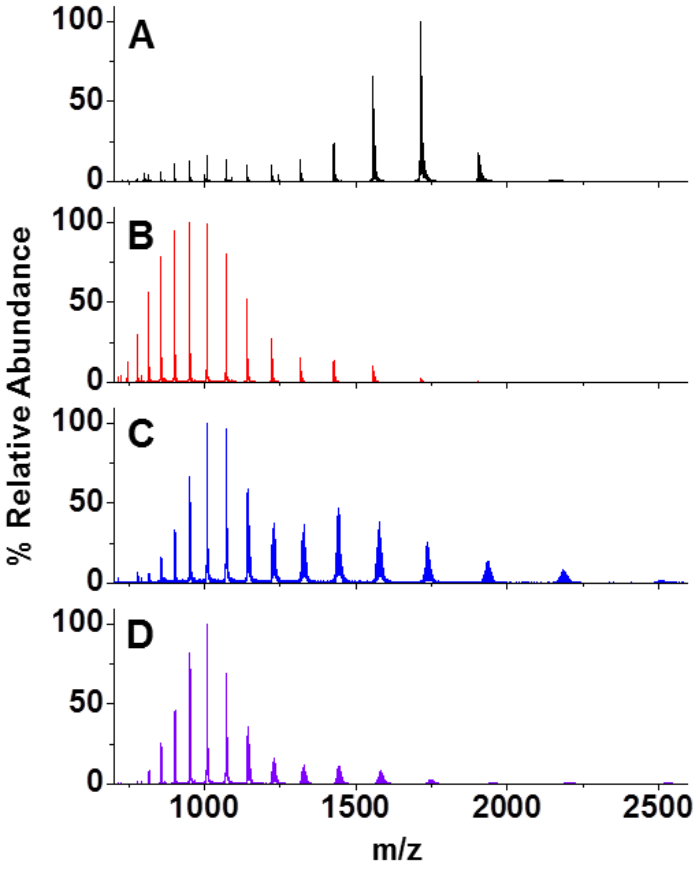

Figure 5.1. Full mass spectra of K48-linked diUbq acquired from (A) water, 0.1% formic acid, (B) 50% methanol, water, 0.1% formic acid, (C) water, 0.1% HCl, and (D) 50% methanol, water, 0.1% HCl.

diUbq ions acquired from solutions containing hydrochloric acid demonstrate abundant ions of the type $[M + nH + xCl]^{(n-x)+}$ to be abbreviated as K48-diUbq$^{(n-x)+}$ (See **Figure 5.2**). K48-linked diUbq ions acquired from formic acid and ammonium acetate buffered solutions are observed of the form K48-$[diUbq + nH]^{n+}$ (to be abbreviated as K48-diUbq^{n+}).

Upon addition of >40% methanol to acidic solution (pH ~ 2), monoUbq is known to populate the "denatured" A-state conformation, wherein part of the N-terminal portion of the β-sheet is retained, but the rest of the structure is in a flexible conformation with a high degree of α-helical character.[24, 105-107] Similarly to that observed of monoUbq ions, K48-linked diUbq acquired from HCl acidified 50% methanolic solutions demonstrate a higher degree of Cl^- adduction than that of K48-linked diUbq acquired from HCl acidified aqueous solution (see **Figure 5.2**). This trend is most apparent of lower charge state ions, and becomes less pronounced with increasing charge state. Note that the abundance of the lower charge states in the spectrum acquired from HCl acidified methanolic solution is significantly lower than that observed of HCl acidified aqueous solution resulting in poor signal-to-noise (see full mass spectra in **Figure 5.1**).

It is well known that ESI-MS charge state distributions can be correlated to protein conformational preference.[98-99] That is, the charge state of a protein in the ESI mass spectrum is related to the solvent accessible surface area (SASA), as related to solvent exposure of basic/acidic residues and the presence of intramolecular interactions.[100-102] For, example, the mass spectra acquired of monoUbq from denaturing acidic/methanolic solution shows a broad distribution of high charge state ions consistent with the increased SASA of the A-state conformation.[30, 94]As noted in Section 3, K48-linked diUbq acquired from water/formic acid solution demonstrate a relatively narrow distribution of high abundance, low charge state ions (10-11+) indicative of a large population of "native-like" ion conformations, and a broad distribution of low

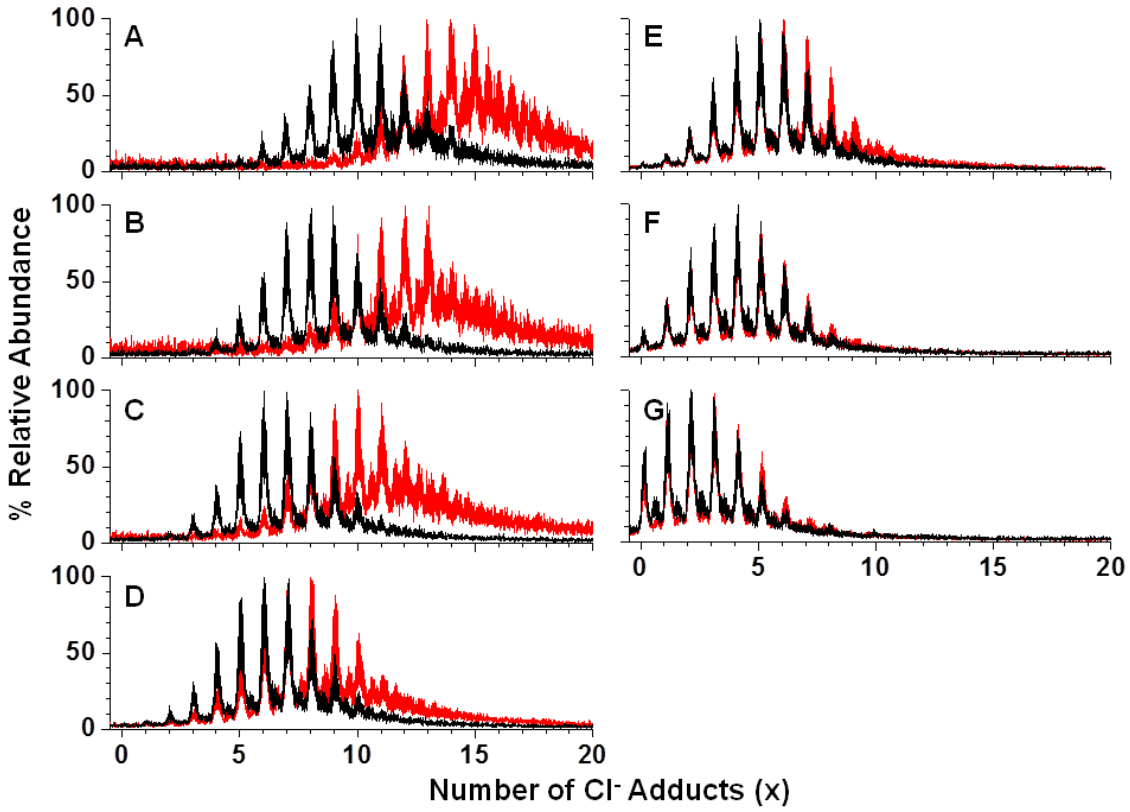

Figure 5.2. Selected regions of the ESI mass spectra of HCl acidified K48-linked diUbq showing protein/adduct ion distributions with charge states of 8+ through 14+ (A-G, respectively) acquired from 99.9% water/0.1% HCl (black) and 49.9% water/50% methanol/0.1% HCl (red). Note that the x-axis has been adjusted to show the number of chloride adducts (x) rather than m/z for ease of comparison.

abundance, high charge states (13 –25+) (see **Figure 3.1**). The full mass spectrum of K48-linked diUbq ions acquired from HCl acidified aqueous solution initially suggests a high degree of denaturation; however, the increased Cl^- adduction observed of lower charge state ions results in artificial signal attenuation because the ion signal is partitioned across increasing numbers of ion signals. Interestingly, the abundance of the 9+, 8+, and even the 7+ populations of K48-diUbq$^{(n-x)+}$ ions is higher than those charge states of K48-diUbq^{n+} ions acquired from formic acid solution. This could be indicative

of decreased SASA due to a more compact conformation or possibly that Cl^- adduct ions form noncovalent bonds with exposed basic side-chains, decreasing their solvent accessibility for protonation. Furthermore, in Section 4 we noted that collisional activation of Ubq-Cl adduct ions results in dissociation of the neutral conjugate acid (HCl). Chait *et al.*[122] and Kim *et al.*[46] have also noted a similar result, but also reported that the adduction and subsequent dissociation of the neutral acid results in a shift to lower average charge states in the mass spectrum, *i.e.* charge reduction.

The addition of 50% methanol to formic acid acidified solution induces a shift to a broad distribution of high charge states of K48-linked diUbq centered at the 18+ charge state (**Figure 5.1A** vs. **B**). The average charge state of K48-diUbq ions acquired from HCl acidified methanolic conditions is higher than that produced from aqueous solution as consistent with methanol induced denaturation and increased SASA (**Figure 5.1C** vs. **D**). However, the average charge state observed from HCl acidified methanolic solution is lower than that observed from formic acid acidified solution; more specifically, the narrower charge state distribution for hydrochloric vs. formic acid solutions suggests depopulation of the highest charge states. The observed increase in Cl^- adduction upon addition of methanol is consistent with increased exposure of Cl^- binding sites due to the increased SASA. Interestingly, the degree of Cl^- adduction becomes increasingly similar with increasing charge state despite the use of denaturing conditions. This similarity in Cl^- adduct distributions observed of higher charge state ions (> 12+) acquired from both solutions suggests those ions demonstrate similar exposure of Cl^- binding sites and are likely more representative of largely unfolded ion populations.

5.3.2. K48- diUbq$^{(n-x)+}$ Ions Populate More Compact Conformers When Compared to K48-diUbq^{n+} Ions

We have previously shown that Cl^- adduction to monoUbq results in the preservation of more compact conformers due to increased resistance to gas-phase unfolding; however, the structure of this compact conformer remains open to speculation due to the limited local structural information provided by ESI-IM-MS analysis. The low energy CCS profiles of protonated K48-linked diUbq ions have been discussed previously (See Section 3, see the top row of **Figure 5.3**). Briefly, the CCS profile of K48-diUbq^{9+} ions suggests two conformational families with CCS values of ~1750 Å^2 (most similar to the theoretical CCS values calculated via MOBCAL for previously reported structures of K48-linked diUbq in solution) and ~1500 Å^2 (attributed to an acid-induced molten globule conformer population). As the charge state increases (< 13+), the CCS profiles are increasingly broad, suggesting a high degree of heterogeneity, and shift to larger CCS values, suggesting little resemblance to the solution phase conformation. High charge state ions (≥ 13+) demonstrate very narrow CCS profiles of extended conformers that likely represent gas-phase equilibrium conformations.

The low energy CCS profiles of all K48-diUbq$^{(n-x)}$ ions exhibit CCS profiles with increased abundance of more compact conformers, some not observed of K48-diUbq^{n+} ions (**Figure 5.3**). The CCS profiles of 9+ K48-diUbq$^{(n-x)+}$ ions suggest an increasing preference for the ~1500 Å^2 conformation (for example see the K48-diUbq$^{(18-9)+}$ ion CCS profile). This may suggest a preference for an acid-induced molten globule

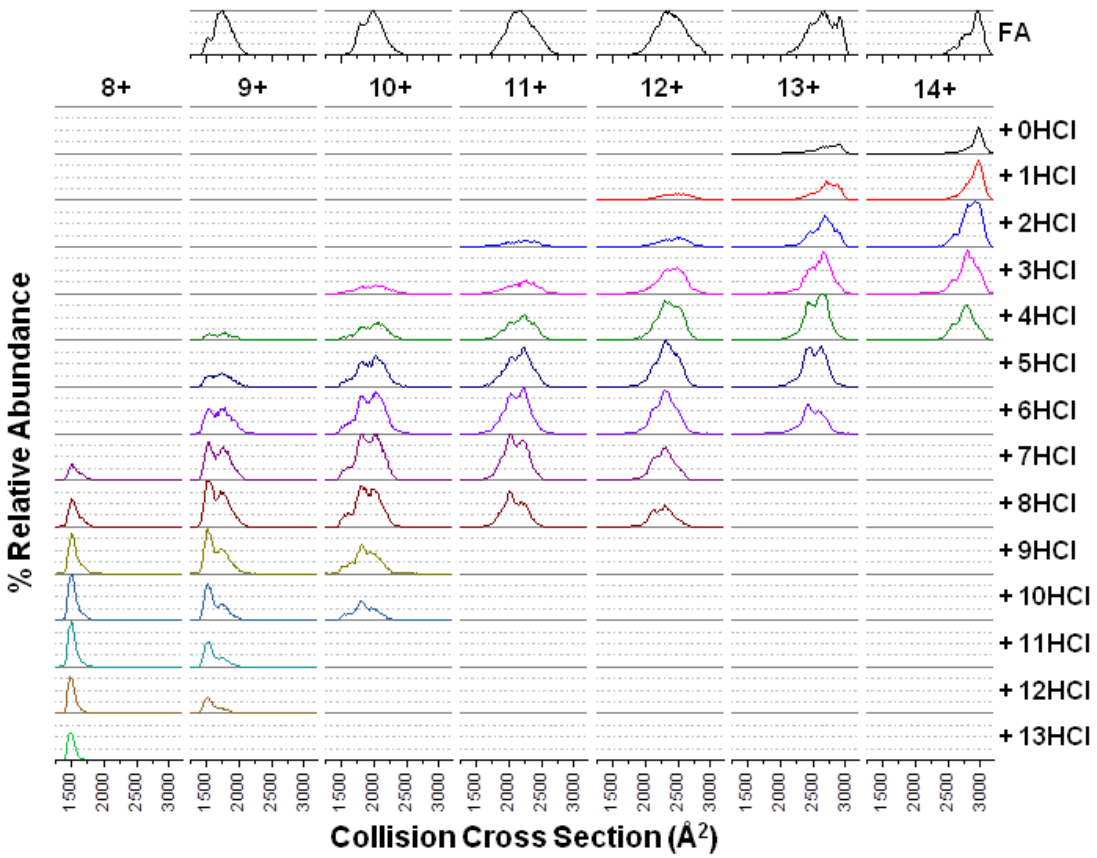

Figure 5.3. CCS profiles of K48-[diUbq + nH]$^{n+}$ acquired from 99.9% water/0.1% formic acid (top, FA) and CCS profiles of K48-[diUbq + nH + xCl]$^{(n-x)+}$ acquired from 99.9% water/0.1% HCl (labeled as "+ xHCl"). Note that all CCS profiles are reported with minimal instrumental collisional energy.

conformation based upon previous assignments; however, this lower CCS is very similar to that of the compact conformers observed of 8+ K48-diUbq(n-x)+ ions. The diUbq8+ ion is not observed in sufficient abundance when acquired from formic acid solution, but is observed when acquired from ammonium acetate buffered solution (see **Figure 2.7**). The CCS profiles of the 7+, 8+, and 9+ charge states of K48-diUbq acquired from

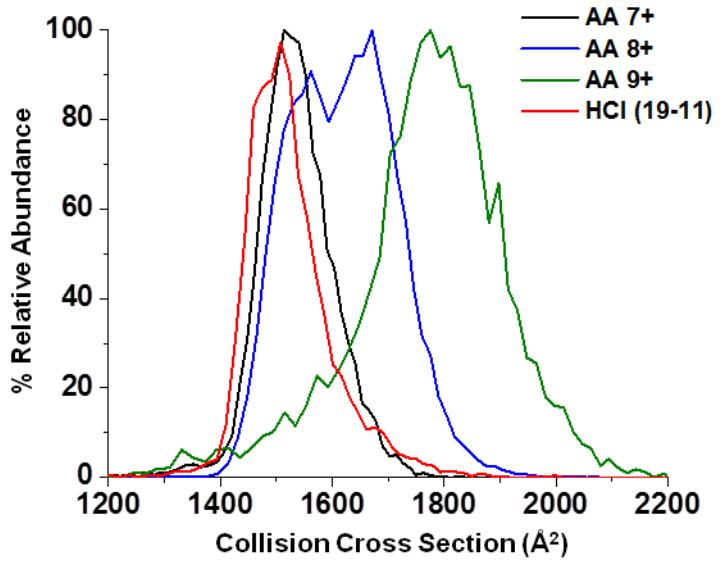

Figure 5.4. CCS profiles of the 7+, 8+, and 9+ charge states of K48-diUbq acquired from 25mM ammonium acetate solution, and the CCS profile of the chloride adducted K48-diUbq$^{(19\text{-}11)+}$ ion with an 8+ charge state acquired from 0.1% hydrochloric acid solution.

buffered solution is shown with the highly chloride adducted K48-diUbq$^{(19\text{-}11)+}$ ion CCS profile for comparison (see **Figure 5.4**). The CCS profile of K48-diUbq^{8+} ions acquired from buffered solution suggests two conformer populations with CCS values of ~1500 Å^2 and ~1700 Å^2. Despite that the K48-diUbq$^{(19\text{-}11)+}$ ion has an overall charge of 8+, the CCS profile of this ion population is superimposable upon the CCS profile of K48-diUbq^{7+} ions and the more compact conformers of K48-diUbq^{8+} ions of acquired from buffered solution. A similar phenomenon is observed of the 10+ charge state of K48-diUbq$^{(n\text{-}x)+}$ ions wherein conformer populations with CCS values of ~1500 Å^2 and ~1780 Å^2 are observed of K48-diUbq$^{(n\text{-}x)+}$ ions with a high degree of Cl^- adduction. These conformers are more abundant with increasing numbers of Cl^- adducts. This suggests

that Cl^- adduction induces the preference for conformers with a similar CCS to the lower charge states suggesting increased retention of the more "native-like" conformers.

The higher charge states of K48-linked diUbq are much less likely to resemble the "native-like" conformers in solution due to the increased coulombic repulsion and collisional activation. Chloride adducted K48-linked diUbq ions with higher charge states (> 10+) exhibit more narrowed CCS profiles than their K48-diUbq^{n+} counterparts suggesting a decrease in conformational heterogeneity. For example, the CCS profiles of 11+ K48-diUbq$^{(n-x)+}$ ions suggests the preference for distinct conformers (CCS ~2000 Å^2 and ~2250 Å^2) rather than the broad distribution observed of K48-diUbq^{11+} ions. The observed larger CCS values suggest that the ions have undergone sufficient collisional activation to result in unfolding. Bartman, *et al.* have previously reported molecular dynamics simulation results that suggest that Ca^{2+} adducted Ubq ions undergo conformational inversion upon collisional activation, wherein the more hydrophobic protein side-chains typically buried within the hydrophobic core are exposed to vacuum and the adduct ions/more polar side-chains are buried within the protein's core.[136] The higher charge states of K48-diUbq$^{(n-x)+}$ ions may populate more compact conformers than their K48-diUbq^{n+}, but the increased collisional activation and coulombic repulsion inherent to these higher charge states may be indicative of a similar effect to that reported by Bartman *et al.*, rather than preservation of more "native-like" conformations.

5.3.3. K48-diUbq$^{(n-x)+}$ Ions Demonstrate Increased Gas-Phase Stability when Compared to K48-diUbq^{n+} Ions

Collisional activation studies provide a means to examine differences in the gas-phase potential energy surface *en route* to gas-phase equilibrium conformation(s) providing a more detailed analysis of differences in noncovalent interactions and relative stabilities. Furthermore, CIU was used in Section 4 to evaluate the gas-phase stabilities of Cl^- adducted monoUbq ions. Here, the results of collisional activation of K48-diUbq$^{(n-x)+}$ ions for the 8+ through 12+ charge state ions are compiled in CIU heat maps shown in **Figure 5.5**, **Figure 5.6**, **Figure 5.7**, **Figure 5.8**, and **Figure 5.9**, respectively. Note that the relative abundance of each K48-diUbq$^{(n-x)+}$ ion at each collision energy level is normalized to the most abundant K48-diUbq$^{(n-x)+}$ ion of that charge state and collision energy; consequently, in each charge state series of K48-diUbq$^{(n-x)+}$ CIU heat maps, the sequential dissociation of neutral HCl can be observed upon collisional activation. However, the appearance and disappearance of each K48-diUbq$^{(n-x)+}$ ion makes discussion of conformational changes (i.e. CIU) more difficult. Consequently, **Figure 5.10A-B**, a compilation the relative abundance and weighted CCS centroid values calculated for each diUbq$^{(n-x)+}$ ion at each collision energy, will be used to aid in the discussion of CIU results.

CIU of various diUbq^{n+} ions was previously reported in Section 3. Briefly, the CIU profiles of K48-diUbq^{n+} are distinctly different from K6-, K11-, and K63-diUbq^{n+} ions; K48-diUbq^{n+} ions undergo smooth, gradual transitions to the more extended

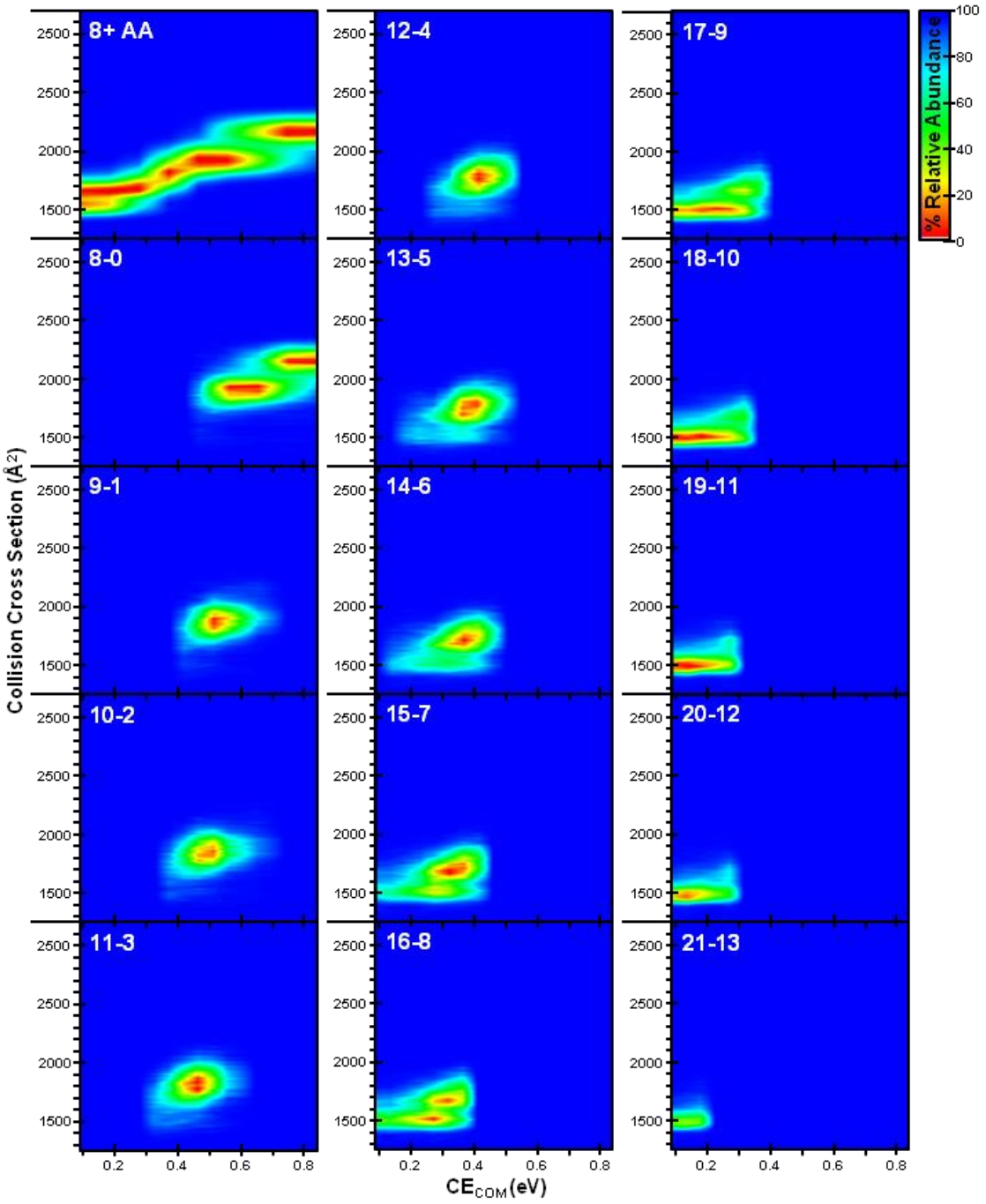

Figure 5.5. CIU heat maps of K48-[diUbq + 8H]$^{8+}$ (denoted AA 8+) acquired from 25mM ammonium acetate buffered solution and all K48-[diUbq + nH + xCl]$^{8+}$ ions acquired from 99.9% water/0.1% HCl (denoted by the adduct ion's (n-x) value).

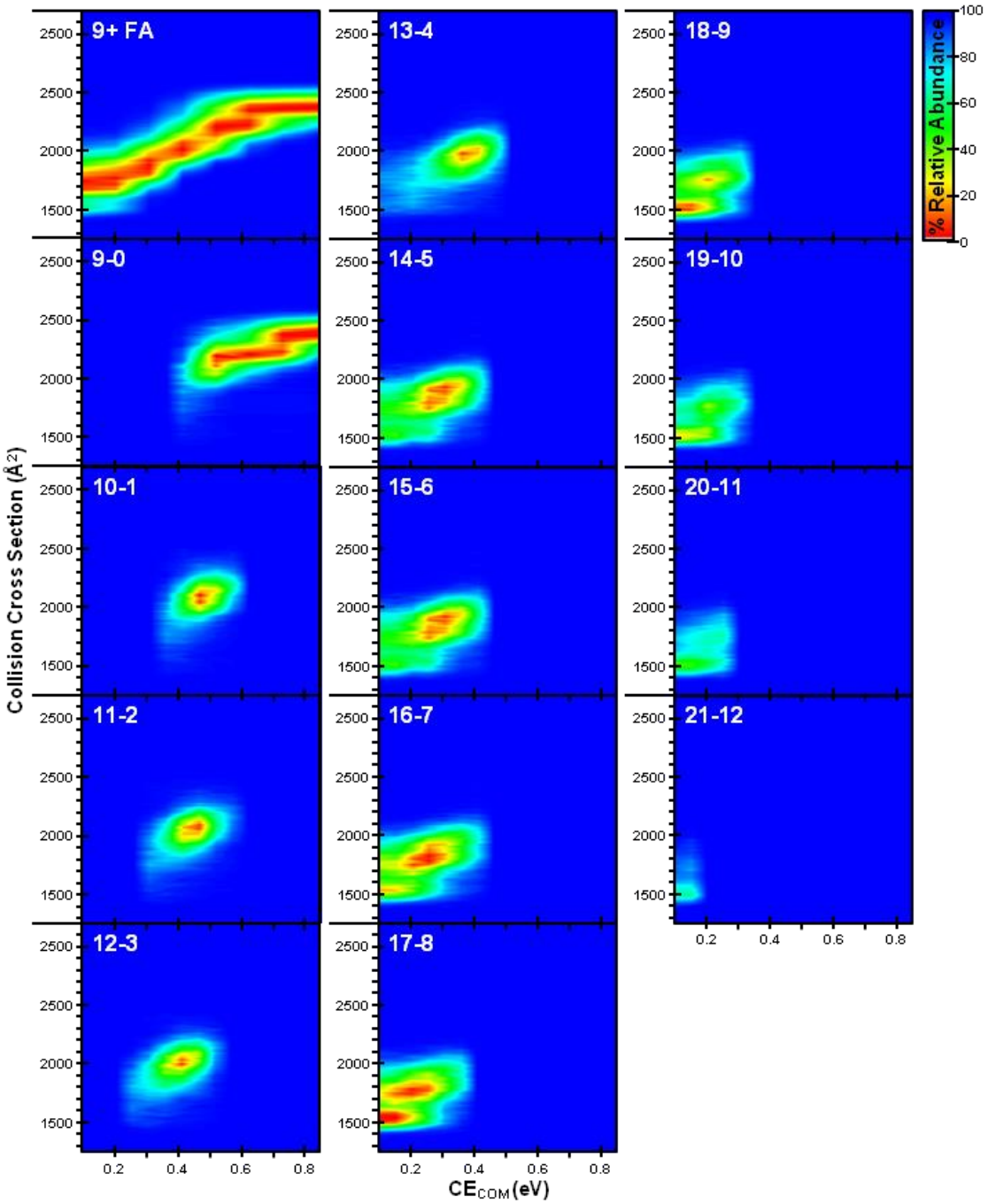

Figure 5.6. CIU heat maps of K48-[diUbq + 9H]$^{9+}$ (denoted FA 9+) acquired from 99.9% water/0.1% formic acid and all K48-[diUbq + nH + xCl]$^{9+}$ ions acquired from 99.9% water/0.1% HCl (denoted by the adduct ion's (n-x) value).

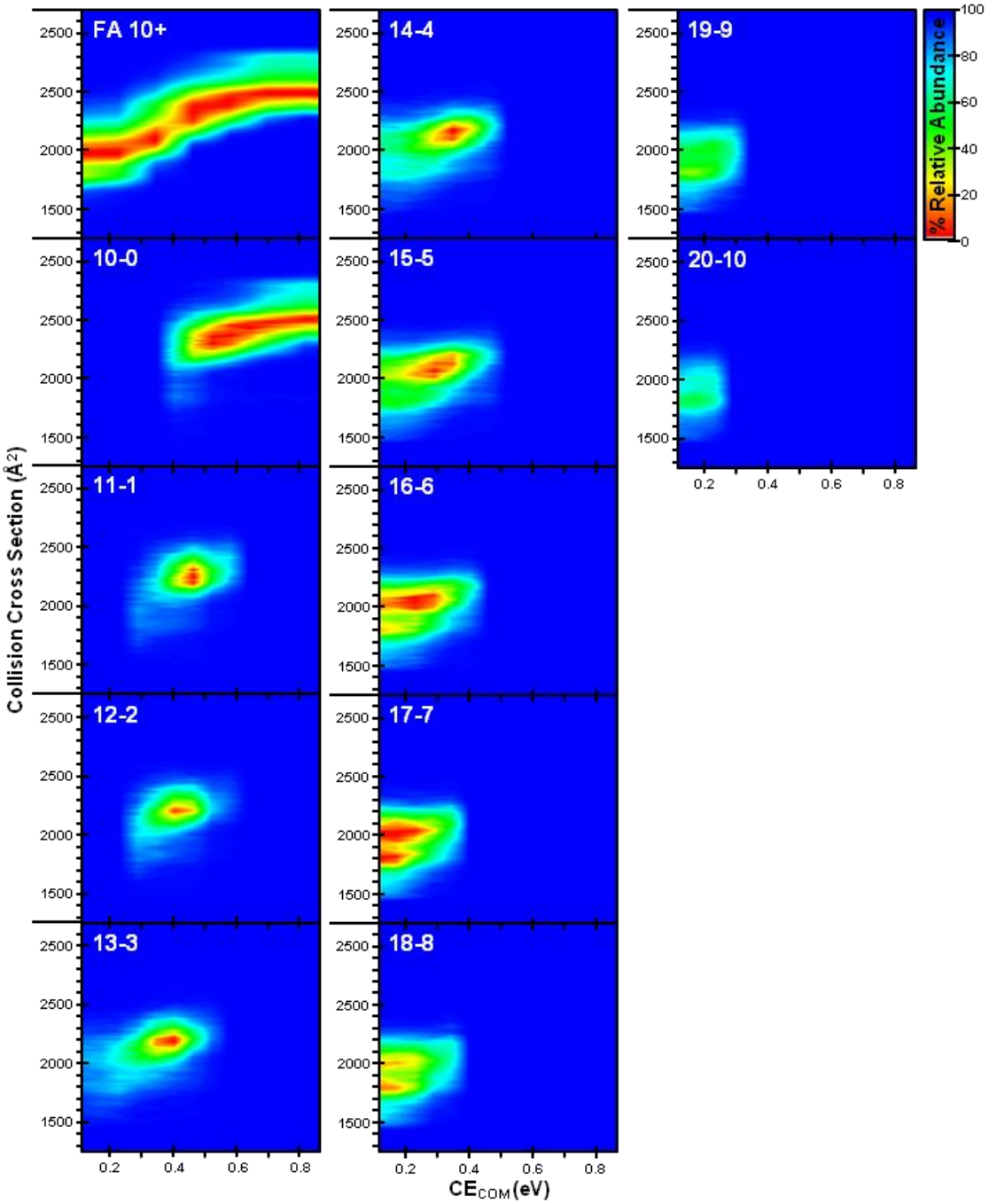

Figure 5.7. CIU heat maps of K48-[diUbq + 10H]$^{10+}$ (denoted FA 10+) acquired from 99.9% water/0.1% formic acid and all K48-[diUbq + nH + xCl]$^{10+}$ ions acquired from 99.9% water/0.1% HCl (denoted by the adduct ion's (n-x) value).

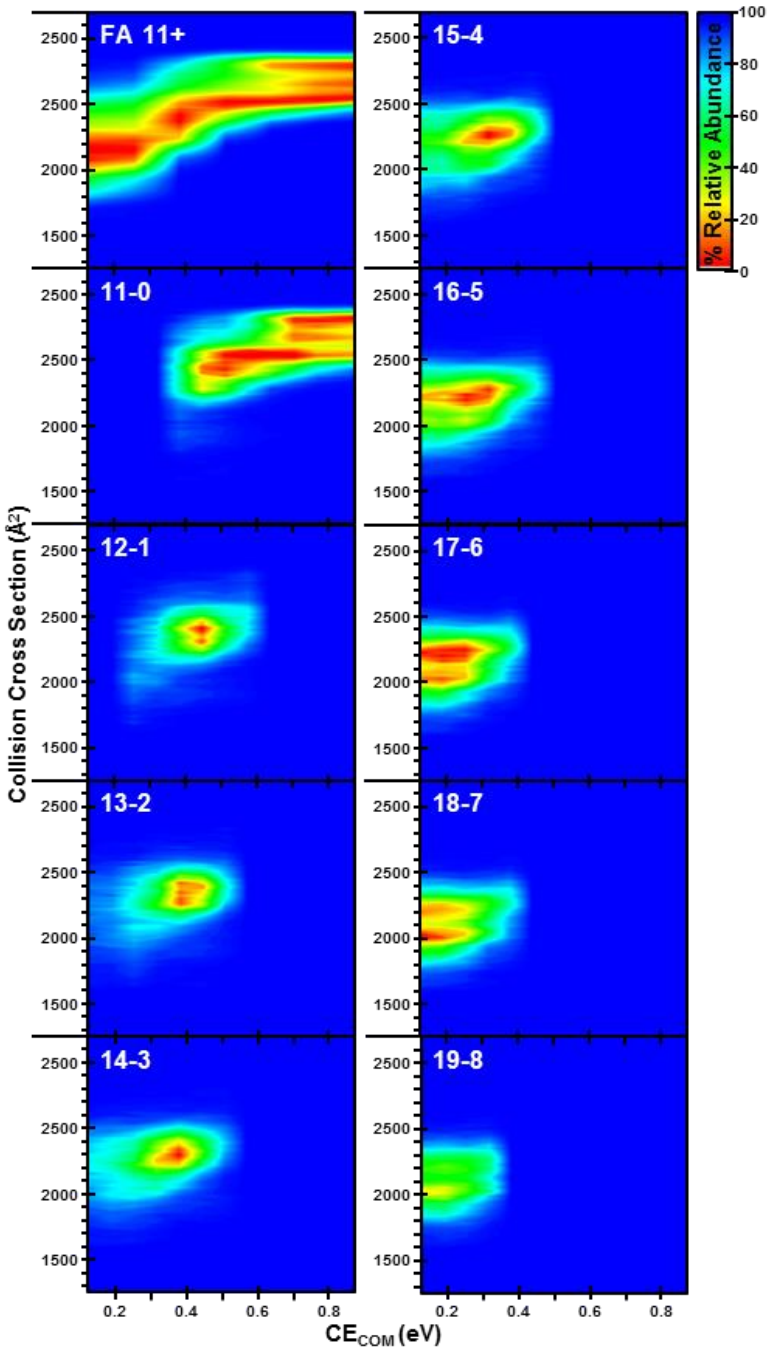

Figure 5.8. CIU heat maps of K48-[diUbq + 11H]$^{11+}$ (denoted FA 11+) acquired from 99.9% water/0.1% formic acid and all K48-[diUbq + nH + xCl]$^{11+}$ ions acquired from 99.9% water/0.1% HCl (denoted by the adduct ion's (n-x) value).

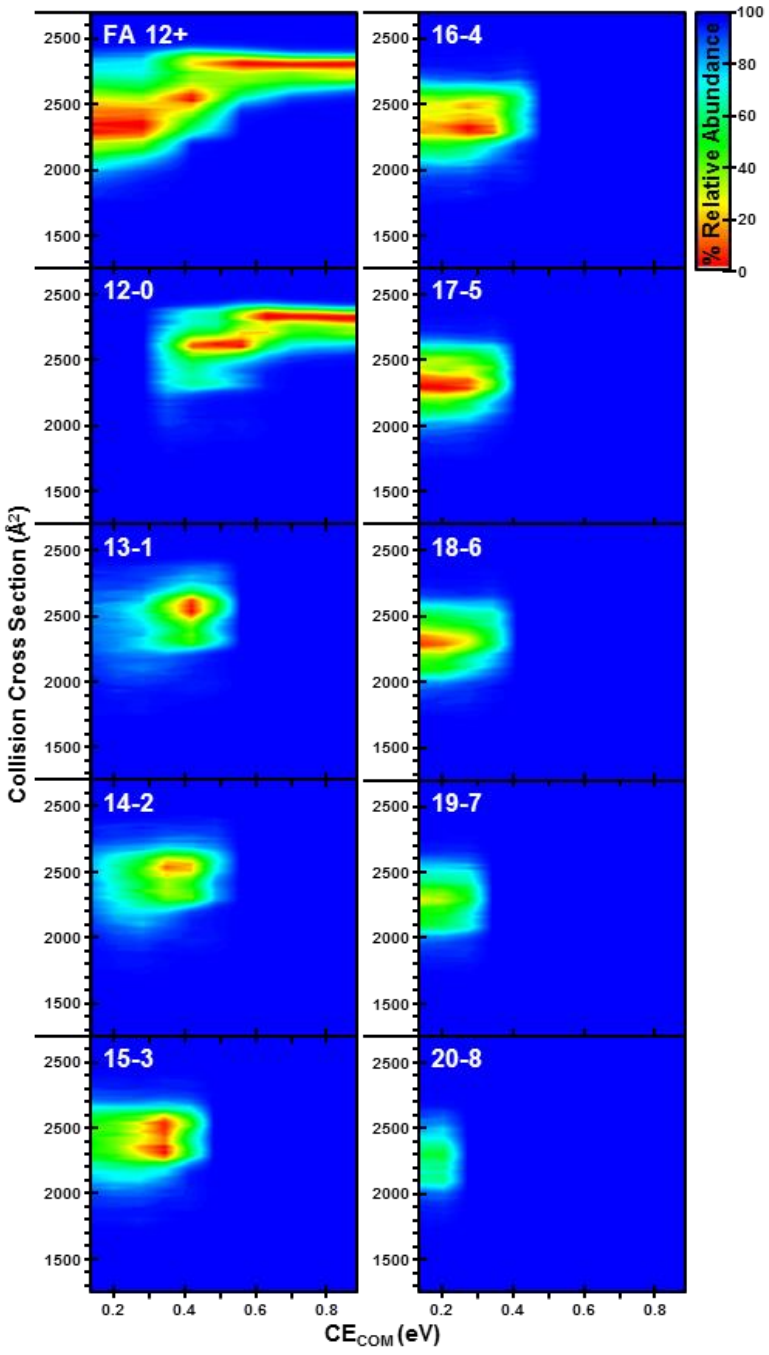

Figure 5.9. CIU heat maps of K48-[diUbq + 12H]$^{12+}$ (denoted FA 12+) acquired from 99.9% water/0.1% formic acid and all K48-[diUbq + nH + xCl]$^{12+}$ ions acquired from 99.9% water/0.1% HCl (denoted by the adduct ion's (n-x) value).

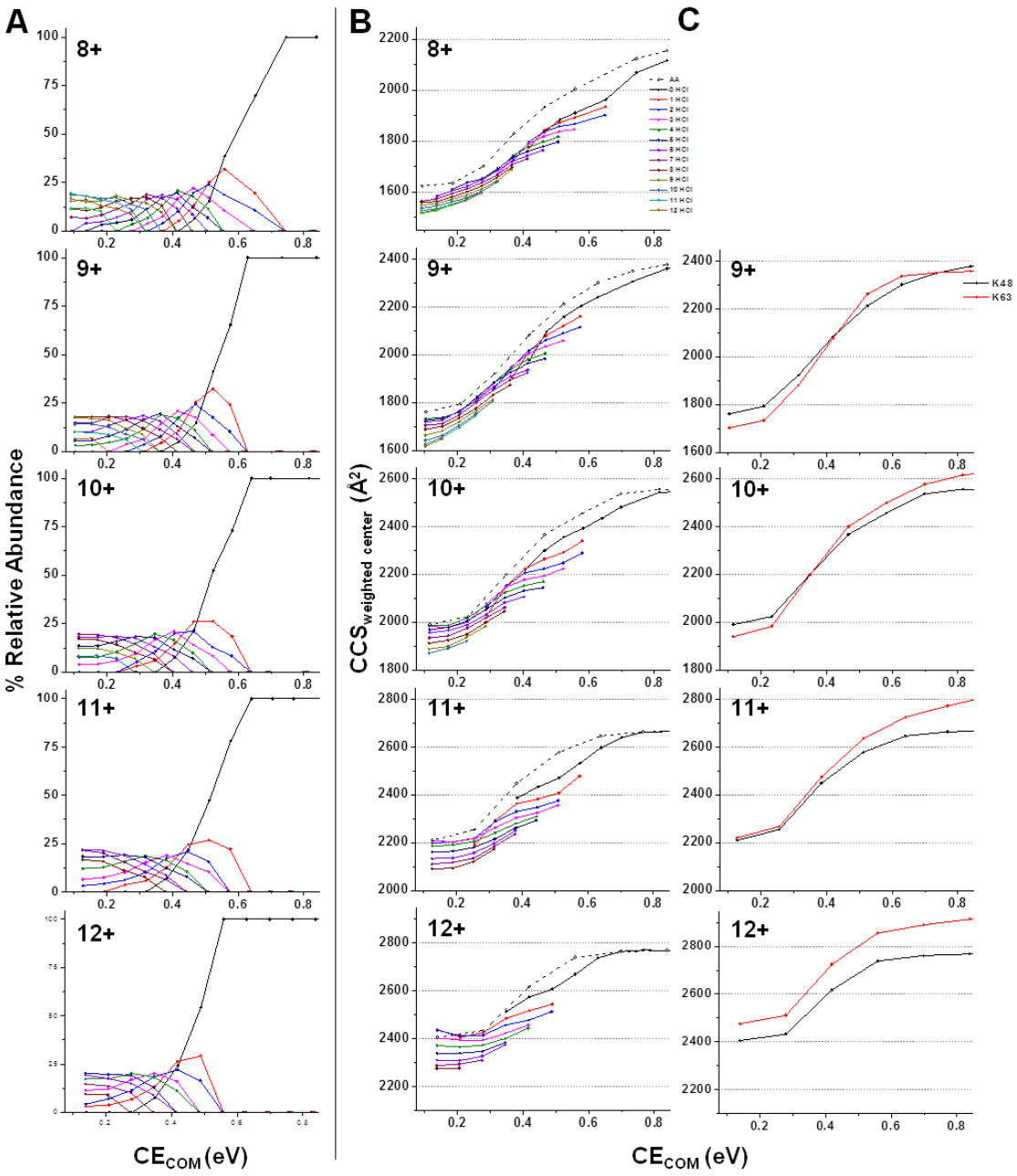

Figure 5.10. (A) Relative abundance of each K48-diUbq$^{(n-x)+}$ ion where the overall charge states are 8-12+ from top to bottom. (B) calculated weighted CCS centroid values of K48-diUbq^{n+} ions (black dash, open circle) and K48-diUbq$^{(n-x)+}$ ions (solid line, solid circle) as a function of center-of-mass frame collision energy. (C) calculated weighted CCS centroid values of K48- and K63-diUbq^{n+} ions acquired from 99.9% water/0.1% formic acid

conformers, whereas the other linkage types demonstrate interconversion through distinct intermediate conformers. The CIU profiles for K48-diUbq^{8+} ions acquired from ammonium acetate solution and CIU profiles for the 9+ through 12+ charge states of K48-diUbq ions acquired from formic acid solution are also included for comparison. These results have been similarly compiled into plots of weighted CCS centroid values calculated for K48- and K63-diUbq^{n+} ions for direct comparison to K48-diUbq$^{(n-x)+}$ ions (See **Figure 5.10C**).

The CIU profile of K48-diUbq^{8+} ions acquired from ammonium acetate solution suggests gradual unfolding reaching a CCS of ~1920 Å^2, followed by a distinct transition to the gas-phase equilibrium conformation (~2150 Å^2). As previously noted, 8+ charge state K48-diUbq$^{(n-x)+}$ ions exhibit an increasingly narrow distribution of compact conformers (CCS of ~1500 Å^2) with each additional adduct, demonstrated in **Figure 5.10B** as an incremental decrease in the weighted CCS centroid with the addition of each adduct. CIU results suggest that this compact conformer is preserved across a range of collision energies (**Figure 5.5**). The CCS of ~1780 Å^2 is not observed in appreciable abundance of the most highly adducted K48-diUbq^{21-13+}, diUbq^{20-12+}, and diUbq^{19-11+} ions. This suggests that these diUbq$^{(n-x)+}$ ions are depopulated at lower energy than that required to populate the more extended conformer, or the large number of chloride adducts form ionic hydrogen bonds and/or salt bridges preventing unfolding to this larger conformer. Subsequent collisional activation results primarily in dissociation of the adduct ions, but also in CIU (see **Figure 5.10B**). Ultimately, the CCS of diUbq^{8-0+} ions settles upon a similar CCS to that of diUbq^{8+} ions acquired from

buffered solution, followed by a distinct transition to a gas-phase equilibrium conformation, but only after a higher collision energy than that required to populate a similar CCS of diUbq^{8+} ions from buffered solution. Interestingly, the most extended conformer is not populated unless all Cl^- adducts have dissociated, suggesting that either the energy required to produce this extended conformer is greater than the energy required for dissociation of all Cl^- adducts, or the Cl^- adduct(s) prevents population of this extended conformation via stabilizing intermolecular interactions. This very similar unfolding pattern is apparent in **Figure 5.10B**, but the average CCS is shifted to reflect the preference for more compact conformers overall.

The CIU profiles of K48-diUbq ions with a 9+ charge state are reported in **Figure 5.6**. As noted previously, highly chloride adducted K48-diUbq$^{(n-x)+}$ ions with a 9+ charge state exhibit a preference for more compact conformers with a CCS of ~1500 $Å^2$. Upon collisional activation, the CIU heat maps suggest a distinct transition to a more extended conformer (~1780 $Å^2$) observed of K48-diUbq^{9+} ions acquired from formic acid solution. Subsequent collisional activation results in sequential dissociation of chloride adducts and CIU that follows an overall similar gradual unfolding profile observed of K48-diUbq^{9+} ions as shown in **Figure 5.10B**, but shifted to lower average CCS representative of the preference for the more compact conformer populations. This same trend is observed of 10+, 11+ and 12+ ion populations.

5.3.4. CIU Suggests That the More Compact Conformers of Low Charge State K48-diUbq$^{(n-x)+}$ Ions are More Collapsed "Native-like" Conformers

As noted previously, the CIU fingerprints of K48-linked diUbq ions and the other linkage types are distinctly different, which is shown in the form of weighted CCS centroid profiles in **Figure 5.10C**. The distinct transitions between intermediate conformers of K63-diUbq^{n+} ions are indicated by a distinctly different weighted CCS centroid profile as a large change in slope for intermediate collision energies. These K63-diUbq$^{(n-x)+}$ weighted CCS centroid profiles are also distinctly different from those observed of K48-diUbq$^{(n-x)+}$ ions. We have previously reported that this unique CIU fingerprint is only observed when I44/I44 hydrophobic patch interactions are preserved (See Section 3). Overall, chloride adduction results in the preference for more compact conformers, and after collision induced depopulation of these compact conformers, the ions unfold in a similar manner to the K48-diUbq^{n+} ions through similar conformers. Interestingly, some of these intermediate conformers of K48-diUbq$^{(n-x)+}$ ions exhibit increased stabilities as evidenced by the weighted CCS centroid reaching some maximum and plateauing rather than further unfolding (see **Figure 5.10**). Therefore, we suggest that the ionic hydrogen bonds/salt bridges involving chloride adducts results in the preference for a more collapsed "native-like" conformer with very similar noncovalent interactions and that resists unfolding in the gas-phase.

K48-linked diUbq exists in equilibrium between closed conformers exhibiting I44/I44 interactions and an "open" conformation exhibiting electrostatic interactions.[34, 37, 53] The I44 hydrophobic patch is surrounded by basic residues (K6, K11, R42, R72,

and H68), the protonation of which may result in coulombic repulsion and possible destabilization of I44/I44 hydrophobic patch interactions.[34, 53] The recently reported noncovalent Ubq homodimer (ncUbq) has been suggested to exhibit similar interfacial interactions.[61, 63, 97] Furthermore, using cryogenic ion mobility mass spectrometry (cryo-IM-MS), Servage *et al.* determined that water plays a significant part in stabilization of ncUbq via occlusion of water from the hydrophobic interface as well as water-bridging the proximal basic side-chains to reduce the effects of coulombic repulsion.[39] Here, chloride adduct ions may perform a similar function in forming salt-bridges/ionic hydrogen bonds bridging the basic residues in close proximity to the I44 hydrophobic patch and resulting in significant gas-phase stabilization of I44/I44 hydrophobic patch interactions. Castañada et al. report that K11-linked diUbq in high concentrations of NaCl exhibits more compact conformers wherein the Ubq subunits are reoriented with respect to conformers observed without the salt.[137] It is therefore possible that the presence of chloride or even ammonium acetate in solution may induce a similar effect on K48-linked diUbq to populate the more compact conformers with a CCS of ~1500Å^2.

5.4. Conclusions

We have previously reported the use of ESI-IM-MS and CIU to probe linkage dependent differences in quaternary structure; furthermore, we have reported that chloride adduction to monoUbq results in the preference for “native-like” conformers and resistance to gas-phase unfolding. Here we investigate the ability of chloride adduct

ions to increase the gas-phase stability of more "native-like" conformations of K48-linked diUbq.

The presence of HCl in solution containing K48-linked diUbq results in abundant ions of the type K48-[diUbq + nH + xCl]$^{(n-x)+}$ (*i.e.* K48-diUbq$^{(n-x)+}$ ions) and an overall increase in abundance of lower charge state ions. The IMS CCS profiles of these chloride adducted diUbq ions suggest retention of more compact conformers. The CCS values of these more compact conformers observed of 8+, 9+, and 10+ charge states of K48-diUbq$^{(n-x)+}$ ions are very similar to the CCS values of lower charge states K48-diUbq^{n+} ions. In particular, chloride adducted K48-diUbq ions with charge states of 8+, 9+, and to a lesser extent 10+ appears to induce preference for the conformational populations with CCSs of ~1500 Å^2 and ~1780 Å^2. The more compact ~1500 Å^2 conformer population of diUbq^{9+} ions has been previously attributed to an acid induced molten globule conformation (see Section 2);[86] however, a conformational population with a similar CCS is also populated by diUbq^{7+} and diUbq^{8+} ions acquired from buffered solution. This suggests that the more compact conformers observed from HCl acidified solution may be "native-like" in conformation.

As noted previously, the CIU fingerprint of K48-diUbq^{n+} ions is unique when compared to other diUbq ions due to the stabilization of the β-sheet subunit structure via I44/I44 hydrophobic patch interactions (see Section 3). From this understanding of the CIU of K48-diUbq^{n+} ions acquired from formic acid solution, we are able to show that not only is a more compact conformer observed of K48-diUbq$^{(n-x)+}$ ions, but also that these ions exhibit "native-like" noncovalent interactions. The lower charge states of

K48-diUbq$^{(n-x)+}$ transition through conformers in a gradual manner similarly to those observed of K48-diUbq^{n+} ions, rather than the distinct transitions observed of diUbq with alternative interfacial interactions. Interestingly, *en route* to the gas-phase equilibrium conformers observed of K48-diUbq^{n+} ions, each K48-diUbq$^{(n-x)+}$ ion reaches some intermediate conformer where collisional activation results not in unfolding in the gas-phase but instead in the dissociation of an additional Cl^- adduct. This suggests that each K48-diUbq$^{(n-x)+}$ has a unique gas-phase equilibrium conformation much lower in CCS than that observed of K48-diUbq^{n+} ions. Finally, K48-diUbq$^{(n-x)+}$ ions that have lost all Cl^- adducts, *i.e.* K48-diUbq$^{(n-0)+}$ ions require more collision energy to populate the most extended conformations than that required of K48-diUbq^{n+} from formic acid solution. This suggests that the dissociation of a Cl^- adduct from K48-linked diUbq ions may result in the dissipation of collision-induced increases in the E_{int}, as noted by Han *et al.* for protein complexes.[74-75]

6. CONCLUSIONS AND FUTURE DIRECTIONS

6.1. Towards a Better Understanding of Polyubiquitin Structure

Here we present evidence that ESI-IM-MS experiments alone lack the resolution necessary to differentiate the unique quaternary structures of different covalently-linked diubiquitin (diUbq) ions; however, CIU analysis produces unique unfolding fingerprints for each diUbq ion allowing for differentiation of these distinct quaternary structures. More specifically, the noncovalent intramolecular interactions of K48-linked diUbq are distinctly different as indicated by conformational broadening and gradual unfolding as opposed to the distinct unfolding intermediate conformational families observed of K6-, K11-, and K63-linked diUbq. We suggest that the interfacial interaction between K48-linked diUbq subunits, *i.e.* I44/I44 hydrophobic patch interactions and noncovalent interactions between proximal basic residues, results in unique gas-phase stabilization against subunit unfolding and thus a more gradual transition to gas-phase equilibrium conformers. This observation is further affirmed by the distinct unfolding transitions observed of K48-linked diUbq upon solvent-induced denaturation, possibly due to disruption of the β-sheet structure containing the I44 hydrophobic patch.

The CIU fingerprints shown for K6-, K11-, and K63-linked diUbq ions demonstrate that the gas-phase unfolding process proceeds through distinct conformational intermediates. Due to the complete inaccessibility of native K63-linked diUbq to form hydrophobic interfacial interactions, “closed” conformers of K63-linked diUbq reported by NMR experiments are shown with purely electrostatic interfacial

interactions.[40, 55] The similarity between the CIU fingerprints of K6-, K11-, and K63-linked diUbq ions could indicate that K6- and K11-linked diUbq form primarily electrostatic interfacial interactions. Furthermore, the differing collision energies necessary to induce unfolding for each linkage type may be evidence of different numbers of salt bridge/ionic hydrogen bonds. Alternatively, the I36 hydrophobic patch is not in a position to provide significant gas-phase stabilization of the Ubq subunits; therefore, any hydrophobic patch interaction involving the I36 patch (*i.e.* I36/I36 or I36/I44) would leave the weakly hydrogen bonded β-sheet of at least one subunit vulnerable to unfolding. Consequently, it is possible that the gradual unfolding pattern observed of K48-linked diUbq is unique.

The CIU fingerprint of ncUbq is nearly identical to that observed of K48-linked diUbq ions; the observation that the other linkage types of diUbq ions demonstrate dramatically different unfolding patterns only solidifies the assumption that ncUbq has a very similar structure to the I44/I44 interfacial K48-linked diUbq. In addition, the depopulation of ncUbq prior to populating the most extended conformation of K48-linked diUbq suggests that subunit interfacial interactions are only completely lost at this point. The stability of I44/I44 interactions with reference to proximal basic residues and the role of water have previously been alluded to by Servage *et al.* using cryo-IM-MS studies.[63] The preference of ncUbq for I44/I44 subunit interfacial interactions suggests that this interface is preferred in solution, and perhaps that it is only the steric hindrance of the covalent tether that prevents K6-, K11-, and K63-linked diUbq from adopting a similar interface. Overall, these studies demonstrate the first step in the application of

ESI-IM-MS and CIU toward interrogating Ubq oligomer quaternary structures, but a large number of questions remain unanswered. This is particularly true of K6- and K11-linked diUbq; even with CIU fingerprints, very few conclusions can be drawn concerning the structures of these molecules.

6.1.1. MDS Simulated Theoretical CIU Structures

Molecular dynamics simulations (MDS) have proven an effective complementary technique to IM-MS experiments in the pursuit of more detailed structural information.[11-13] MDS can provide the means to monitor changes in structure/CCS as a function of temperature and thus mimic the CIU experiment.[29, 72] Thus a theoretical CIU map might be calculated from differing starting structures extracted from the Protein Data Bank and used to interrogate experimental CIU fingerprints. In particular, these studies would make further interrogation of the more biologically relevant longer, heterogeneous, or branched polyUbq structures more fruitful.

6.1.2. Thermal Analysis of PolyUbq Solution-Phase Stability and Structural Transitions

Using differential scanning calorimetry (DSC), Morimoto *et al.* report that the thermal stability of polyUbq decreases as a function of chain length, the thermal stability is lower for K63-linked polyUbq vs. K48-linked polyUbq, and although monoUbq refolds upon cooling, thermal unfolding of polyUbq is irreversible which was attributed to the heat-induced formation of fibrils.[138] Similarly, recent investigations have determined that of metal ions, Cu(II) uniquely influences monoUbq thermal stability[139]

and induces Ubq aggregation.[140] Cong *et al.*[141] and El-Baba *et al.*[142] have recently developed solution-phase temperature control units for interface with ESI-IM-MS measurements. Of particular note, El-Baba *et al.* demonstrate the use of solution-phase unfolding analysis to probe the thermal denaturation of Ubq.[142] Thermal analysis of Ubq using ESI-IM-MS resulted in a distinct transition in average charge state indicative of the transition from a folded to a denatured state such that the thermal unfolding temperature is found in good agreement with the literature; furthermore, IM-MS analysis revealed unique denatured states.[142] Solution-phase thermal denaturation, followed by ESI-IM-MS provides a means to interrogate the relative stability of each of the linkage types of diUbq as well as probe any conformational changes induced by thermal denaturation prior to large scale aggregation. Furthermore, similar thermal denaturation analyses could provide insight into the structural effects of Cu(II) binding to monoUbq, as well as interrogate the interfacial interactions of early low mass aggregates.

6.2. Towards a Better Understanding of Protein-Salt Interactions: The Pursuit of Hofmeister Effects

The Hofmeister series is the ordering of cations and anions based upon their ability to "salt in" or "salt out" a protein. The mechanism(s) of these effects is still oft debated, but generally is attributed to either direct interaction of the ions with the protein, perturbation of water structure, or a combination thereof.[112-117] Anions tend to have the strongest influence on protein structure owing to their high affinity for the protein backbone.[112, 116-118] In particular, the halide motif, *i.e.* "the interaction motif of a

non-bonded halogen ion with two or more electrophiles simultaneously," is relatively prolific throughout the PDB.[119] Here, we have presented evidence that chloride adduction results in an increase in gas-phase stability of more compact conformers of both monoUbq and K48-linked diUbq. Chloride ions are capable of a multitude of simultaneous direct interactions with basic side-chains, polar side-chains, and backbone moieties. Therefore, we posit that the chloride adducts participate in a network of coordinated ionic hydrogen bonds and salt-bridges, thus linking the protein backbone and inducing resistance to gas-phase unfolding. Furthermore, we report that the lower average charge states of K48-linked diUbq ions acquired from HCl solution than those acquired from formic acid and the remarkably similar CIU fingerprints suggest not only the preference for more compact conformers, but also a higher retention of more "native-like" non-covalent interactions.

6.2.1. The Effects of Salt on PolyUbq Solution-Phase Structures

Castañada *et al.* report that K11-linked diUbq in high concentrations of NaCl exhibits more compact conformers wherein the Ubq subunits are reoriented with respect to conformers observed without the salt.[137] It is therefore possible that the presence of chloride in solution may induce a similar effect on K48-linked diUbq resulting in the population of the more compact conformer population with a CCS of ~1500Å^2. A similar study using K11-linked diUbq could clarify whether a salt-induced more compact solution-phase conformer is being observed, or the preservation of more "native-like" conformers via resistance to gas-phase unfolding. Furthermore, heat-

controlled ESI-IM-MS experiments could directly probe the influence of HCl or other salts on the thermal stability of the various diUbq ions.

6.2.2. The Effect of Halide Adduction on MonoUbq Gas-Phase Stability

The studies presented in this thesis have focused on the use of chloride adduction for gas-phase stabilization of Ubq. Han *et al.* used a range of anions for the gas-phase stabilization of protein complexes; chloride was adept at stabilizing the protein complex, whereas the presence of iodide had little to no stabilizing effect on the protein complex.[143] Interestingly, Merenbloom *et al.* did not observe chloride adducts, but did note that monoUbq ions with large numbers of iodide adducts exhibited a more compact conformer than the elongated conformers observed without adducts.[73] However, these studies do little to clarify under what conditions and to what extent does iodide stabilize or destabilize protein structure both in solution and in the gas-phase. The Hofmeister series orders the halides as $F^- < Cl^- < Br^- < I^-$ largely due to their differing charge densities. The smaller halides with high charge density on the left tend to contribute to the ordering of water molecules and "salt-out" proteins, *i.e.* are more kosmotropic, whereas those to the larger halides with much more diffuse charge tend to disrupt water structure/ordering and "salt-in" proteins , *i.e.* are more chaotropic. [144] Furthermore, the halides differ in their binding affinities for the different basic residues as well as the site of interaction; for example, iodide and bromide tend to exhibit more interactions with nonpolar moieties and different backbone coordination propensities than fluoride or chloride.

Abundant ions of the type $[M + nH + xX]^{(n-x)+}$ are observed in the ESI-MS mass spectra of monoUbq acquired from 10mM HCl, HBr, and HI solutions (see **Figure 6.1** in black, red, and blue, respectively). The numbers of observed anion adducts increases in the order of $Cl^- < Br^- < I^-$; note that fluoride is not observed as an adduct ion. Kim *et al.* have reported MDS simulations demonstrating the behavior of chloride in an ESI droplet containing HCl and the small amphipathic peptide substance P.[70] Because chloride ions have a relatively high affinity for water, the chloride ions remain associated with water and few leave the droplet through fission events. In the final stages of desolvation, the remaining chloride anions cluster around the basic residues of the peptide and participate

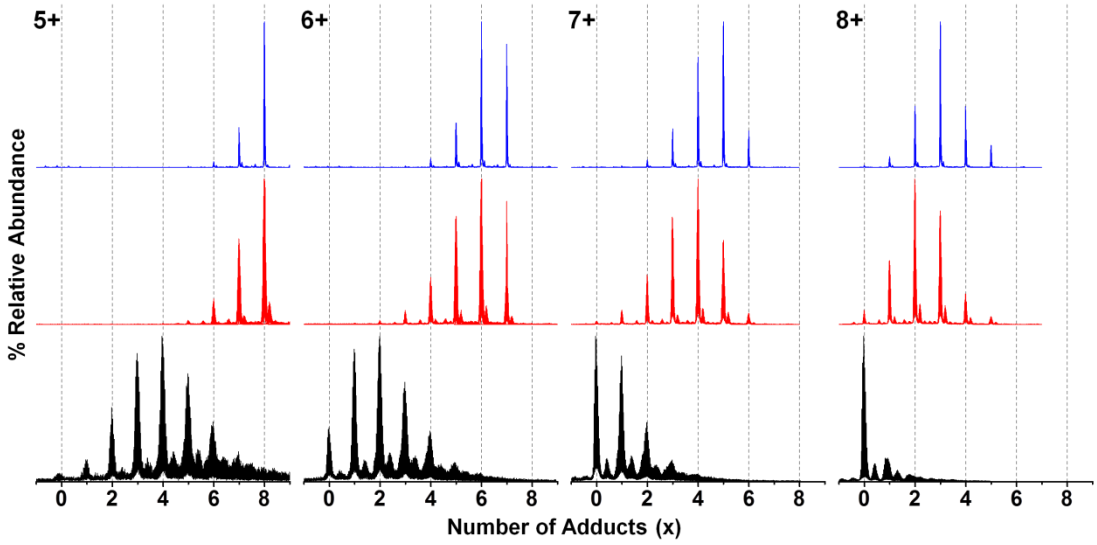

Figure 6.1. Selected regions of the ESI mass spectra of HCl (black), HBr (red), and HI (blue) acidified ubiquitin showing 5 – 8+ ions (from left to right) where a distribution of $[Ubq + nH + xX]^{(n-x)+}$ ions are observed. Note that the x-axis has been adjusted to show the number of halide adducts (x) rather than m/z for ease of comparison.

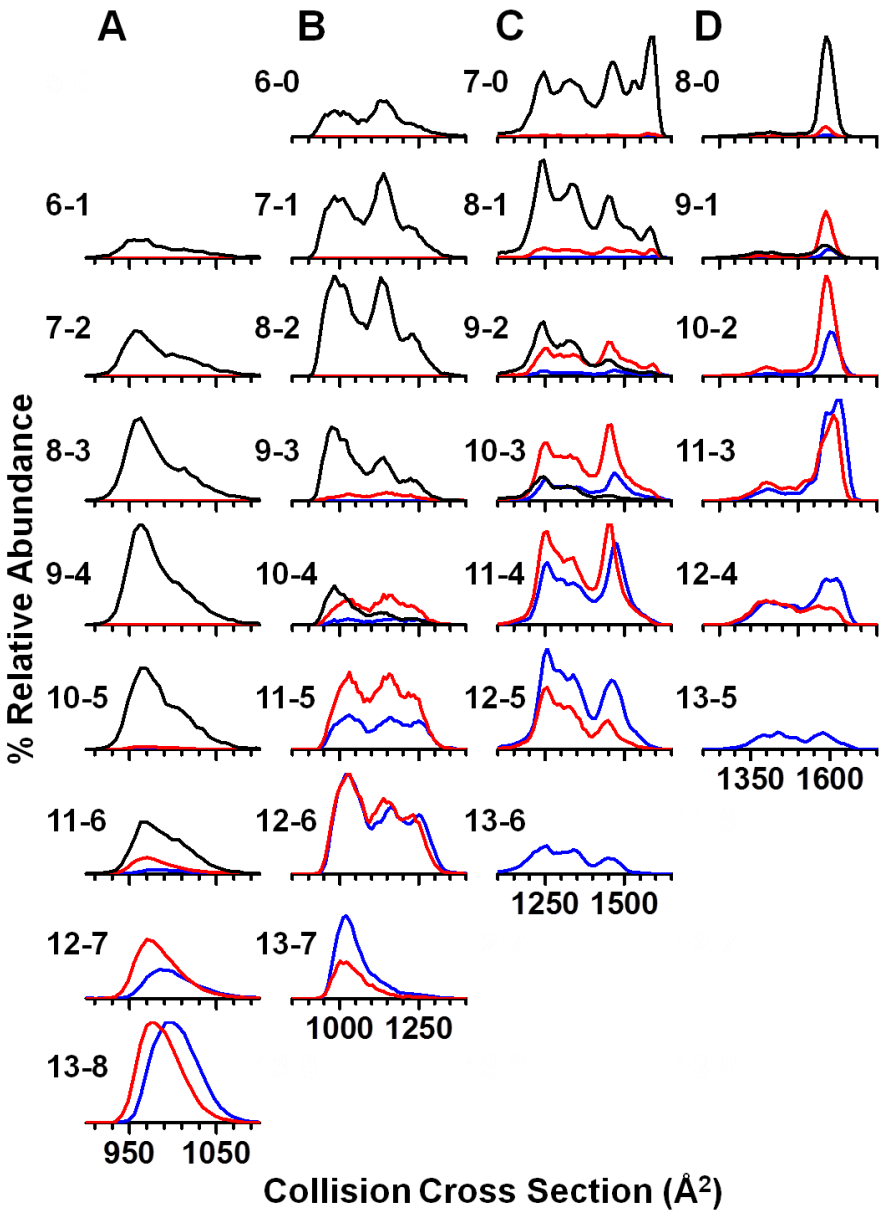

Figure 6.2. CCS profiles of $[Ubq + nH + xX]^{(n-x)+}$ ions acquired with minimal collision energy and 1000-fold excess of HCl (black), HBr (blue) and HI (red). The notation to the left of each CCS profile denotes the values of n and x of the selected ion population (as n-x). The CCS profiles of A through D correspond to ubiquitin ions where the total charges are 5+, 6+, 7+, and 8+, respectively. Note that the % relative abundance of each CCS profile is scaled according to the relative abundance of said ion to the other adduct ions of the same charge state. For example, the $[Ubq + 9H + 4Cl]^{5+}$ ion is the most abundant of the $[Ubq + nH + xCl]^{5+}$ ion population and as such is scaled to 100% relative abundance.

of intermolecular charge solvation. Bromide and iodide have relatively low water affinities which may suggest the preference to directly bind to the protein as opposed to being fully hydrated or may drive their migration to the surface of the droplet.[145] The increased abundance of bromide and iodide adducts suggests that the decreased water affinity of these anions drives their association with the protein within the droplet.

As noted previously for chloride adducted monoUbq ions, the CCS profiles of highly adducted $[Ubq + nH + xX]^{(n-x)+}$ ions acquired with minimal collision energy from HBr and HI solution suggests an increased preference for more compact conformers (See **Figure 6.2**). These compact conformers are shifted slightly to larger CCS values, which could indicate a change in conformation or a general increase in size induced by the addition of eight relatively large iodide or bromide ions. Interestingly, more bromide and iodide adducts are required to induce a similar preference for compact conformers as that observed for chloride adduction, *i.e.* seven bromide and seven iodide adducts are necessary to completely depopulate the intermediate conformation of 6+ Ubq ions, but only four chloride induces a similar preference.

A compilation of collisional activation results for chloride, bromide, and iodide adducted ubiquitin ions with a total charge of 5+ and 6+ are shown in **Figure 6.3** and **Figure 6.4**, respectively (see Section 5 for details concerning data analysis, CIU heat maps are shown in Appendix B). Interestingly, the most extended gas-phase equilibrium conformations are only observed upon complete dissociation of all halide adducts. Chloride adducted monoUbq ions follow a similar unfolding trajectory as that observed

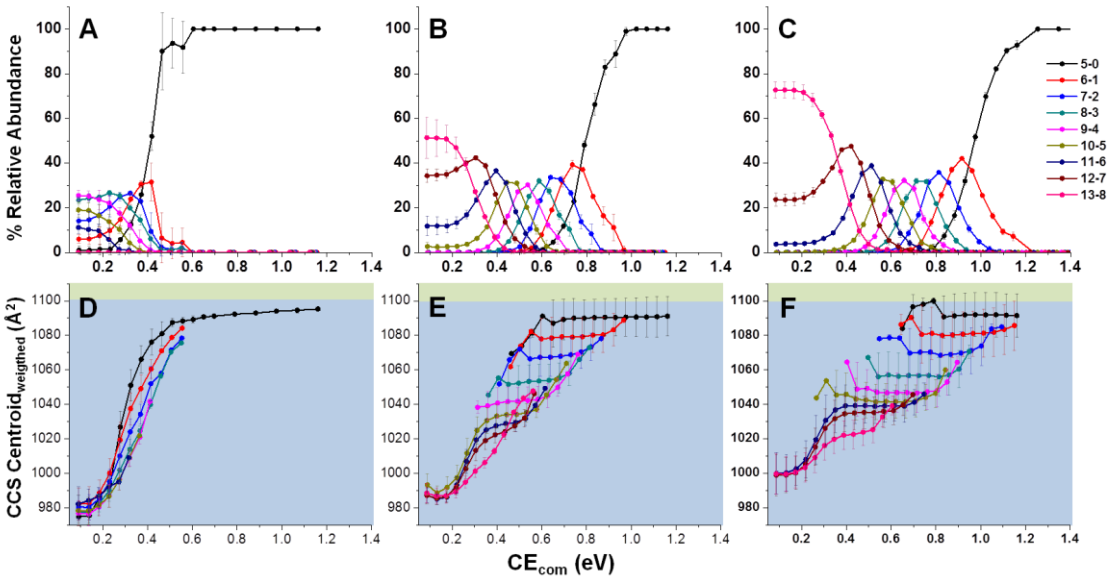

Figure 6.3. Collisional activation of 5+ adduct ion populations. (A-C) Relative abundance of each [Ubq + nH + xX]$^{5+}$ adduct and (D-F) calculated weighted CCS centroid values as a function of center-of-mass frame collision energy where the adduct anions (X) are Cl^-, Br^-, and I^- (left to right, respectively). Note that the % relative abundance of each ion population is scaled according to the abundance of the other adduct ions of the same charge state such that the sum of all [Ubq + nH + xX]$^{5+}$ ions of each charge and at each collision energy is 100%. Background color coding denotes the transition from >50% C conformer ions (blue) to >50% I conformer ions (green).

of unadducted monoUbq ions (See the [M + 5H]$^{5+}$ ion unfolding pattern acquired from HCl containing solution in **Figure 6.3D** and the unfolding pattern of [M + 6H]$^{6+}$ ions acquired from 0.1% formic acid solution shown in **Figure 6.4D**), but with increased preference for more compact conformers despite collisional activation. The bromide and iodide adducted monoUbq ions instead appear to reach some gas-phase equilibrium conformer that is stabilized across a range of collision energies; unfolding of this conformer is not observed without dissociation of an additional bromide or iodide adduct. This could be a similar effect to that proposed by Bartman *et al.* wherein

collisional activation of ion adducted protein results in structural inversion to an alternative gas-phase structure.[136] Overall these results show that chloride, bromide, and iodide adduction induce gas-phase stabilization of the target protein; however, further analysis is necessary to comment on the actual structure of these ions. Toward that end, additional analysis using K48-linked diUbq ions similar to that reported in Section 5 could shed more light on the effect of bromide and iodide adducts on protein structure.

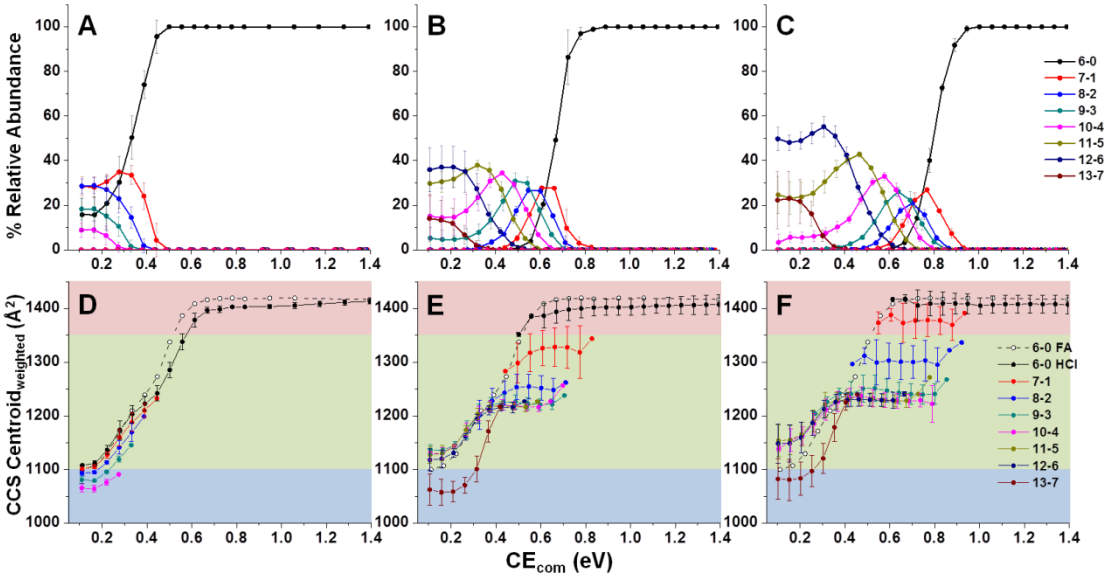

Figure 6.4. Collisional activation of 6+ adduct ion populations. (A-C) Relative abundance of each $[Ubq + nH + xX]^{6+}$ adduct and (D-F) calculated weighted CCS centroid values as a function of center-of-mass frame collision energy where the adduct anions (X) are Cl^-, Br^-, and I^- (left to right, respectively). Note that the % relative abundance of each ion population is scaled according to the abundance of the other adduct ions of the same charge state such that the sum of all $[Ubq + nH + xX]^{6+}$ ions of each charge and at each collision energy is 100%. The calculated weighted CCS centroid values of the $[Ubq + 6H]^{6+}$ ion population acquired from 0.1% formic acid as a function of center-of-mass frame collision energy is shown for comparison (open circle, black dash). Background color coding denotes the transition from >50% C conformer ions (blue) to >50% I conformer ions (green), and to >50% E conformer ions (red).

6.2.3. Using ESI-IM-MS and Thermal Analysis to Gain Insight into "Salting-in" and "Salting-out" Processes

Overall, the work presented here provides insight into the effect of halide adduction on gas-phase protein structure and stability; however, these studies provide little insight into the effect of halides on protein solution-phase structure, *i.e.* Hofmeister effects. It has been previously shown using differential scanning calorimetry (DSC) that chloride binding induces significant thermal stabilization of monoUbq.[123] A similar study monitored the secondary structural changes induced by thermal denaturation using circular dichroism in the presence of various salts.[146] The previously noted thermal analysis ESI-IM-MS experiment[142] provides the means to expand this analysis to both other salts and polyUbq ions, wherein ESI-IM-MS could be used to probe more global structural changes.

Here a preliminary analysis of the solution-phase heat-induced unfolding of monoUbq in formic acid and hydrochloric acid solutions is presented. Thermal control was established using a simple "coffee cup apparatus" wherein the capillary containing the sample was submerged within a coffee cup containing various temperatures of water in-line with the ESI source. The resulting full ESI mass spectra are shown in **Figure 6.5** and **Figure 6.6** for formic acid and HCl containing solutions, respectively. The influence of solution temperature on charge state is observed similar to that of El-Baba *et al.*[142]; however, the CCS profiles of each ion population was identical to those acquired without solution-phase heating, suggesting that the Waters Synapt G2 HDMS instrument lacks the resolution to identify the heat-induced conformers noted. **Figure 6.7** shows the

calculated average charge state of ions acquired from each temperature and using both solutions conditions (note that the abundance of each ion was calculated from the area of the ion's CCS profile; chloride adduct ions were included in the average charge state calculation based upon their total charge).

The average charge state of Ubq ions acquired from formic acid and HCl solution at 2°C is ~7.4 and ~7.6, respectively, suggesting that Ubq ions electrosprayed from HCl

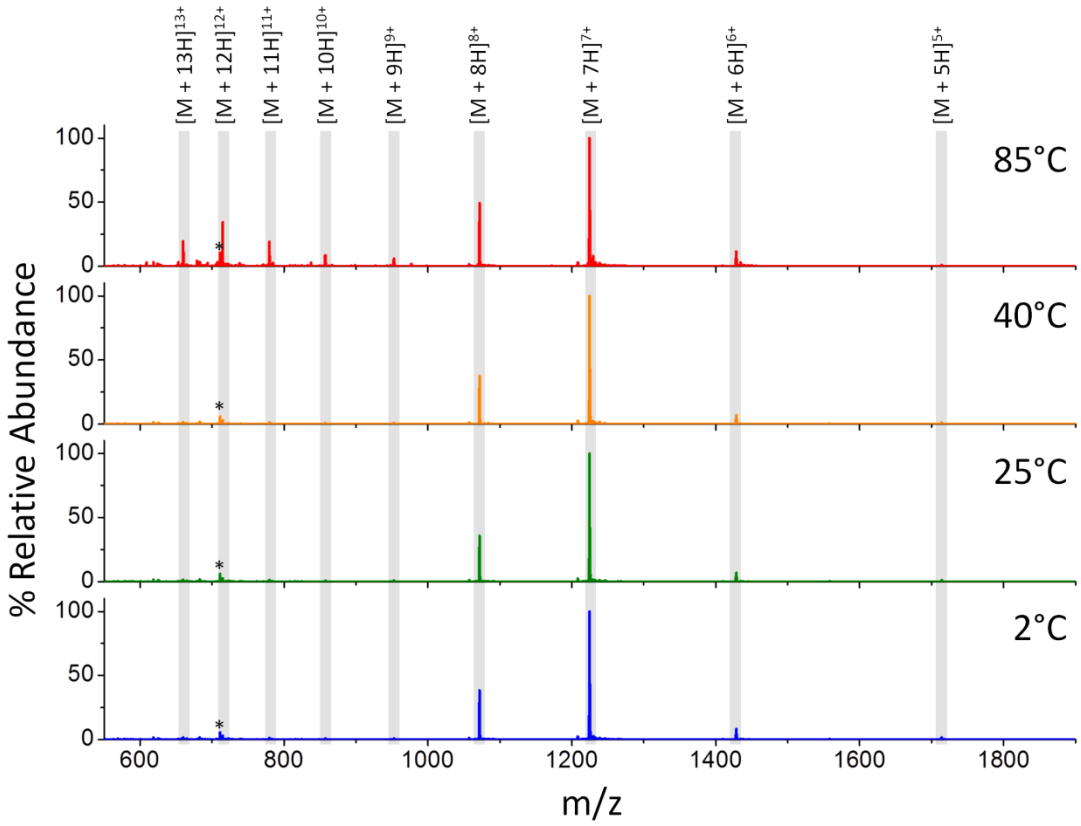

Figure 6.5. Full mass spectra of ubiquitin ions acquired from 99.9% water/0.1% formic acid at various solution temperatures.

solution may contain a higher population of denatured conformers; however, the average charge state of monoUbq ions incubated at ~85°C in formic acid solution is relatively higher than the average charge state observed at the same temperature from HCl solution. In fact, the average charge state of monoUbq acquired from HCl solution changes relatively little despite the large fluctuation in solution temperature. The large number of low charge states remaining for both solution conditions at 85°C suggests that

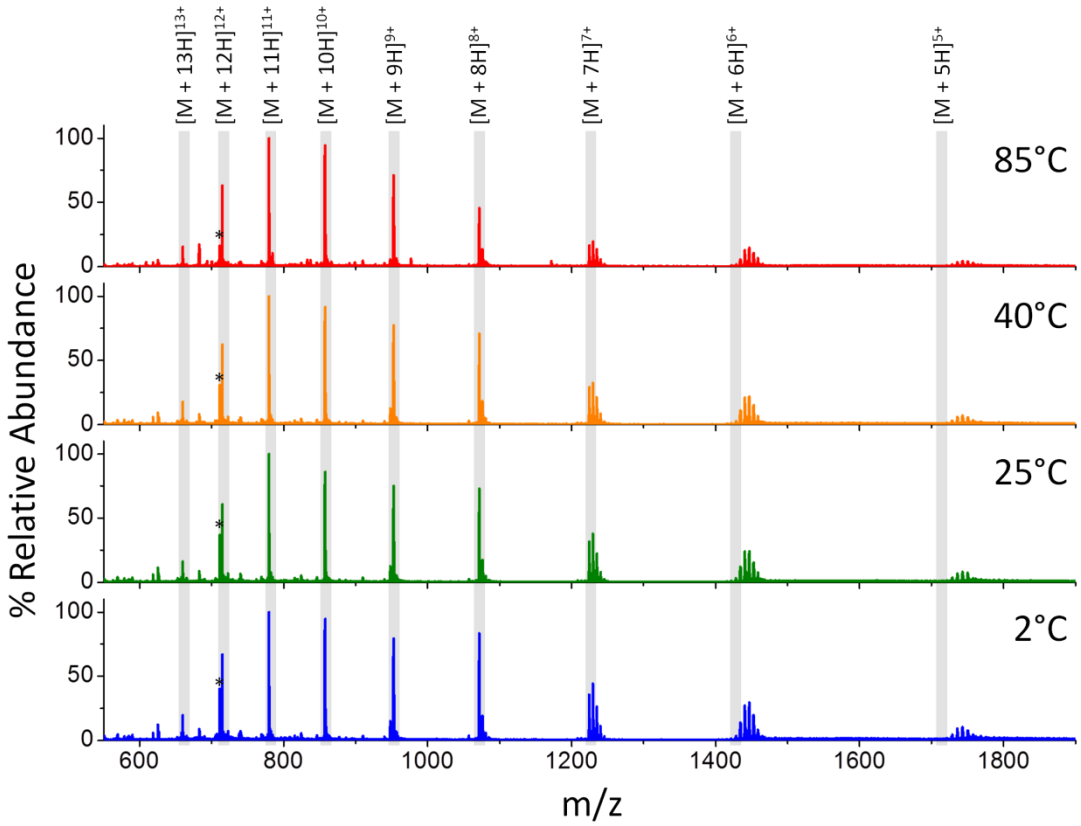

Figure 6.6. Full mass spectra of ubiquitin ions acquired from 99.9% water/0.1% hydrochloric acid at various solution temperatures.

the thermal denaturation of monoUbq in both solution conditions is incomplete, but it is apparent that the unfolding transition temperature for monoUbq acquired from HCl solution will be higher than that observed from formic acid solution. More precise analysis concerning the effects of chloride and other ionic solutes on the solution-phase thermal denaturation of proteins as observed through changes in average ESI-MS charge state and possible changes in ESI-IM-MS CCS profiles could provide new insight into the "salting in" and "salting out" effects observed for Hofmeister salts. A particularly interesting study would probe the influence of ammonium acetate, the most common ESI-MS buffer for native MS analyses, and other buffers on the solution-phase stability of various proteins.

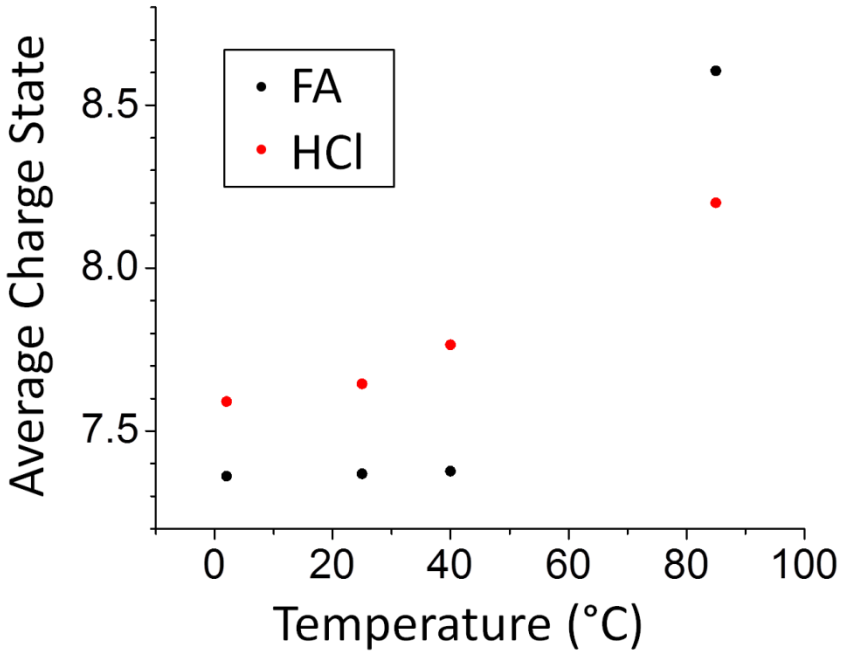

Figure 6.7. Calculated average charge states of ubiquitin ions acquired from 99.9% water and either 0.1% formic acid (black) or 0.1% hydrochloric acid (red).

REFERENCES

1. Bork, P.; Jensen, L. J.; Von Mering, C.; Ramani, A. K.; Lee, I.; Marcotte, E. M., Protein interaction networks from yeast to human. *Curr. Opin. Struct. Biol.* **2004,** *14* (3), 292-299.
2. Laatikainen, R.; Niemitz, M.; Malaisse, W. J.; Biesemans, M.; Willem, R., A computational strategy for the deconvolution of NMR spectra with multiplet structures and constraints: Analysis of overlapping 13C-2H multiplets of 13C enriched metabolites from cell suspensions incubated in deuterated media. *Magn. Reson. Med.* **1996,** *36* (3), 359-365.
3. Ryabov, Y. E.; Fushman, D., A Model of Interdomain Mobility in a Multidomain Protein. *J. Am. Chem. Soc.* **2007,** *129* (11), 3315-3327.
4. Chylla, R. A.; Hu, K.; Ellinger, J. J.; Markley, J. L., Deconvolution of Two-Dimensional NMR Spectra by Fast Maximum Likelihood Reconstruction: Application to Quantitative Metabolomics. *Anal. Chem.* **2011,** *83* (12), 4871-4880.
5. Loo, J. A., Studying noncovalent protein complexes by electrospray ionization mass spectrometry. *Mass Spectrom. Rev.* **1997,** *16*, 1-23.
6. Heck, A. J. R., Native mass spectrometry : a bridge between interactomics and structural biology. *Nat. Methods* **2008,** *5* (11), 927-933.
7. Cubrilovic, D.; Biela, A.; Sielaff, F.; Steinmetzer, T.; Klebe, G.; Zenobi, R., Quantifying Protein-Ligand Binding Constants using Electrospray Ionization

Mass Spectrometry: A Systematic Binding Affinity Study of a Series of Hydrophobically Modified Trypsin Inhibitors. *J. Am. Soc. Mass Spectrom.* **2012,** *23* (10), 1768-77.

8. Laganowsky, A.; Reading, E.; Hopper, J. T. S.; Robinson, C. V., Mass spectrometry of intact membrane protein complexes. *Nat. Protoc.* **2013,** *8* (4), 639-51.

9. Zhou, M.; Jones, C. M.; Wysocki, V. H., Dissecting the Large Noncovalent Protein Complex GroEL with Surface-Induced Dissociation and Ion Mobility–Mass Spectrometry. *Anal. Chem.* **2013,** *85* (17), 8262-8267.

10. Zhang, X.; Julian, R. R., Investigating the gas phase structure of KIX with radical directed dissociation and molecular dynamics: Retention of the native structure. *Int. J. Mass Spectrom.* **2011,** *308* (2–3), 225-231.

11. Fernandez-Lima, F. A.; Wei, H.; Gao, Y. Q.; Russell, D. H., On the structure elucidation using ion mobility spectrometry and molecular dynamics. *J. Phys. Chem. A* **2009,** *113* (29), 8221-34.

12. Pierson, N. A.; Chen, L.; Valentine, S. J.; Russell, D. H.; Clemmer, D. E., Number of solution States of bradykinin from ion mobility and mass spectrometry measurements. *J. Am. Chem. Soc.* **2011,** *133* (35), 13810-3.

13. Chen, L.; Shao, Q.; Gao, Y.-q.; Russell, D. H., Molecular Dynamics and Ion Mobility Spectrometry Study of Model beta-hairpin peptide Trpzip1. *J. Phys. Chem. A* **2011,** *115* (17), 4427-4435.

14. Wysocki, V. H.; Jones, C. M.; Galhena, A. S.; Blackwell, A. E., Surface-induced dissociation shows potential to be more informative than collision-induced dissociation for structural studies of large systems. *J. Am. Soc. Mass Spectrom.* **2008,** *19* (7), 903-913.

15. Zhong, Y.; Han, L.; Ruotolo, B. T., Collisional and Coulombic unfolding of gas-phase proteins: high correlation to their domain structures in solution. *Angew. Chem.* **2014,** *53* (35), 9209-12.

16. Hopper, J. T. S.; Oldham, N. J., Collision induced unfolding of protein ions in the gas phase studied by ion mobility-mass spectrometry: the effect of ligand binding on conformational stability. *J. Am. Soc. Mass Spectrom.* **2009,** *20* (10), 1851-8.

17. Freeke, J.; Robinson, C. V.; Ruotolo, B. T., Residual counter ions can stabilise a large protein complex in the gas phase. *Int. J. Mass Spectrom.* **2010,** *298*, 91-98.

18. Laganowsky, A.; Reading, E.; Allison, T. M.; Ulmschneider, M. B.; Degiacomi, M. T.; Baldwin, A. J.; Robinson, C. V., Membrane proteins bind lipids selectively to modulate their structure and function. *Nature* **2014,** *510* (7503), 172-5.

19. Liu, J.; Konermann, L., Cation-induced stabilization of protein complexes in the gas phase: mechanistic insights from hemoglobin dissociation studies. *J. Am. Soc. Mass Spectrom.* **2014,** *25* (4), 595-603.

20. Eschweiler, J. D.; Rabuck-Gibbons, J. N.; Tian, Y.; Ruotolo, B. T., CIUSuite: A Quantitative Analysis Package for Collision Induced Unfolding Measurements of Gas-Phase Protein Ions. *Anal. Chem.* **2015,** *87* (22), 11516-22.

21. Wagner, N. D.; Kim, D.; Russell, D. H., Increasing Ubiquitin Ion Resistance to Unfolding in the Gas Phase Using Chloride Adduction: Preserving More "Native-Like" Conformations Despite Collisional Activation. *Anal. Chem.* **2016,** *88* (11), 5934-5940.

22. Fenwick, R. B.; van den Bedem, H.; Fraser, J. S.; Wright, P. E., Integrated description of protein dynamics from room-temperature X-ray crystallography and NMR. *Proc. Natl. Acad. Sci.* **2014,** *111* (4), E445-E454.

23. Nyon, M. P.; Prentice, T.; Day, J.; Kirkpatrick, J.; Sivalingam, G. N.; Levy, G.; Haq, I.; Irving, J. A.; Lomas, D. A.; Christodoulou, J.; Gooptu, B.; Thalassinos, K., An integrative approach combining ion mobility mass spectrometry, X-ray crystallography, and nuclear magnetic resonance spectroscopy to study the conformational dynamics of α(1)-antitrypsin upon ligand binding. *Protein Sci.* **2015,** *24* (8), 1301-1312.

24. Lenkinski, R. E.; Chen, D. M.; Glickson, J. D.; Goldstein, G., Nuclear magnetic resonance studies of the denaturation of ubiquitin. *Biochim. Biophys. Acta* **1977,** *494* (1), 126-130.

25. Vijay-Kumar, S.; Bugg, C. E.; Wilkinson, K. D.; Cook, W. J., Three-dimensional structure of ubiquitin at 2.8 A resolution. *Proc. Natl. Acad. Sci.* **1985,** *82* (11), 3582-3585.

26. Sloper-Mould, K. E.; Jemc, J. C.; Pickart, C. M.; Hicke, L., Distinct functional surface regions on ubiquitin. *J. Biol. Chem.* **2001,** *276* (32), 30483-9.

27. Komander, D.; Rape, M., The Ubiquitin Code. *Annu. Rev. Biochem.* **2012,** *81*, 203-29.

28. Koeniger, S. L.; Clemmer, D. E., Resolution on structural transitions of elongated states of ubiquitin. *J. Am. Soc. Mass Spec.* **2007,** *18*, 322-331.

29. Segev, E.; Wyttenbach, T.; Bowers, M. T.; Gerber, R. B., Conformational evolution of ubiquitin ions in electrospray mass spectrometry: molecular dynamics simulations at gradually increasing temperatures. *Phys. Chem. Chem. Phys.* **2008,** *10* (21), 3077-3082.

30. Wyttenbach, T.; Bowers, M. T., Structural stability from solution to the gas phase: native solution structure of ubiquitin survives analysis in a solvent-free ion mobility-mass spectrometry environment. *J. Phys. Chem. B* **2011,** *115* (42), 12266-75.

31. Dikic, I.; Wakatsuki, S.; Walters, K. J., Ubiquitin-binding domains - from structures to functions. *Nat. Rev. Mol. Cell Biol.* **2009,** *10* (10), 659-71.

32. Wickliffe, K. E.; Williamson, A.; Meyer, H. J.; Kelly, A.; Rape, M., K11-linked ubiquitin chains as novel regulators of cell division. *Trends Cell Biol.* **2011,** *21* (11), 656-63.

33. Husnjak, K.; Dikic, I., Ubiquitin-binding proteins: decoders of ubiquitin-mediated cellular functions. *Annu. Rev. Biochem* **2012,** *81*, 291-322.

34. Lai, M. Y.; Zhang, D.; Laronde-Leblanc, N.; Fushman, D., Structural and biochemical studies of the open state of Lys48-linked diubiquitin. *Biochim. Biophys. Acta* **2012,** *1823* (11), 2046-56.

35. Castaneda, C. A.; Kashyap, T. R.; Nakasone, M. A.; Krueger, S.; Fushman, D., Unique structural, dynamical, and functional properties of k11-linked polyubiquitin chains. *Structure* **2013,** *21* (7), 1168-81.

36. Avram, H., The Ubiquitin System. In *Ubiquitin and the Biology of the Cell*, Peters, J.-M.; Harris, J. R.; Finley, D., Eds. Springer US: 1998.

37. Varadan, R.; Walker, O.; Pickart, C.; Fushman, D., Structural Properties of Polyubiquitin Chains in Solution. *J. of Mol. Biol.* **2002,** *324* (4), 637-647.

38. Varadan, R.; Assfalg, M.; Haririnia, A.; Raasi, S.; Pickart, C.; Fushman, D., Solution conformation of Lys63-linked di-ubiquitin chain provides clues to functional diversity of polyubiquitin signaling. *J. Biol. Chem.* **2004,** *279* (8), 7055-63.

39. Fushman, D.; Wilkinson, K. D., Structure and recognition of polyubiquitin chains of different lengths and linkage. *F1000 Biol. Rep.* **2011,** *3*, 26.

40. Ye, Y.; Blaser, G.; Horrocks, M. H.; Ruedas-Rama, M. J.; Ibrahim, S.; Zhukov, A. A.; Orte, A.; Klenerman, D.; Jackson, S. E.; Komander, D., Ubiquitin chain conformation regulates recognition and activity of interacting proteins. *Nature* **2012,** *492* (7428), 266-70.

41. Collins, C. A.; Brown, E. J., Cytosol as battleground: ubiquitin as a weapon for both host and pathogen. *Trends Cell Biol.* **2010,** *20* (4), 205-13.

42. Kleiger, G.; Mayor, T., Perilous journey: a tour of the ubiquitin-proteasome system. *Trends Cell Biol.* **2014,** *24* (6), 352-9.

43. Schnell, J. D.; Hicke, L., Non-traditional functions of ubiquitin and ubiquitin-binding proteins. *J. Biol. Chem.* **2003,** *278* (38), 35857-60.

44. Kulathu, Y.; Komander, D., Atypical ubiquitylation — the unexplored world of polyubiquitin beyond Lys48 and Lys63 linkages. *Nat. Rev. Mol. Cell Biol.* **2012,** *13* (8), 508-523.

45. Bennett, E. J.; Harper, J. W., DNA damage: ubiquitin marks the spot. *Nat. Struct. Mol. Biol.* **2008,** *15* (1), 20-22.

46. Chen, Z. J.; Sun, L. J., Nonproteolytic functions of ubiquitin in cell signaling. *Mol. Cell* **2009,** *33* (3), 275-86.

47. Wertz, I. E.; Newton, K.; Seshasayee, D.; Kusam, S.; Lam, C.; al., e., Phosphorylation and linear ubiquitin direct A20 inhibition of inflammation. *Nature* **2015,** *528* (7582), 370-5.

48. Peisley, A.; Wu, B.; Xu, H.; Chen, Z. J.; Hur, S., Structural basis for ubiquitin-mediated antiviral signal activation by RIG-I. *Nature* **2014,** *509* (7498), 110-4.

49. Durcan, T. M.; Tang, M. Y.; Pérusse, J. R.; Dashti, E. A.; Aguileta, M. A.; McLelland, G. L.; Gros, P.; Shaler, T. A.; Faubert, D.; Coulombe, B.; Fon, E. A., USP8 regulates mitophagy by removing K6-linked ubiquitin conjugates from parkin. *The EMBO Journal* **2014,** *33* (21), 2473-2491.

50. Ross, C. A.; Pickart, C. M., The ubiquitin-proteasome pathway in Parkinson's disease and other neurodegenerative diseases. *Trends Cell Biol.* **2004,** *14* (12), 703-11.

51. Bennett, E. J.; Shaler, T. A.; Woodman, B.; Ryu, K. Y.; Zaitseva, T. S.; Becker, C. H.; Bates, G. P.; Schulman, H.; Kopito, R. R., Global changes to the ubiquitin system in Huntington's disease. *Nature* **2007,** *448* (7154), 704-8.

52. Hoeller, D.; Dikic, I., Targeting the ubiquitin system in cancer therapy. *Nature* **2009,** *458* (7237), 438-44.

53. Ryabov, Y.; Fushman, D., Interdomain mobility in di-ubiquitin revealed by NMR. *Proteins* **2006,** *63* (4), 787-96.

54. Komander, D.; Reyes-Turcu, F.; Licchesi, J. D. F.; Odenwaelder, P.; Wilkinson, K. D.; Barford, D., Molecular discrimination of structurally equivalent Lys 63-linked and linear polyubiquitin chains. *EMBO Reports* **2009,** *10* (5), 466-473.

55. Liu, Z.; Gong, Z.; Jiang, W. X.; Yang, J.; Zhu, W. K.; Guo, D. C.; Zhang, W. P.; Liu, M. L.; Tang, C., Lys63-linked ubiquitin chain adopts multiple conformational states for specific target recognition. *eLIFE* **2015,** *4*, DOI: 10.7554/eLife.05767.

56. Matsumoto, M. L.; Wickliffe, K. E.; Dong, K. C.; Yu, C.; Bosanac, I.; Bustos, D.; Phu, L.; Kirkpatrick, D. S.; Hymowitz, S. G.; Rape, M.; Kelley, R. F.; Dixit, V. M., K11-Linked Polyubiquitination in Cell Cycle Control Revealed by a K11 Linkage-Specific Antibody. *Mol. Cell* **2010,** *39* (3), 477-484.

57. Bremm, A.; Komander, D., Emerging roles for Lys11-linked polyubiquitin in cellular regulation. *Trends Biochem. Sci* **2011,** *36* (7), 355-363.

58. Virdee, S.; Ye, Y.; Nguyen, D. P.; Komander, D.; Chin, J. W., Engineered diubiquitin synthesis reveals Lys29-isopeptide specificity of an OTU deubiquitinase. *Nat. Chem. Biol.* **2010,** *6* (10), 750-757.

59. Fushman, D., Exploring Polyubiquitin as a Flexible Multiple-Ligand Binding Platform. *Structure* **2017,** *25* (1), 1-3.

60. Castaneda, C. A.; Chaturvedi, A.; Camara, C. M.; Curtis, J. E.; Krueger, S.; Fushman, D., Linkage-specific conformational ensembles of non-canonical polyubiquitin chains. *Phys. Chem. Chem. Phys* **2016,** *18* (8), 5771-5788.

61. Liu, Z.; Zhang, W. P.; Xing, Q.; Ren, X.; Liu, M.; Tang, C., Noncovalent dimerization of ubiquitin. *Angew. Chem. Int. Ed.* **2012,** *51*, 469-472.

62. Levin-Kravets, O.; Shohat, N.; Prag, G., Tetrameric Assembly of Monoubiquitin Accurately Mimics the Lys11 Polyubiquitin Chain Structure. *Biochemistry* **2015,** *54* (30), 4704-10.

63. Servage, K. A.; Silveira, J. A.; Fort, K. L.; Clemmer, D. E.; Russell, D. H., Water-Mediated Dimerization of Ubiquitin Ions Captured by Cryogenic Ion Mobility-Mass Spectrometry. *J. Phys. Chem. Lett.* **2015,** *6* (24), 4947-4951.

64. Xu, P.; Duong, D. M.; Seyfried, N. T.; Cheng, D.; Xie, Y.; Robert, J.; Rush, J.; Hochstrasser, M.; Finley, D.; Peng, J., Quantitative Proteomics Reveals the Function of Unconventional Ubiquitin Chains in Proteasomal Degradation. *Cell* **2009,** *137* (1), 133-145.

65. Breuker, K.; McLafferty, F. W., Stepwise evolution of protein native structure with electrospray into the gas phase, 10^{-12} to 10^{2} s. *Proc. Natl. Acad. Sci.* **2008,** *105* (47), 18145-18152.

66. Lee, S.-W.; Freivogel, P.; Schindler, T.; Beauchamp, J. L., Freeze-Dried Biomolecules: FT-ICR Studies of the Specific Solvation of Functional Groups and Clathrate Formation Observed by the Slow Evaporation of Water from Hydrated Peptides and Model Compounds in the Gas Phase. *J. Am. Chem. Soc.* **1998,** *120* (45), 11758-11765.

67. Silveira, J. A.; Servage, K. A.; Gamage, C. M.; Russell, D. H., Cryogenic ion mobility-mass spectrometry captures hydrated ions produced during electrospray ionization. *J. Phys. Chem. A* **2013,** *117* (5), 953-61.

68. Sun, Y.; Vahidi, S.; Sowole, M. A.; Konermann, L., Protein Structural Studies by Traveling Wave Ion Mobility Spectrometry: A Critical Look at Electrospray Sources and Calibration Issues. *J. Am. Soc. Mass Spec.* **2015,** *27* (1), 31-40.

69. Skinner, O. S.; McLafferty, F. W.; Breuker, K., How ubiquitin unfolds after transfer into the gas phase. *J. Am. Soc. Mass Spec.* **2012,** *23* (6), 1011-4.

70. Kim, D.; Wagner, N.; Wooding, K.; Clemmer, D. E.; Russell, D. H., Ions from Solution to the Gas Phase: A Molecular Dynamics Simulation of the Structural Evolution of Substance P during Desolvation of Charged Nanodroplets Generated by Electrospray Ionization. *J. Am. Chem. Soc.* **2017,** *139* (8), 2981-2988.

71. Merenbloom, S. I.; Flick, T. G.; Williams, E. R., How Hot are Your Ions in TWAVE Ion Mobility Spectrometry? *J. Am. Soc. Mass Spec.* **2011,** (November).

72. Chen, S. H.; Russell, D. H., How Closely Related Are Conformations of Protein Ions Sampled by IM-MS to Native Solution Structures? *J. Am. Soc. Mass Spec.* **2015**.

73. Merenbloom, S. I.; Flick, T. G.; Daly, M. P.; Williams, E. R., Effects of select anions from the Hofmeister series on the gas-phase conformations of protein ions measured with traveling-wave ion mobility spectrometry/mass spectrometry. *J. Am. Soc. Mass Spec.* **2011,** *22* (11), 1978-90.

74. Han, L.; Hyung, S.-J.; Ruotolo, B. T., Dramatically stabilizing multiprotein complex structure in the absence of bulk water using tuned Hofmeister salts. *Faraday Discuss.* **2013,** *160*, 371-371.

75. Han, L.; Ruotolo, B. T., Hofmeister salts recover a misfolded multiprotein complex for subsequent structural measurements in the gas phase. *Angew. Chem. Int. Ed. Engl.* **2013,** *52* (32), 8329-32.

76. Rodier, F.; Bahadur, R. P.; Chakrabarti, P.; Janin, J., Hydration of protein–protein interfaces. *Prot.: St., Func., Bioinf.* **2005,** *60* (1), 36-45.

77. Hirano, T.; Serve, O.; Yagi-Utsumi, M.; Takemoto, E.; Hiromoto, T.; Satoh, T.; Mizushima, T.; Kato, K., Conformational Dynamics of Wild-type Lys-48-linked Diubiquitin in Solution. *J. Biol. Chem.* **2011,** *286* (43), 37496-37502.

78. Ruotolo, B. T.; Benesch, J. L. P.; Sandercock, A. M.; Hyung, S.-J.; Robinson, C. V., Ion mobility-mass spectrometry analysis of large protein complexes. *Nat. Protoc.* **2008,** *3* (7), 1139-52.

79. Pettersen, E. F.; Goddard, T. D.; Huang, C. C.; Couch, G. S.; Greenblatt, D. M.; Meng, E. C.; Ferrin, T. E., UCSF Chimera—A visualization system for exploratory research and analysis. *J. Comput. Chem.* **2004,** *25* (13), 1605-1612.

80. Mesleh, M. F.; Hunter, J. M.; Shvartsburg, A. A.; Schatz, G. C.; Jarrold, M. F., Structural Information from Ion Mobility Measurements: Effects of the Long-Range Potential. *J. Phys. Chem.* **1996,** *100* (40), 16082-16086.

81. Shvartsburg, A. A.; Jarrold, M. F., An exact hard-spheres scattering model for the mobilities of polyatomic ions. *Chem. Phys. Lett.* **1996,** *261* (1–2), 86-91.

82. Baldwin, R. L.; Rose, G. D., Molten globules, entropy-driven conformational change and protein folding. *Curr. Opin. Struct. Biol.* **2013,** *23* (1), 4-10.

83. Kebarle, P.; Verkerk, U. H., Electrospray: from ions in solution to ions in the gas phase, what we know now. *Mass Spectrom. Rev.* **2009,** *28* (6), 898-917.

84. Zhang, Y.; Vuković, L.; Rudack, T.; Han, W.; Schulten, K., Recognition of Poly-Ubiquitins by the Proteasome through Protein Refolding Guided by Electrostatic and Hydrophobic Interactions. *J. Phys. Chem. B* **2016,** *120* (33), 8137-8146.

85. Bogan, A. A.; Thorn, K. S., Anatomy of hot spots in protein interfaces. *J. of Mol. Biol.* **1998,** *280* (1), 1-9.

86. Scarff, C.; Thalassinos, K.; Hilton, G.; Scrivens, J., Travelling wave ion mobility mass spectrometry studies of protein structure: biological significance and

comparison with X-ray crystallography and nuclear magnetic resonance spectroscopy measurements. *Rapid Commun. Mass Spectrom.* **2008,** *22* (20), 3297-3304.

87. Jurneczko, E.; Barran, P. E., How useful is ion mobility mass spectrometry for structural biology? The relationship between protein crystal structures and their collision cross sections in the gas phase. *The Analyst* **2011,** *136* (1), 20-8.

88. Konermann, L.; Vahidi, S.; Sowole, M. a., Mass spectrometry methods for studying structure and dynamics of biological macromolecules. *Anal. Chem.* **2014,** *86* (1), 213-32.

89. Ho, Y.; Gruhler, A.; Heilbut, A.; Bader, G. D.; Moore, L.; Adams, S.-L.; Millar, A.; Taylor, P.; Bennett, K.; Boutilier, K.; Yang, L.; Wolting, C.; Donaldson, I.; Schandorff, S.; Shewnarane, J.; Vo, M.; Taggart, J.; Goudreault, M.; Muskat, B.; Alfarano, C.; Dewar, D.; Lin, Z.; Michalickova, K.; Willems, A. R.; Sassi, H.; Nielsen, P. A.; Rasmussen, K. J.; Andersen, J. R.; Johansen, L. E.; Hansen, L. H.; Jespersen, H.; Podtelejnikov, A.; Nielsen, E.; Crawford, J.; Poulsen, V.; Sorensen, B. D.; Matthiesen, J.; Hendrickson, R. C.; Gleeson, F.; Pawson, T.; Moran, M. F.; Durocher, D.; Mann, M.; Hogue, C. W. V.; Figeys, D.; Tyers, M., Systematic identification of protein complexes in Saccharomyces cerevisiae by mass spectrometry. *Nature* **2002,** *415* (6868), 180-183.

90. Krogan, N. J.; Cagney, G.; Yu, H.; Zhong, G.; Guo, X.; Ignatchenko, A.; Li, J.; Pu, S.; Datta, N.; Tikuisis, A. P.; Punna, T.; Peregrín-Alvarez, J. M.; Shales, M.; Zhang, X.; Davey, M.; Robinson, M. D.; Paccanaro, A.; Bray, J. E.; Sheung, A.;

Beattie, B.; Richards, D. P.; Canadien, V.; Lalev, A.; Mena, F.; Wong, P.; Starostine, A.; Canete, M. M.; Vlasblom, J.; Wu, S.; Orsi, C.; Collins, S. R.; Chandran, S.; Haw, R.; Rilstone, J. J.; Gandi, K.; Thompson, N. J.; Musso, G.; St Onge, P.; Ghanny, S.; Lam, M. H. Y.; Butland, G.; Altaf-Ul, A. M.; Kanaya, S.; Shilatifard, A.; O'Shea, E.; Weissman, J. S.; Ingles, C. J.; Hughes, T. R.; Parkinson, J.; Gerstein, M.; Wodak, S. J.; Emili, A.; Greenblatt, J. F., Global landscape of protein complexes in the yeast Saccharomyces cerevisiae. *Nature* **2006,** *440* (7084), 637-643.

91. Taverner, T.; Hernández, H.; Sharon, M.; Ruotolo, B. T.; Matak-Vinković, D.; Devos, D.; Russell, R. B.; Robinson, C. V., Subunit Architecture of Intact Protein Complexes from Mass Spectrometry and Homology Modeling. *Acc. Chem. Res.* **2008,** *41* (5), 617-627.

92. Uetrecht, C.; Rose, R. J.; van Duijn, E.; Lorenzen, K.; Heck, A. J. R., Ion mobility mass spectrometry of proteins and protein assemblies. *Chem. Soc. Rev.* **2010,** *39* (5), 1633-55.

93. Brutscher, B.; Bruschweiler, R.; Ernst, R. R., Backbone dynamics and structural characterization of the partially folded A state of ubiquitin by 1H, 13C, and 15N nuclear magnetic resonance spectroscopy. *Biochemistry* **1997,** *36*, 13043-13053.

94. Babu, K. R.; Moradian, A.; Douglas, D. J., The Methanol-Induced Conformational Transitions of B-Lactoglobulin, Cytochrome c, and Ubiquitin at Low pH : A Study by Electrospray Ionization Mass Spectrometry. *J. Am. Soc. Mass Spec.* **2001,** *12*, 317-328.

95. Jackson, S. E., Ubiquitin: a small protein folding paradigm. *Org. & Biomol. Chem.* **2006,** *4* (10), 1845-53.

96. Shi, H.; Atlasevich, N.; Merenbloom, S. I.; Clemmer, D. E., Solution Dependence of the Collisional Activation of Ubiquitin [M + 7H](7+) Ions. *J. Am. Soc. Mass Spec.* **2014**, 21-26.

97. Wagner, N. D.; Russell, D. H., Defining Noncovalent Ubiquitin Homodimer Interfacial Interactions through Comparisons with Covalently Linked Diubiquitin. *J. Am. Chem. Soc.* **2016,** *138* (51), 16588-16591.

98. Chowdhury, S. K.; Katta, V.; Chait, B. T., Probing conformational changes in proteins by mass spectrometry. *J. Am. Chem. Soc.* **1990,** *112* (24), 9012-9013.

99. Loo, J. A.; Loo, R. R. O.; Udseth, H. R.; Edmonds, C. G.; Smith, R. D., Solvent-induced conformational changes of polypeptides probed by electrospray-ionization mass spectrometry. *Rapid Commun. Mass Spectrom.* **1991,** *5* (3), 101-105.

100. Iavarone, a. T.; Jurchen, J. C.; Williams, E. R., Effects of solvent on the maximum charge state and charge state distribution of protein ions produced by electrospray ionization. *J. Am. Soc. Mass Spectrom.* **2000,** *11* (11), 976-85.

101. Hall, Z.; Robinson, C. V., Do charge state signatures guarantee protein conformations? *J. Am. Soc. Mass Spectrom.* **2012,** *23* (7), 1161-8.

102. Hamdy, O. M.; Julian, R. R., Reflections on charge state distributions, protein structure, and the mystical mechanism of electrospray ionization. *J. Am. Soc. Mass Spectrom.* **2012,** *23* (1), 1-6.

103. Ly, T.; Julian, R. R., Elucidating the Tertiary Structure of Protein Ions in Vacuo with Site Specific Photoinitiated Radical Reactions. *J. Am. Chem. Soc.* **2010,** *132* (25), 8602-8609.

104. Lee, J. W.; Heo, S. W.; Lee, S. J. C.; Ko, J. Y.; Kim, H.; Kim, H. I., Probing Conformational Changes of Ubiquitin by Host-Guest Chemistry Using Electrospray Ionization Mass Spectrometry. *J. Am. Soc. Mass Spectrom.* **2012**.

105. Harding, M. M., Williams, D. H., Woolfson, D. N., Characterization of a Partially Denatured State of a Protein by Two-Dimensional NMR: Reduction of the Hydrophobic Interactions in Ubiquitin. *Biochemistry* **1990,** *30*, 3120-3128.

106. Brutscher, B.; Bruschweiler, R.; Ernst, R. R., Backbone dynamics and structural characterization of the partially folded A state of ubiquitin by 1H, 13C, and 15N nuclear magnetic resonance spectroscopy. *Biochemistry* **1997,** *36* (42), 13043-53.

107. Babu, K. R.; Moradian, A.; Douglas, D. J., The Methanol-Induced Conformational Transitions of B-Lactoglobulin, Cytochrome c, and Ubiquitin at Low. *J. Am. Soc. Mass Spectrom.* **2000,** *12*, 317-328.

108. Shi, H.; Pierson, N. a.; Valentine, S. J.; Clemmer, D. E., Conformation types of ubiquitin [M+8H]8+ Ions from water:methanol solutions: evidence for the N and A States in aqueous solution. *J. Phys. Chem. B* **2012,** *116* (10), 3344-52.

109. Eschweiler, J. D.; Martini, R. M.; Ruotolo, B. T., Chemical Probes and Engineered Constructs Reveal a Detailed Unfolding Mechanism for a Solvent-Free Multidomain Protein. *J. Am. Chem. Soc.* **2017,** *139* (1), 534-540.

110. Shi, H.; Clemmer, D. E., Evidence for Two New Solution States of Ubiquitin by IMS–MS Analysis. *The Journal of Physical Chemistry B* **2014,** *118*, 3498-3506.

111. Loo, R. R. O.; Loo, J. A., Salt Bridge Rearrangement (SaBRe) Explains the Dissociation Behavior of Noncovalent Complexes. *J. Am. Soc. Mass Spectrom.* **2016,** *27* (6), 975-990.

112. Jungwirth, P.; Cremer, P. S., Beyond Hofmeister. *Nature Chemistry* **2014,** *6* (4), 261-3.

113. Xie, W. J.; Gao, Y. Q., A Simple Theory for the Hofmeister Series. *J. Phys. Chem. Let.* **2013,** *4* (24), 4247-4252.

114. Cacace, M. G.; Landau, E. M.; Ramsden, J. J., The Hofmeister series: salt and solvent effects on interfacial phenomena. *Q. Rev. Biophys.* **1997,** *30* (3), 241-77.

115. Rembert, K. B.; Paterova, J.; Heyda, J.; Hilty, C.; Jungwirth, P.; Cremer, P. S., Molecular mechanisms of ion-specific effects on proteins. *J. Am. Chem. Soc.* **2012,** *134* (24), 10039-46.

116. Shimizu, S.; McLaren, W. M.; Matubayasi, N., The Hofmeister series and protein-salt interactions. *J. Chem. Phys.* **2006,** *124* (23), 234905-234905.

117. Zhang, Y.; Cremer, P. S., Interactions between macromolecules and ions: The Hofmeister series. *Curr. Op. in Chem. Bio.* **2006,** *10* (6), 658-63.

118. Pegram, L. M.; Record, M. T., Jr., Quantifying the roles of water and solutes (denaturants, osmolytes, and Hofmeister salts) in protein and model processes using the solute partitioning model. *Methods. Mol. Biol.* **2009,** *490*, 179-93.

119. Zhou, P.; Tian, F.; Zou, J.; Ren, Y.; Liu, X.; Shang, Z., Do halide motifs stabilize protein architecture? *J. Phys. Chem. B* **2010,** *114* (47), 15673-15686.

120. Hamada, D.; Kidokoro, S.; Fukada, H.; Takahashi, K.; Goto, Y., Salt-induced formation of the molten globule state of cytochrome c studied by isothermal titration calorimetry. *PNAS* **1994,** *91* (October), 10325-10329.

121. Sinibaldi, F.; Piro, M. C.; Coletta, M.; Santucci, R., Salt-induced formation of the A-state of ferricytochrome c--effect of the anion charge on protein structure. *The FEBS Journal* **2006,** *273* (23), 5347-57.

122. Mirza, U. a.; Chait, B. T., Effects of anions on the positive ion electrospray ionization mass spectra of peptides and proteins. *Anal. Chem.* **1994,** *66* (18), 2898-2904.

123. Makhatadze, G. I.; Lopez, M. M.; Richardson, J. M.; Thmos, S. T., Anion binding to the ubiquitin molecule. *Protein Sci.* **1998,** *7* (3), 689-697.

124. Brutscher, B.; Bruschweiler, R.; Ernst, R. R., *Biochemistry* **1997,** *36*, 13043-13053.

125. Hoerner, J. K.; Xiao, H.; Kaltashov, I. A., Structural and dynamic characteristics of a partially folded state of ubiquitin revealed by hydrogen exchange mass spectrometry. *Biochemistry* **2005,** *44* (33), 11286-94.

126. Sharawy, M.; Consta, S., Effect of counterions on the charging mechanisms of a macromolecule in aqueous nanodrops. *J. Chem. Phys.* **2014,** *141* (10), 104321.

127. Konermann, L.; McAllister, R. G.; Metwally, H., Molecular Dynamics Simulations of the Electrospray Process: Formation of NaCl Clusters via the Charged Residue Mechanism. *J. Phys. Chem. B* **2014,** *118* (41), 12025-12033.

128. Gunsteren, W. F. V. A. N., Molecular dynamics simulations of the native and partially folded states of ubiquitin : Influence of methanol cosolvent , pH , and temperature on the protein structure and dynamics. *Protein Sci.* **2007,** *16*, 1101-1118.

129. Sharawy, M.; Consta, S., Effect of counterions on the charging mechanisms of a macromolecule in aqueous nanodrops. *J. Chem. Phys.* **2014,** *141* (10), 104321.

130. Malevanets, A.; Consta, S., Variation of droplet acidity during evaporation. *J. Chem. Phys.* **2013,** *138* (18), 184312.

131. Chang, T. M.; Berden, G.; Oomens, J.; Williams, E. R., Halide anion binding to Gly3, Ala3 and Leu3. *Int. J. Mass Spectrom.* **2014,** *377*, 440-447.

132. Zhou, P.; Ren, Y.; Tian, F.; Zou, J.; Shang, Z., Halogen-ionic bridges: Do they exist in the biomolecular world? *J. Chem. Theory and Comp.* **2010,** *6* (7), 2225-2241.

133. Demireva, M.; Oomens, J.; Berden, G.; Williams, E. R., The Ionic Hydrogen/Deuterium Bonds between Diammoniumalkane Dications and Halide Anions. *ChemPlusChem* **2013,** *78* (9), 995-1004.

134. Warnke, S.; von Helden, G.; Pagel, K., Protein structure in the gas phase: the influence of side-chain microsolvation. *J. Am. Chem. Soc.* **2013,** *135* (4), 1177-80.

135. Mautner, M., The Ionic Hydrogen Bond Mautner 2005.pdf. *Chem. Rev.* **2005,** *105*, 213-284.

136. Bartman, C. E.; Metwally, H.; Konermann, L., Effects of Multidentate Metal Interactions on the Structure of Collisionally Activated Proteins: Insights from Ion Mobility Spectrometry and Molecular Dynamics Simulations. *Anal. Chem.* **2016,** *88* (13), 6905-6913.

137. Castañeda, Carlos A.; Kashyap, Tanuja R.; Nakasone, Mark A.; Krueger, S.; Fushman, D., Unique Structural, Dynamical, and Functional Properties of K11-Linked Polyubiquitin Chains. *Structure* **2013,** *21* (7), 1168-1181.

138. Morimoto, D.; Walinda, E.; Fukada, H.; Sou, Y.-S.; Kageyama, S.; Hoshino, M.; Fujii, T.; Tsuchiya, H.; Saeki, Y.; Arita, K.; Ariyoshi, M.; Tochio, H.; Iwai, K.; Namba, K.; Komatsu, M.; Tanaka, K.; Shirakawa, M., The unexpected role of polyubiquitin chains in the formation of fibrillar aggregates. *Nature Communications* **2015,** *6*, 6116.

139. Milardi, D.; Arnesano, F.; Grasso, G.; Magrì, A.; Tabbì, G.; Scintilla, S.; Natile, G.; Rizzarelli, E., Ubiquitin Stability and the Lys 63-Linked Polyubiquitination Site Are Compromised on Copper Binding. *Angew. Chem. Int. Ed.* **2007,** *46* (42), 7993-7995.

140. Arnesano, F.; Scintilla, S.; Calò, V.; Bonfrate, E.; Ingrosso, C.; Losacco, M.; Pellegrino, T.; Rizzarelli, E.; Natile, G., Copper-Triggered Aggregation of Ubiquitin. *PLOS ONE* **2009,** *4* (9), e7052.

141. Cong, X.; Liu, Y.; Liu, W.; Liang, X.; Russell, D. H.; Laganowsky, A., Determining Membrane Protein–Lipid Binding Thermodynamics Using Native Mass Spectrometry. *J. Am. Chem. Soc.* **2016,** *138* (13), 4346-4349.

142. El-Baba, T. J.; Woodall, D. W.; Raab, S. A.; Fuller, D. R.; Laganowsky, A.; Russell, D. H.; Clemmer, D. E., Melting Proteins: Evidence for Multiple Stable Structures upon Thermal Denaturation of Native Ubiquitin from Ion Mobility Spectrometry-Mass Spectrometry Measurements. *J. Am. Chem. Soc.* **2017,** *139* (18), 6306-6309.

143. Han, L.; Hyung, S.-J.; Mayers, J. J. S.; Ruotolo, B. T., Bound anions differentially stabilize multiprotein complexes in the absence of bulk solvent. *J. Am. Chem. Soc.* **2011,** *133* (29), 11358-67.

144. Zhang, Y.; Cremer, P. S., Chemistry of Hofmeister anions and osmolytes. *Annu. Rev. Phys. Chem.* **2010,** *61*, 63-83.

145. Gladich, I.; Shepson, P. B.; Carignano, M. A.; Szleifer, I., Halide Affinity for the Water−Air Interface in Aqueous Solutions of Mixtures of Sodium Salts. *The Journal of Physical Chemistry A* **2011,** *115* (23), 5895-5899.

146. Sedlák, E.; Stagg, L.; Wittung-Stafshede, P., Effect of Hofmeister ions on protein thermal stability: roles of ion hydration and peptide groups? *Arch. Biochem. Biophys.* **2008,** *479* (1), 69-73.

APPENDIX A

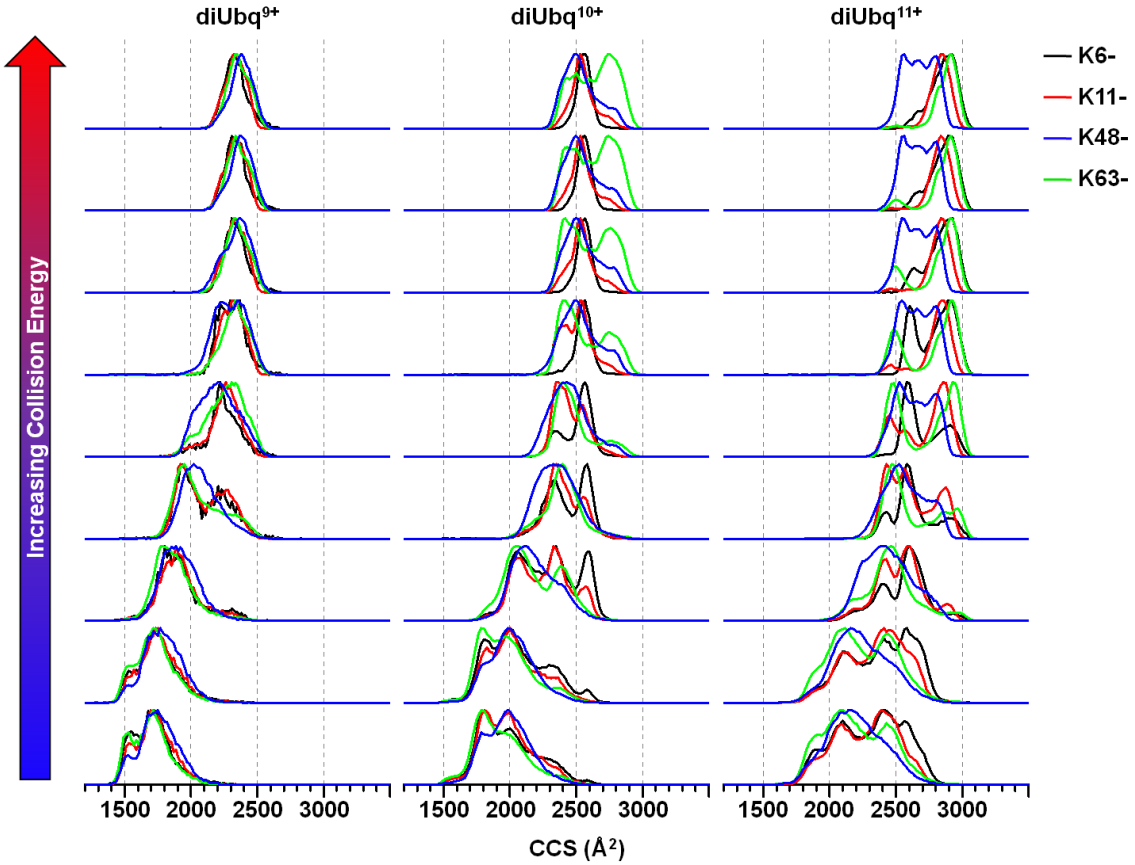

Figure A.1 Stacked CCS profiles after varying degrees of collisional activation (collision voltage was 5-45V in 5V increments) for 9 – 11+ charge states (left to right) of protonated K6- (black), K11- (red), K48- (blue) and K63- (green) linked diUbq acquired from 99.9% water/0.1% formic acid.

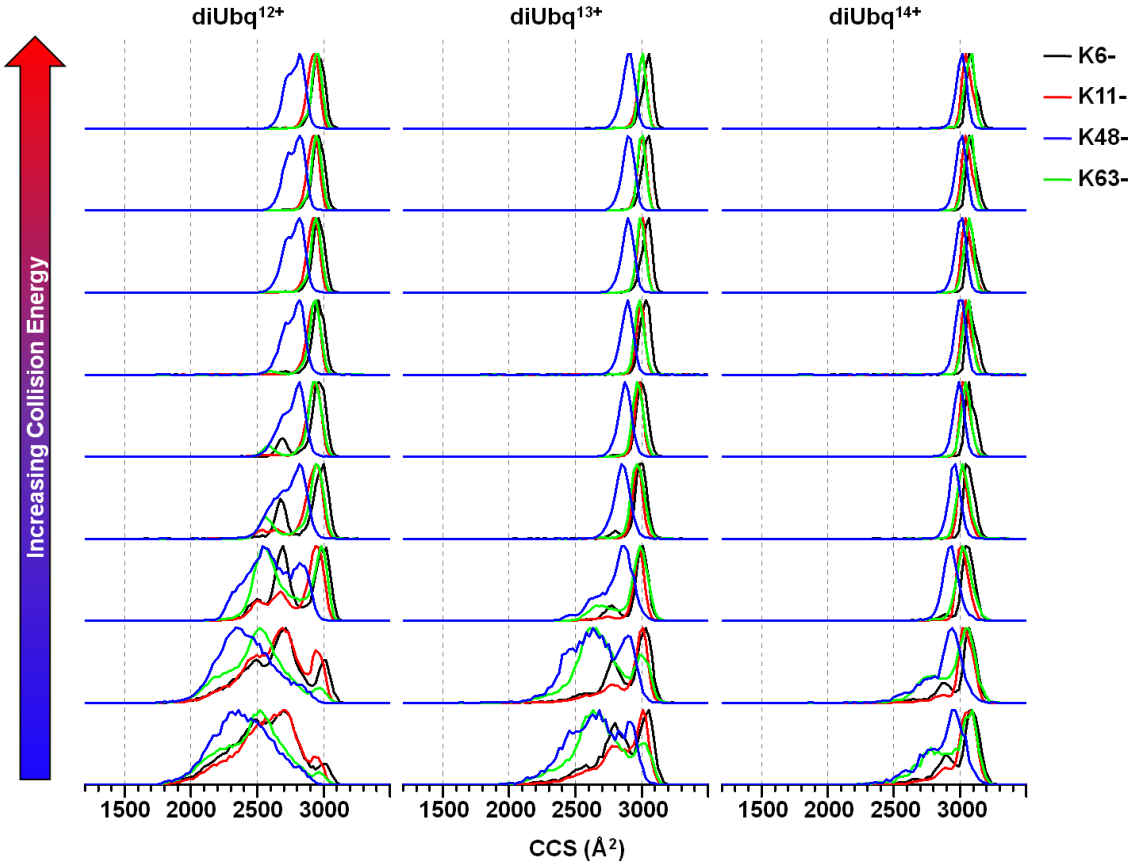

Figure A.2. Stacked CCS profiles after varying degrees of collisional activation (collision voltage was 5-45V in 5V increments) for 12 – 14+ charge states (left to right) of protonated K6- (black), K11- (red), K48- (blue) and K63- (green) linked diUbq acquired from 99.9% water/0.1% formic acid.

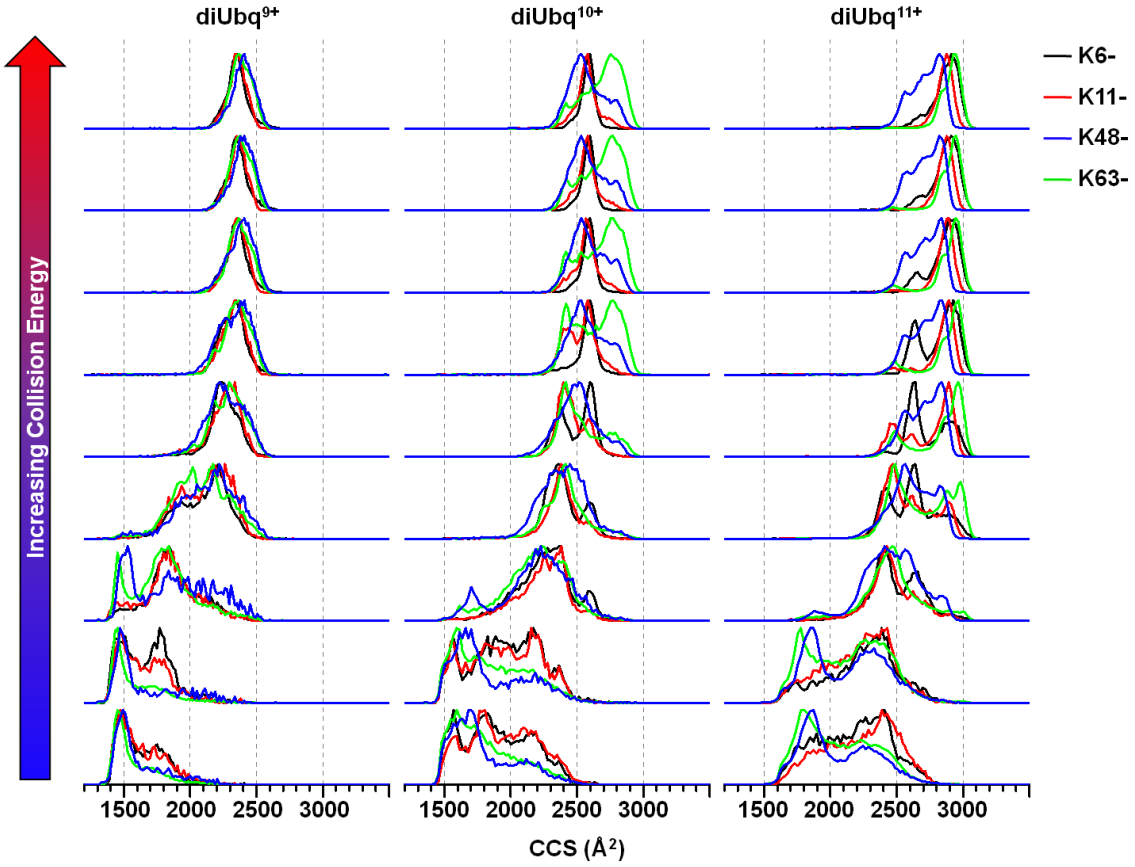

Figure A.3. Stacked CCS profiles after varying degrees of collisional activation (collision voltage was 5-45V in 5V increments) for 9 – 11+ charge states (left to right) of protonated K6- (black), K11- (red), K48- (blue) and K63- (green) linked diUbq acquired from 49.9% water/50% methanol/0.1% formic acid.

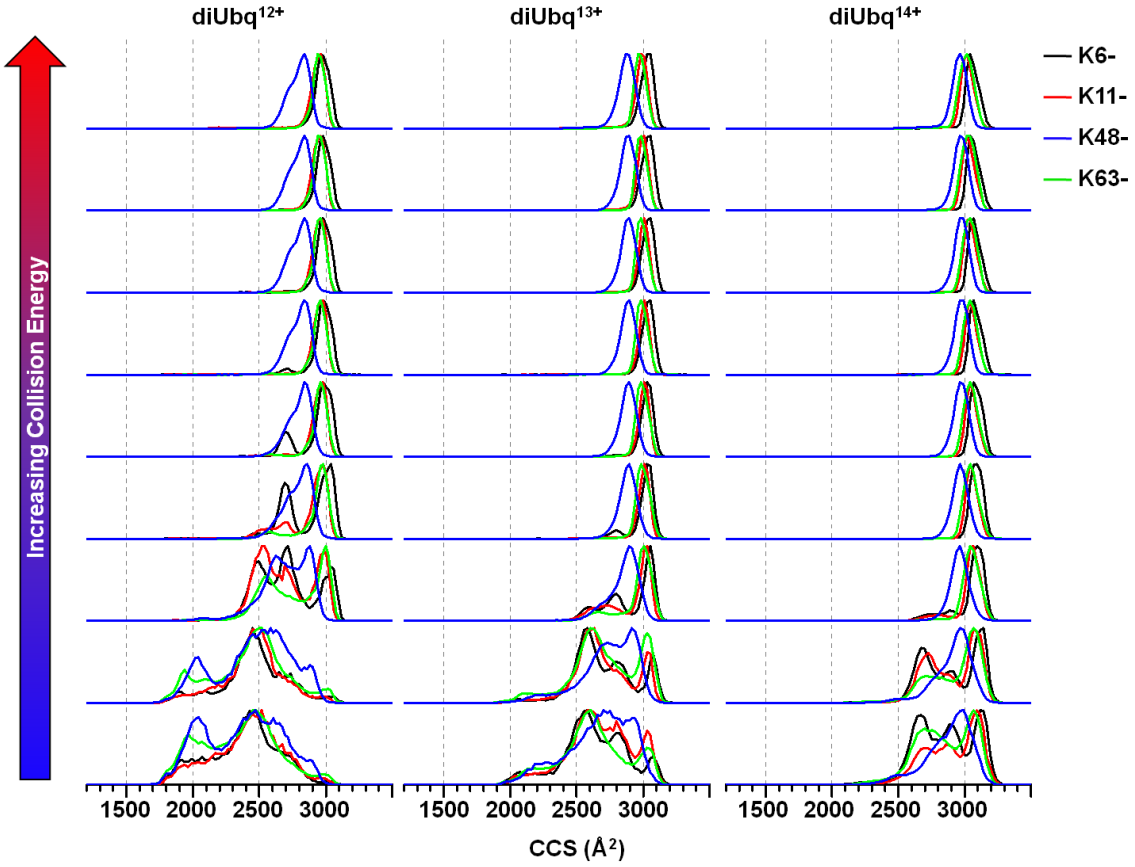

Figure A.4. Stacked CCS profiles after varying degrees of collisional activation (collision voltage was 5-45V in 5V increments) for 12 – 14+ charge states (left to right) of protonated K6- (black), K11- (red), K48- (blue) and K63- (green) linked diUbq acquired from 49.9% water/50% methanol/0.1% formic acid.

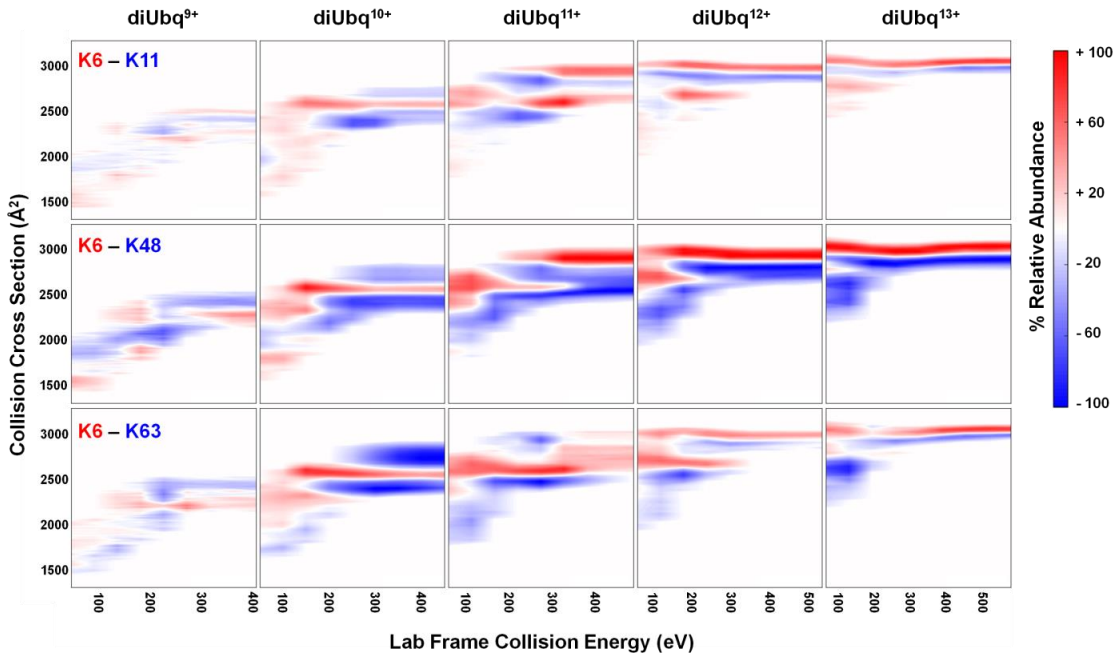

Figure A.5. Difference plots acquired using CIUSuite where K11-, K48-, and K63-linked diUbq ion CIU profiles (blue) are subtracted from K6-linked diUbq ion CIU profiles (red). The CIU profiles were acquired from 99.9% water/0.1% formic acid.

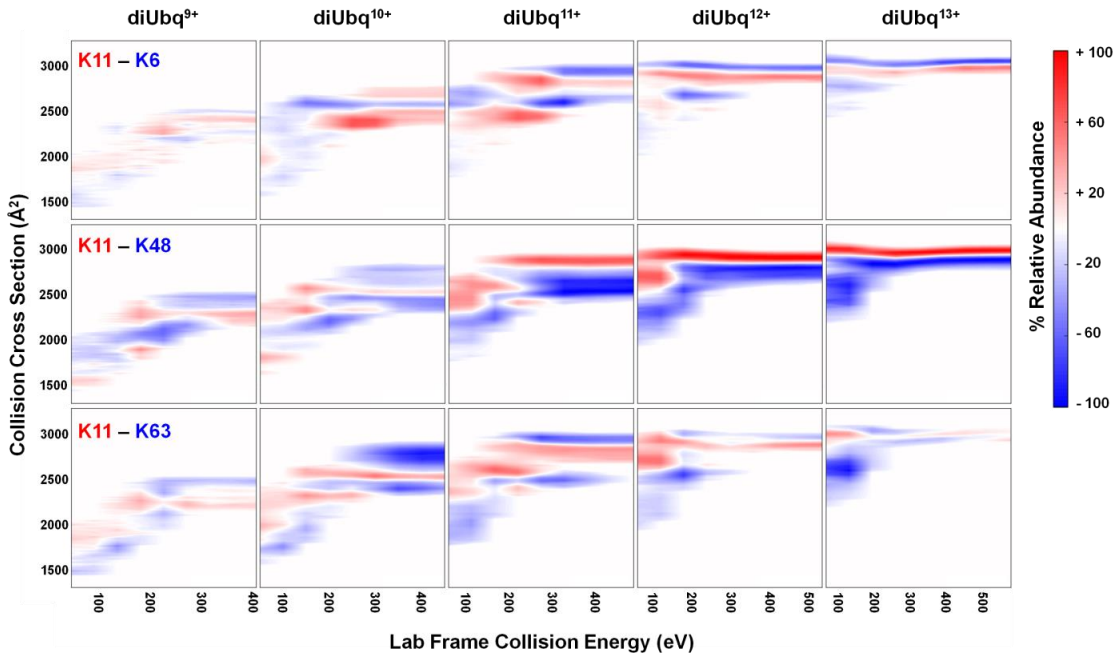

Figure A.6. Difference plots acquired using CIUSuite where K6-, K48-, and K63-linked diUbq ion CIU profiles (blue) are subtracted from K11-linked diUbq ion CIU profiles (red). The CIU profiles were acquired from 99.9% water/0.1% formic acid.

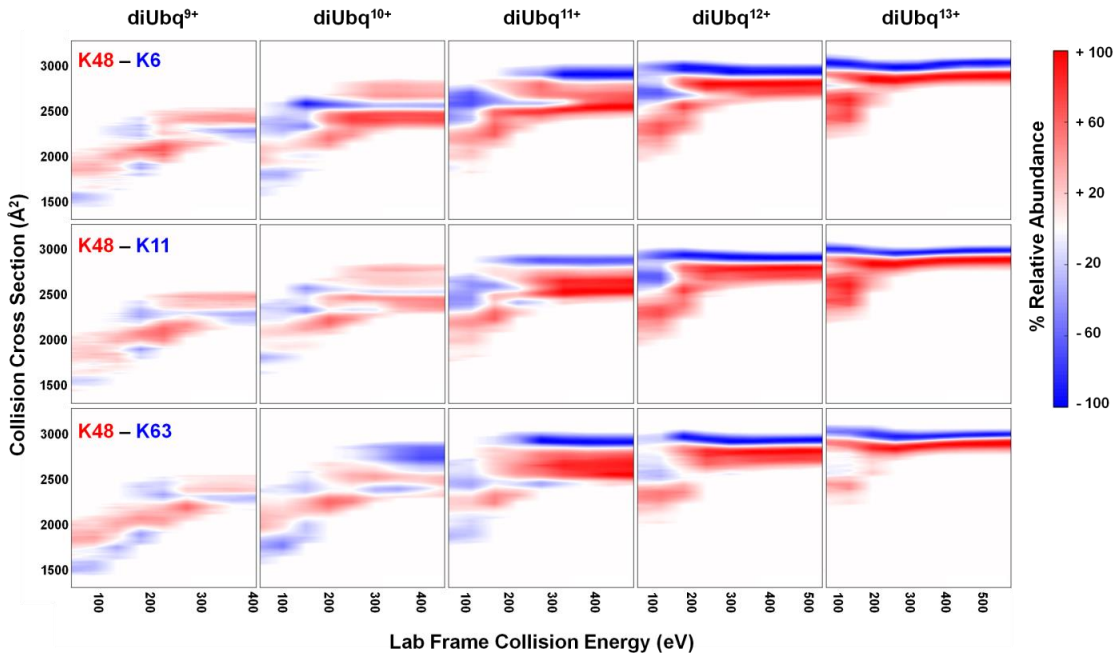

Figure A.7. Difference plots acquired using CIUSuite where K6-, K11-, and K63-linked diUbq ion CIU profiles (blue) are subtracted from K48-linked diUbq ion CIU profiles (red). The CIU profiles were acquired from 99.9% water/0.1% formic acid.

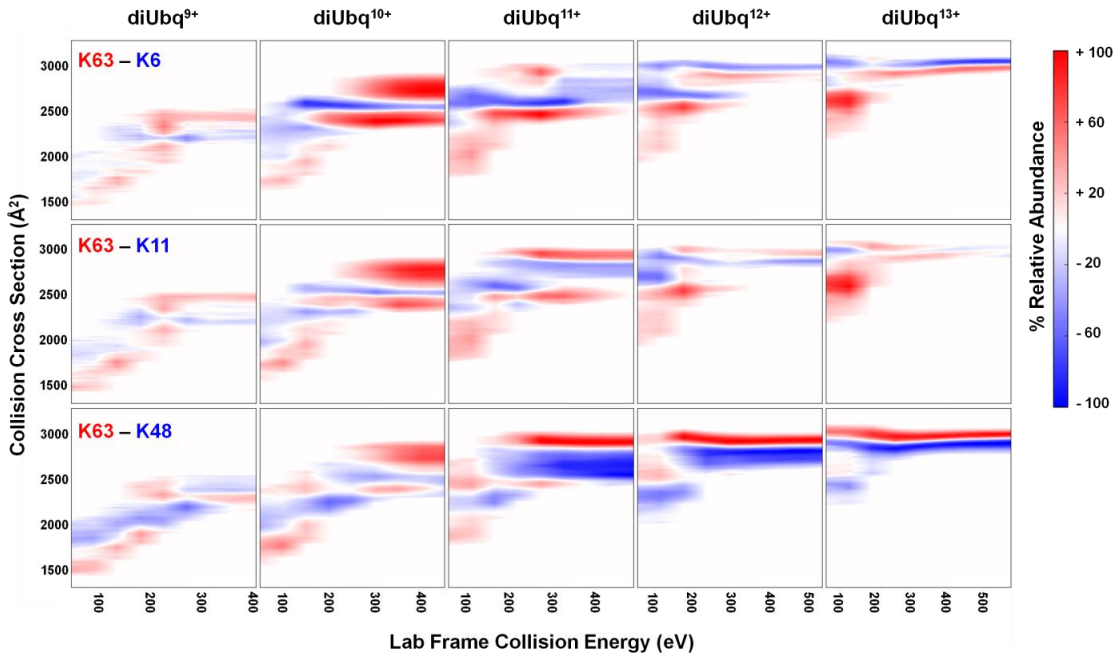

Figure A.8. Difference plots acquired using CIUSuite where K6-, K11-, and K48-linked diUbq ion CIU profiles (blue) are subtracted from K63-linked diUbq ion CIU profiles (red). The CIU profiles were acquired from 99.9% water/0.1% formic acid.

A)	K6	K11	K48	K63
K6	--	7.63511	17.6889	12.1854
K11	7.63511	--	16.4435	11.0331
K48	17.6889	16.4435	--	15.3618
K63	12.1854	11.0331	15.3618	--
B)	K6	K11	K48	K63
K6	--	16.3807	27.0205	33.8335
K11	16.3807	--	16.3053	25.1512
K48	27.0205	16.3053	--	20.2881
K63	33.8335	25.1512	28.2625	--
C)	K6	K11	K48	K63
K6	--	20.8333	35.7486	24.2159
K11	20.8333	--	33.9711	21.4117
K48	35.7486	33.9711	--	35.8188
K63	24.2159	21.4117	35.8188	--
D)	K6	K11	K48	K63
K6	--	19.6005	44.6714	19.8442
K11	19.6005	--	44.4018	18.8066
K48	44.6714	44.4018	--	39.3972
K63	19.8442	18.8066	39.3972	--
E)	K6	K11	K48	K63
K6	--	23.2105	51.1201	28.9788
K11	23.2105	--	50.7267	25.0742
K48	51.1201	50.7267	--	39.2652
K63	28.9788	25.0742	39.2652	--

Table A.1. RMSD values comparing the CIU heat maps of each linkage type acquired from 99.9% water and 0.1% formic acid where the charge state is 9-13+ (A-E, respectively) determined using the compare function of CIUSuite.

	9+	10+	11+	12+	13+
K6	15.4925	19.5302	16.5448	20.843	25.5902
K11	17.561	17.82	16.0994	23.8314	28.0258
K48	25.6599	20.2881	21.6354	19.3996	15.4605
K63	20.5176	19.2573	19.148	13.5917	26.3195

Table A.2. RMSD values comparing the CIU heat maps acquired from 99.9% water/0.1% formic acid and 50% methanol/49.9% water/0.1% formic acid conditions for each linkage type and charge state.

APPENDIX B

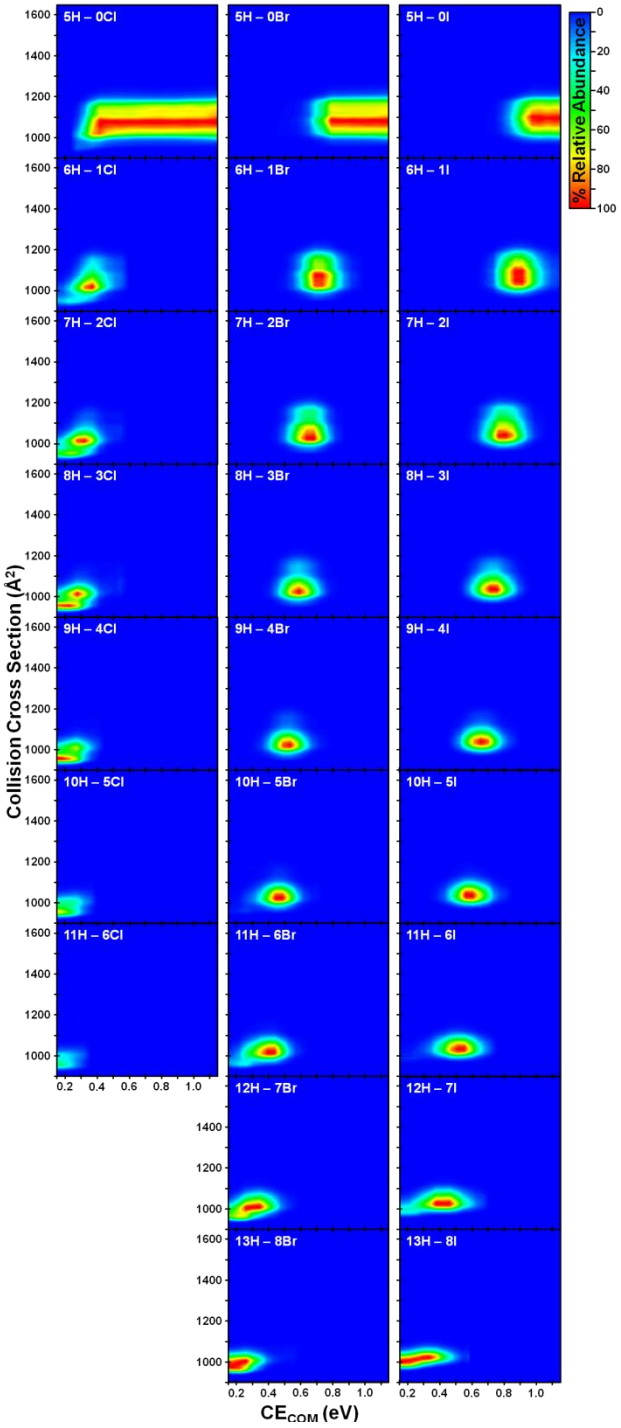

Figure B.1. CIU heat maps of all $[Ubq + nH + xX]^{5+}$ ions where the anion adducts are Cl^-, Br^- and I^- from left to right, respectively. Each heat map is labeled according to their n and x values (n-x).

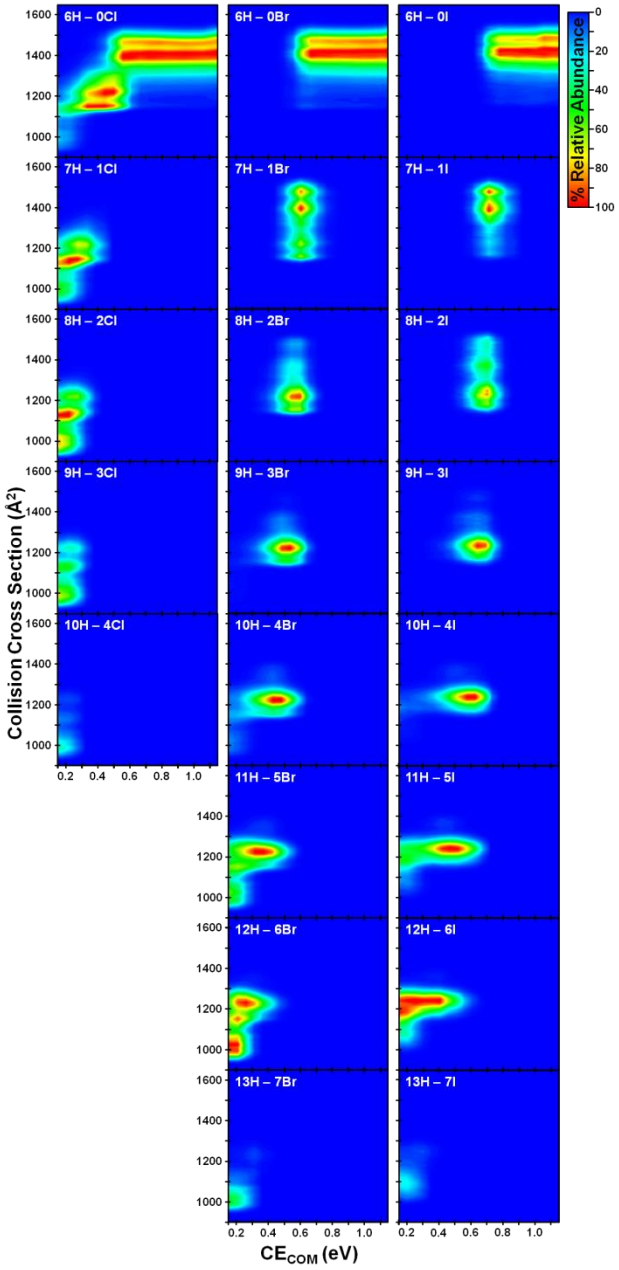

Figure B.2. CIU heat maps of all $[Ubq + nH + xX]^{6+}$ ions where the anion adducts are Cl^-, Br^- and I^- from left to right, respectively. Each heat map is labeled according to their n and x values (n-x).